Lawrence Berkeley National Laboratory
Recent Work

Title
EXPERIMENTAL TEST OF LOCAL HIDDEN-VARIABLE THEORIES

Permalink
https://escholarship.org/uc/item/2f18n5nk

Author
Freedman, Stuart Jay.

Publication Date
1972-05-01

eScholarship.org Powered by the California Digital Library
University of California

RECEIVED
LAWRENCE
RADIATION LABORATORY

DOCUMENTS SECTION

LBL-391

EXPERIMENTAL TEST OF LOCAL HIDDEN-VARIABLE THEORIES

Stuart Jay Freedman
(Ph. D. Thesis)

May 5, 1972

AEC Contract No. W-7405-eng-48

For Reference

Not to be taken from this room

LBL-391

DISCLAIMER

This document was prepared as an account of work sponsored by the United States Government. While this document is believed to contain correct information, neither the United States Government nor any agency thereof, nor the Regents of the University of California, nor any of their employees, makes any warranty, express or implied, or assumes any legal responsibility for the accuracy, completeness, or usefulness of any information, apparatus, product, or process disclosed, or represents that its use would not infringe privately owned rights. Reference herein to any specific commercial product, process, or service by its trade name, trademark, manufacturer, or otherwise, does not necessarily constitute or imply its endorsement, recommendation, or favoring by the United States Government or any agency thereof, or the Regents of the University of California. The views and opinions of authors expressed herein do not necessarily state or reflect those of the United States Government or any agency thereof or the Regents of the University of California.

0 0 0 0 5 7 0 2 1 7 6

EXPERIMENTAL TEST OF LOCAL HIDDEN-VARIABLE THEORIES

Contents

0 0 0 0 3 7 0 2 1 7 8

EXPERIMENTAL TEST OF LOCAL HIDDEN-VARIABLE THEORIES

Stuart Jay Freedman

Department of Physics
and
Lawrence Berkeley Laboratory
University of California
Berkeley, California

May 5, 1972

ABSTRACT

This thesis describes a measurement of the linear polarization correlation of the photons emitted in the atomic cascade $4p^2\ {}^1S_0 \rightarrow 4s4p\,{}^1P_1 \rightarrow 4s^2\ {}^1S_0$ of calcium. It has been shown by Bell that local hidden-variable theories yield predictions for an idealized correlation of this type which are in conflict with the predictions of quantum mechanics. This result is expressed in terms of an inequality that was subsequently generalized and made applicable to the present experiment. The simplest form of this inequality is

$$\delta = \left(\frac{R(22\tfrac{1}{2}^\circ)}{R_o} - \frac{R(67\tfrac{1}{2}^\circ)}{R_o} \right) - \frac{1}{4} \leq 0 \ ,$$

where $R(\phi)$ is the coincidence rate with angle ϕ between the polarizers, and R_o is the rate with polarizers removed. The present experiment yields $\delta = 0.050 \pm 0.008$, violating this inequality. Furthermore, the results for $R(\phi)/R_o$ show no evidence of any deviation from the predictions of quantum mechanics. Thus this experiment verifies the quantum-

mechanical predictions and provides strong evidence against the validity of local hidden-variable theories.

0 0 0 0 3 7 0 2 1 7 7

I. INTRODUCTION

The usual interpretation of quantum mechanics is self-consistent, yet it has often been suggested that a more deterministic formulation (a hidden-variable theory) may be possible. Recently, J. S. Bell (B65) has considered a class of hidden-variable theories constrained by a natural condition of locality. He noted that these theories yield predictions in conflict with some of the statistical predictions of ordinary quantum mechanics. Bell's result takes the form of an inequality (Bell's inequality), valid for any local hidden-variable theory, but violated by certain quantum-mechanical predictions.

Bell's inequality was generalized to realizable systems by Clauser, Horne, Shimony, and Holt (CHSH69, H70), who pointed out that the generalized inequality could be tested experimentally, but that existing data were insufficient for this purpose.

The present experiment is a test of the generalized inequality. This thesis describes a measurement of the polarization correlation of the two photons emitted in the $4p^2\ {}^1S_0 \rightarrow 4s4p\,{}^1P_1 \rightarrow 4s^2\ {}^1S_0$ cascade of calcium. The method is similar to that of Kocher and Commins (KC67). The results of this experiment are compared with the predictions of quantum mechanics and the inequalities imposed by local hidden-variable theories (FC72). The experimental results are consistent with quantum mechanics and provide strong evidence against the validity of local hidden-variable theories.

A. Hidden-Variable Theories

Quantum-mechanical predictions have a statistical nature that has led some physicists to speculate that the theory is incomplete. In a more complete theory, physical states would be precisely specified, and measurements would be free of dispersion. These theories are called hidden-variable theories, after the additional quantities needed for complete specification of states. These quantities are hidden because quantum mechanics can be interpreted without them, and there is yet no observational evidence that demands their existence.*

Of course, any useful hidden-variable theory must be capable of describing the quantum-mechanical properties of nature, including the observed dispersion of the results of identical measurements made on identically prepared systems. To accomplish this, a quantum state is associated with an ensemble of hidden-variable states. The result of a particular measurement is then, in principle, determined, and the apparent dispersion in repeated measurements is due to ignorance of what particular hidden-variable state had been chosen from the initial ensemble.

For a long time it appeared that the usefulness of such a scheme had been decided in a famous proof by J. Von Neumann (V32). Contained in the conclusions of this proof is the assertion that all hidden-variable theories are impossible, all being inconsistent with the well-verified properties of quantum mechanics.

---

* For an excellent discussion of the motivation for a deterministic substructure for quantum mechanics, see Ref. B57.

0 0 0 0 5 7 0 2 1 7 9

J. S. Bell (B66) has reexamined Von Neumann's proof and has argued that its essential assumption is unduly restrictive. In the same paper, Bell examined other proofs of the impossibility of hidden-variable theories, concluding that, while some restrict the form of possible theories, none rule them out altogether.

It is not the purpose of this thesis to enter into the controversy over the validity of the various proofs of the impossibility of hidden-variable theories. It should be pointed out, however, that there are specific examples of hidden-variable theories whose predictions are consistent with quantum mechanics. That mathematically valid impossibility proofs and specific examples of theories exist, is evidence of disagreement about what constitutes a hidden-variable theory. The essential question is: What properties of quantum mechanics, in addition to its statistical predictions, should be retained in a hidden-variable theory?*

B. Local Hidden-Variable Theories; Bell's Inequality

The particular class of hidden-variable theories to be tested here, local hidden-variable theories, is best described in the context in which it was originally discussed by Bell. Bell (B65) considered an idealized case of measurements made on spatially separated but quantum-mechanically correlated systems, namely, measurements of the

---

* For some specific examples of hidden-variable theories, see Refs. B52a, B52b, BB66 , B66. For proofs of the impossibility of hidden variables, see JP63, G68, KS67,Mi67. For discussions of the validity of the impossibility proofs and the examples, see B72, G70, B66. For a more complete bibliography on hidden variables, see Gr70, B72, DG71.

components of spin of two spin-½ particles initially in a state of total angular momentum zero (the singlet state). This system had been shown by Bohm (B51, BA57)* to be an example of a peculiar aspect of quantum mechanics first pointed out by Einstein, Podolsky, and Rosen (EPR35).† The two-spin-½ system is analogous to the two-photon system that is investigated in this experiment.

Consider two spin-½ particles initially in the singlet state and moving freely in opposite directions along the z axis. The spin part of the quantum-mechanical state vector for this system is

$$\psi = \frac{1}{\sqrt{2}} [u_+(1)\, u_-(2) - u_-(1)\, u_+(2)] , \qquad (I.1)$$

where u_+ and u_- are eigenstates of some components of the spin operator $\vec{\sigma}$, and 1 and 2 refer to the particles. Only the portion of the state vector describing the spin angular momentum need be considered.

If, when the particles are separated, any component of one particle's spin is measured, then, because the total angular momentum is zero, one may conclude that the same component of the other particle's spin is in the opposite direction. Furthermore, this is independent of

---

* This system is often included in discussions of hidden-variable theories. The idealized experiment that is discussed here is called "Bohm's Gedankenexperiment."

† In their 1935 paper, Einstein et al. discussed the quantum-mechanical properties of momentum and position measurements made on spatially separated but previously interacting particles. They concluded that quantum mechanics must be incomplete. In fact, it was an attempt to implement this completion that led Bell to formulate the problem in terms of a local hidden-variable theory.

0 0 0 0 3 7 0 2 1 8 0

the direction chosen for the initial measurement. Apparently, the state ofoneparticle can be prepared by performing a measurement on the other particle, even though the particles are separated in space.

This peculiar correlation led Bell to speculate on an alternative description. In terms of a hidden-variable scheme, a correlation between the particles merely results from information disclosed by the first measurement which allows the results of measurements on the other particle to be anticipated. This additional information previously existed in the two-particle system (as the value of some hidden variable), but was not included in the "incomplete" quantum-mechanical description.

Bell considered the following model. One assumes that the results of all possible spin measurements on particle 1 (2) are determined by the value of some hidden-variable, λ_1 (λ_2). The exact form of the hidden variables need not be specified; for notational convenience we take them to be continuous parameters. A measurement of the spin of particle 1 is associated with a deterministic function $A(\hat{a}, \lambda_1)$, where $\hat{a}$ represents parameters of the measuring device – say, the orientation of a Stern-Gerlach magnet. Another function $B(\hat{b}, \lambda_2)$, is associated with measurements on particle 2. These functions take on the values corresponding to the two possible results of a measurement of a component of spin. We let $A(\hat{a}, \lambda_1) = \pm 1$ and $B(\hat{b}, \lambda_2) = \pm 1$.

The essential condition of locality has already been assumed. In particular, the function $A(\hat{a}, \lambda_1)$ is independent of the orientation $\hat{b}$ of the other measuring device, and vice versa. This is a natural

assumption in a hidden-variable description, because it is unreasonable for the result of a measurement involving one of the particles to be affected by the orientation of a distant measuring device.

To describe repeated measurements on identically prepared systems, one assumes that each hidden-variable state is associated with the pair λ_1, λ_2 which is chosen according to a probability distribution $\rho(\lambda_1, \lambda_2)$. We assume $\rho(\lambda)$ is normalized:

$$\int_{\Gamma_1,\Gamma_2} \rho(\lambda_1,\lambda_2)d\lambda_1 d\lambda_2 = 1 ,$$

where Γ_1 (Γ_2) is the space from which λ_1 (λ_2) is chosen. For notational convenience and without loss of generality, one can associate a single hidden variable λ with the pair λ_1, λ_2.

The quantum-mechanical expectation value for the product of individual spin measurements in the directions $\hat{a}$ and $\hat{b}$ is given by the following expectation value:

$$E(\hat{a}, \hat{b}) = \langle \psi | \hat{a}\cdot\vec{\sigma}_1 \; \hat{b}\cdot\vec{\sigma}_2 | \psi \rangle = -\hat{a}\cdot\hat{b} . \qquad (I.2)$$

The analogous quantity in the local hidden-variable theory is the correlation function, defined by

$$P(\hat{a}, \hat{b}) = \int \rho(\lambda) \; A(\hat{a}, \lambda) \; B(\hat{b}, \lambda) \; d\lambda . \qquad (I.3)$$

The content of Bell's observation is that no function given by this expression (Eq. I.3) for any $\rho(\lambda)$, $A(\hat{a}, \lambda)$, or $B(\hat{b}, \lambda)$ can equal the quantum-mechanical expectation value, Eq. I.2, for all $\hat{a}$ and $\hat{b}$.

0 0 0 0 3 7 0 2 1 8 1

Therefore, no local hidden-variable theory is consistent with this particular prediction of quantum mechanics.

The condition of locality is absolutely essential to Bell's conclusion. In particular, the more general expression

$$\bar{P}(\hat{a}, \hat{b}) = \int \rho(\lambda) A(\hat{a}, \hat{b}, \lambda) B(\hat{a}, \hat{b}, \lambda) d\lambda \qquad (I.4)$$

can be made to equal $E(\hat{a}, \hat{b})$ for all $\hat{a}$ and $\hat{b}$ (see Ref. B66).

In his original derivation, Bell used the condition

$$A(\hat{a}, \lambda) = -B(\hat{a}, \lambda) \qquad (I.5)$$

for all λ. This condition makes $P(\hat{a}, \hat{b})$ consistent with $E(\hat{a}, \hat{b})$, at least for measurements in the same direction ($\hat{a} = \hat{b}$). The assumption of perfect correlation is unrealistic for an actual experiment, but it can be shown that a discrepancy between quantum mechanics and local hidden-variable theories can be obtained without it (see Sec. II.A).

Using Eq. I.5, Eq. I.3 can be rewritten as

$$P(\hat{a}, \hat{b}) = -\int \rho(\lambda) A(\hat{a}, \lambda) A(\hat{b}, \lambda) d\lambda \ .$$

Considering the three measurement directions $\hat{a}$, $\hat{b}$, and $\hat{c}$, and recalling that $A(\hat{a}, \lambda) = \pm 1$ and $B(\hat{b}, \lambda) = \pm 1$, we have

$$P(\hat{a}, \hat{b}) - P(\hat{a}, \hat{c}) = -\int \rho(\lambda) [A(\hat{a}, \lambda) A(\hat{b}, \lambda) - A(\hat{a}, \lambda) A(\hat{c}, \lambda)] d\lambda$$

$$= \int \rho(\lambda) A(\hat{a}, \lambda) A(\hat{b}, \lambda) [A(\hat{b}, \lambda) A(\hat{c}, \lambda) - 1] d\lambda \ ;$$

hence,

$$|P(\hat{a}, \hat{b}) - P(\hat{a}, \hat{c})| \leq \int \rho(\lambda) [1 - A(\hat{b}, \lambda) A(\hat{c}, \lambda)] \ ,$$

and finally,

$$|P(\hat{a}, \hat{b}) - P(\hat{a}, \hat{c})| \leq 1 + P(\hat{b}, \hat{c}) \ . \qquad (I.6)$$

Note that the fact that $\rho(\lambda)$ is normalized has been used.

It will now be seen that inequality I.6 is inconsistent with the quantum-mechanical expectation value. Let $\hat{a}$, $\hat{b}$, $\hat{c}$ be coplanar, and let $\alpha = \cos^{-1}(\hat{a}\cdot\hat{b})$, $\beta = \cos^{-1}(\hat{b}\cdot\hat{c})$, and $\alpha+\beta = \cos^{-1}(\hat{a}\cdot\hat{c})$. Then, on substitution of the quantum-mechanical expectation values into I.6, we have

$$|-\cos\alpha + \cos(\alpha + \beta)| \leq 1 - \cos\beta \ .$$

With $\alpha = \beta = 60°$, we get the contradiction $1 \leq \frac{1}{2}$.

C. Gleason's Theorem

The discrepancy between quantum mechanics and local hidden-variable theories can be understood in another way by employing a theorem due to Gleason (G57).* Gleason's theorem was considered by Bell (B66), who pointed out that it limits the form of any hidden-variable theory that is to agree with the statistical predictions of quantum mechanics.†

Consider a system whose quantum-mechanical description is associated with a Hilbert space on which there are at least three non-trivial observables (hermitian operators) A, B, and C, having the

---

* Similar conclusions can be made from a different theorem proved by Jauch and Piron (JP63). See also Ref. B66.

† For discussions of Gleason's theorem in the present context, see Refs. B72, H70, S70.

0 0 0 0 3 7 0 2 1 8 2

following commutation properties: $[A, B] = 0$; $[A, C] = 0$; and $[B, C] \neq 0$. According to Gleason's theorem, there exists no single deterministic function which can be used to represent the measurement corresponding to the operator A. In order to construct a theory which describes measurements as deterministic functions of hidden variables, one must specify the other observable (whether B or C) which could have been measured along with A. Thus, Gleason's theorem requires that all hidden-variable theories be contextual, i.e., the results of a given measurement can be predicted only in the context of other measurements that could be made at the same time.

For a spin measurement on a single spin-½ particle, Gleason's theorem does not apply. The Hilbert space for this system is two-dimensional, and there aren't three hermitian operators (excluding the identity operator) satisfying the required commutation relations. Furthermore, Bell (B66) has constructed an example of a hidden-variable theory describing spin measurements on a spin-½ particle. This theory is not contextual, yet it agrees with quantum mechanics.

For systems consisting of two spin-½ particles, the appropriate Hilbert space is four-dimensional, and Gleason's theorem does apply. However, the theory discussed in the previous section was not contextual. In fact, in a contextual hidden-variable theory for this system, the correlation function is given by Eq. I.4. In order to define a measurement function for one particle, it is necessary to specify the component of the other particle's spin that could be measured at the same time.

The condition of locality has been used to avoid making the theory contextual. But, by Gleason's theorem, the resulting non-contextual hidden-variable theory must be inconsistent with quantum mechanics. This fact is confirmed by application of Bell's inequality.

These considerations point out an essential difference between quantum-mechanical and local hidden-variable descriptions. In quantum mechanics, a multiparticle state is represented by a single vector in a Hilbert space; the individual states of the component particles are not specified in this framework. On the other hand, in a local hidden-variable theory, the component particles are always in well-defined states. Thus it is not surprising that a discrepancy appears when one considers systems like the singlet state of two spin-½ particles, because, for this system, the two views are clearly inconsistent.

D. The Ideal Two-Photon System

The system that is investigated in this experiment consists of two distinguishable photons, γ_1 and γ_2, emitted in an atomic cascade. To a good approximation, the atom cascades via electric dipole transitions through angular-momentum states $J = 0 \rightarrow J = 1 \rightarrow J = 0$. The following heuristic argument (H70) is sufficient to determine the resulting quantum-mechanical two-photon state in the ideal case, in which the photons travel in opposite directions along the z axis.

The initial and final atomic angular momentum is zero; hence, by conservation of angular momentum, the two photons are in a combined state of angular momentum zero. The most general state of this kind is

$$|\gamma_1\gamma_2\rangle = a|R_+\rangle_1|L_+\rangle_2 + b|L_+\rangle_1|R_+\rangle_2 + c|R_-\rangle_1|L_-\rangle_2 + d|L_-\rangle_1|R_-\rangle_2$$
$$+ e|R_+\rangle_1|R_-\rangle_2 + f|L_+\rangle_1|L_-\rangle_2 + g|R_-\rangle_1|R_+\rangle_2 + h|L_-\rangle_1|L_+\rangle_2 ,$$

where $|R_+\rangle_1$ is the eigenstate of a right-hand circularly polarized photon traveling along the +z axis. The subscripts label the photons, which are distinguishable by their energies.

Since the parities of the initial and final atomic states are the same, the parity of the two-photon state must be even. This implies that a = d, b = c, e = h, and f = g.

The initial state (atom alone, J = 0) is invariant under rotations by 180° about the x axis. The portion of the final state which refers to the atom is similarly invariant; hence the two-photon state must also be invariant. This implies that a = b and e = f.

Finally, if we require that γ_1 move along the +z axis and γ_2 move along the -z axis, we have

$$|\gamma_1\gamma_2\rangle = \frac{1}{\sqrt{2}}\left(|R_+\rangle_1|R_-\rangle_2 + |L_+\rangle_1|L_-\rangle_2\right) ,$$

where the remaining constant has been set equal to $1/\sqrt{2}$ for proper normalization.

Transforming to a linear-polarization basis, and picking a separate right-handed coordinate system for each photon (the z axis of each system points in the direction of the photon's motion and the x and y axes are parallel), we have

$$|\gamma_1\gamma_2\rangle = \frac{1}{\sqrt{2}}\left(|x\rangle_1|x\rangle_2 - |y\rangle_1|y\rangle_2\right) .$$

This state is clearly analogous to the singlet state of two electrons. As with the singlet state, the eigenstate of one particle can be inferred from a measurement made on the other particle.

In a representation that exploits the binary character of photon polarization, we have

$$|\gamma_1\gamma_2\rangle = \frac{1}{\sqrt{2}}\left[\begin{pmatrix}1\\0\end{pmatrix}_1\begin{pmatrix}1\\0\end{pmatrix}_2 - \begin{pmatrix}0\\1\end{pmatrix}_1\begin{pmatrix}0\\1\end{pmatrix}_2\right] . \qquad (I.7)$$

In this representation a measurement of a photon's linear polarization in an arbitrary direction perpendicular to the z axis is associated with a hermitian operator of the form

$$O_i(\phi_i) = \begin{bmatrix}\cos 2\phi_i & \sin 2\phi_i\\ \sin 2\phi_i & -\cos 2\phi_i\end{bmatrix} . \qquad (I.8)$$

The expectation value for joint polarization measurements is

$$E(\phi) = \langle\gamma_1\gamma_2|O_1(\phi_1)\ O_2(\phi_2)|\gamma_1\gamma_2\rangle = \cos 2\phi\ , \qquad (I.9)$$

where ϕ is the angle between the polarizers.

The local hidden-variable restriction for the two-photon system is obtained by replacing Eq. I.5 by the condition

$$A(\hat{a},\ \lambda) = B(\hat{a},\ \lambda)\ .$$

The resulting inequality is

$$|P(\alpha) - P(\alpha + \beta)| \leq 1 - P(\beta)\ ,$$

where α and β are defined as before (Sect. I.B). The quantum-mechanical

0 0 0 0 3 7 0 2 1 8 4

expectation value, Eq. I.9, violates this restriction (for example, when $\alpha = \beta = 30°$).

E. Other Experiments

There are few examples of two-particle correlations which can provide a decisive test between local hidden-variable theories and quantum mechanics. A practical experiment requires a suitable method of preparation of correlated states and adequate measuring devices. Of course, to be a test, the quantum-mechanical predictions must violate the local hidden-variable restrictions.

The possibility of an experimental test using spin-½ particles (Bohm's Gedankenexperiment) is slight.* Presumably, Stern-Gerlach magnets could be used as measuring devices, but the difficulty of directing particles into these devices would severely limit the count rate. Magnetic fields could not be employed to direct the particle, because they would also cause the spins to precess. Scattering asymmetries provide another method of inferring spin, but this is too insensitive for a decisive test. If the measuring devices are not strongly correlated with the individual particle spins, the observed spin-spin correlation between the particles is weakened, and the quantum-mechanical predictions will no longer violate the inequality.

The state of the two 0.5-MeV γ-rays resulting from positronium

---

* For discussions of some relevant correlations and other experimental possibilities, see Refs. PS60, D61, I61, F71.

annihilation is analogous to the state prepared in this experiment. Experimental verification of the quantum-mechanical predictions for this system was first proposed by Wheeler (W46). The experiment has been performed by many groups (H48, BB48, VD49, WS50, H51, BBL55). The first precise measurement was made by Wu and Shaknov in 1950. Although there were some slight discrepancies in some of the early experiments, the results are generally in good agreement with quantum mechanics.

Efficient polarizers are not available for the 0.5-MeV gamma rays, so the polarizations are inferred from the azimuthal asymmetry of Compton scattering (the Klien-Nishina formula). Thus, this experiment examines the polarization-dependent joint distribution for Compton scattering. It has been shown by Horne that exact verification of the quantum-mechanical predictions cannot provide evidence against local hidden-variable theories (H70).

Langhoff (L60) and Kasday, Ullman, and Wu (KUW70) have repeated the experiment with greater precision. These experiments include measurements of the polarization correlation at intermediate angles between 0° and 90°. The results of these experiments are in excellent agreement with quantum mechanics. By applying additional assumptions concerning the nature of Compton scattering, Kasday et al. have shown that their data can be scaled so that they violate the restrictions of local hidden-variable theories (presumably, Langhoff's data can be similarly scaled). However, specific local hidden-variable theories have been constructed that can explain this violation and the agreement with quantum mechanics (see Ref. K70).

0 0 0 0 3 7 0 2 1 8 5

In the Kocher-Commins experiment, the polarization correlation for optical photons from the same cascade studied here was observed at 0° and 90° only. It will be seen (Sect. II) that observations at intermediate angles are required to test local hidden-variables. In addition, the polarizers (polaroid sheet) were not efficient enough for a decisive test.* Their result for the ratio of the photon coincidence rate with polarizers perpendicular to the rate with polarizers parallel is consistent with the quantum-mechanical prediction.†

F. Outline of the Experiment

The experimental scheme is an extension of the one used by Kocher and Commins (KC67). The basic idea is simple: Photons emitted in an atomic cascade are counted in coincidence, the coincidence rate being observed as a function of the individual photon polarization states.

A schematic diagram of the experimental apparatus is shown in Fig. 1. A beam of calcium atoms intersects the filtered output of a

---

* It has been suggested that, with additional assumptions, the requirement for highly efficient polarizers can be relaxed (FR71). Although these assumptions are somewhat weaker than those used by Kasday et al. (K70), they are unnecessary, since adequate polarizers can be obtained.

† The positron annihilation experiment and the Kocher-Commins experiment are sufficient to rule out another proposed solution to the measurement problem pointed out by Einstein et al. (EPR35). This solution was suggested by Furry (F36) and discussed by Bohm and Aharonov (BA57), who pointed out that the data from the experiment of Wu and Shaknov (WS50) rules out the Furry hypothesis. Using his own data, Kocher (K67a) came to similar conclusions.

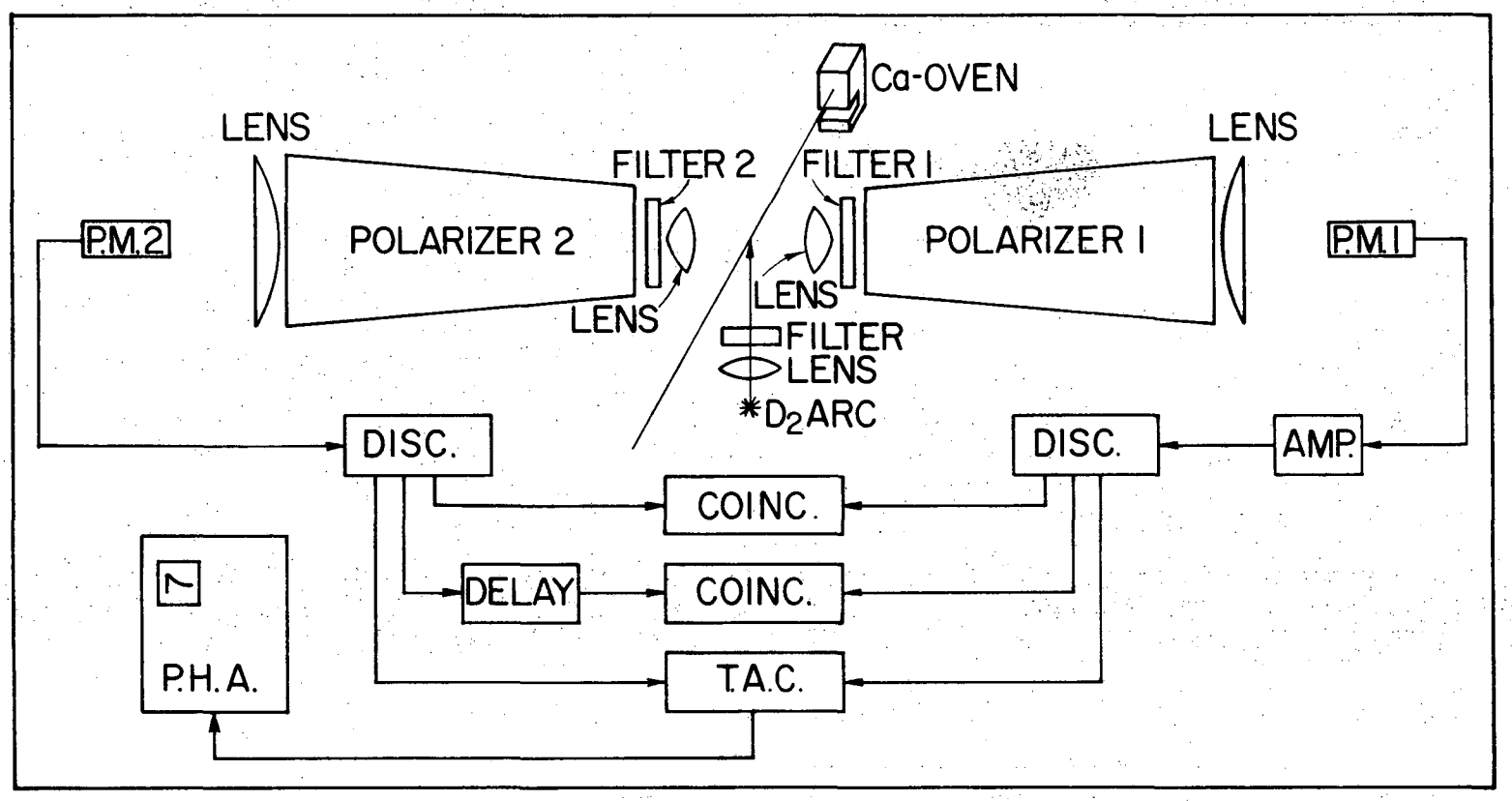

XBL 7112-1792

Fig. 1. Schematic diagram of the apparatus and associated counting electronics. Scalers (not shown) monitor the outputs of the discriminators and coincidence modules.

0 0 0 0 3 7 0 2 1 8 6

deuterium arc lamp. The lamp filter passes photons with energies corresponding to the upper resonance states of calcium. The dominant excitation mode proceeds by resonance excitation to the $3d4p\,^1P_1$ state (see Fig. 2). Some of the excited atoms decay to the $4p^2\ ^1S_0$ state and then cascade to the ground state with the emission of two photons: γ_1 at 5513 Å and γ_2 4227 Å.

Naturally-occurring calcium atoms are virtually all isotopes having nuclear spin zero (99.855% spin zero, LHP67). Hence, for nearly all the atoms, the angular momentum of each state of the cascade is given by the total electronic angular momentum J.

The interaction region is viewed by two symmetrically placed detector systems, each consisting of two lenses, a wavelength filter, a rotatable and removable linear polarizer, and a photon detector.

In each detector system, photons of one type (either γ_1 or γ_2) are selected by an interference filter and formed into a nearly parallel beam by the first lens. The polarization states of the photons are analyzed by highly efficient pile-of-plates polarizers. The photons which pass through a polarizer are focused by the second lens onto the face of a photomultiplier, which is used as a single-photon detector.

Photons γ_1 and γ_2 are counted in coincidence in order to insure that they came from the same decaying calcium atom. The following quantities are measured:

$R(\phi)$: the coincidence rate for two-photon detection as a function of the angle ϕ between the planes of linear polarization defined by the orientation of the two inserted polarizers;

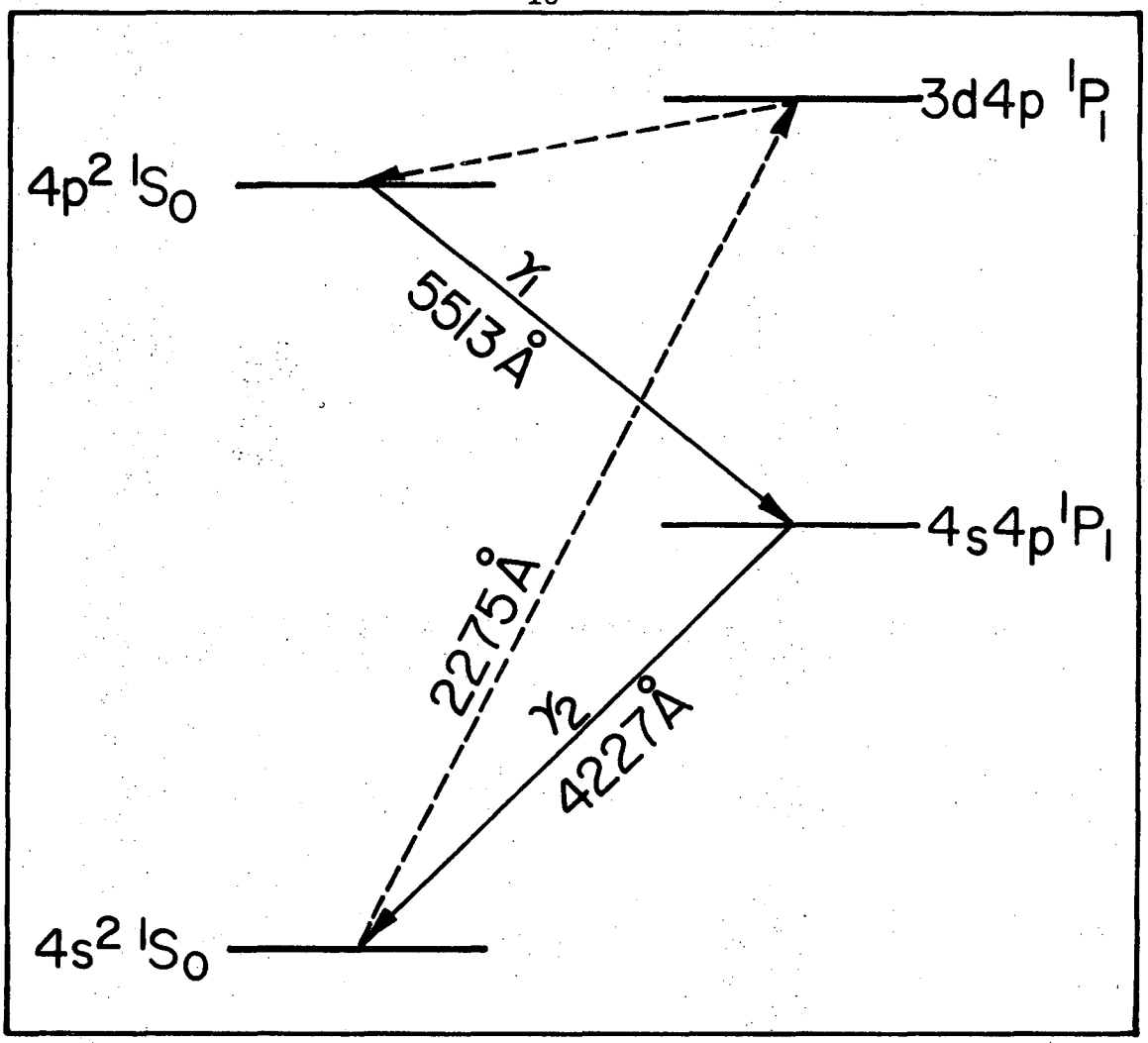

XBL 723-517

Fig. 2. Level scheme of calcium showing the observed cascade and the dominant excitation mode.

0 0 0 0 3 7 0 : 1 8 7

R_1: the coincidence rate with polarizer 2 removed;

R_2: the coincidence rate with polarizer 1 removed;

R_o: the coincidence rate with both polarizers removed.

These rates are determined by correcting the observed coincidence rates for the random coincidence background (accidental-coincidence rate). The quantum-mechanical predictions for the measured rates will be seen to violate the restrictions imposed by local hidden-variable theories.

In addition to ordinary coincidence counting, a time delay-coincidence system provides a spectrum of the arrival time difference between γ_1 and γ_2. This gives the lifetime of the $4s4p\,^1P_1$ state and provides a check on the consistency of the experiment.

II. THEORY

A. Generalization of Bell's Inequality

In this section we will prove the generalization of Bell's inequality. This discussion follows the notation and style of a recent proof by Bell (B70). For other methods of proving the generalized inequality, see Refs. H70, B72, W70, and CHSH69.

As before, we consider an ensemble of particle pairs and two spatially separated measuring devices. The particles from each pair move so that one enters device 1 and the other device 2. Each device performs a measurement that can have one of two possible outcomes. We assume that the result of each measurement is determined by the value of a hidden variable λ, corresponding to the particular particle pair, and carried along by each of the particles. The ensemble is associated with distribution function $\rho(\lambda)$, which gives the probability that a particular pair has a given value of λ. $\rho(\lambda)$ satisfies the normalization condition

$$\int_{\Gamma} \rho(\lambda) d\lambda = 1 \ , \qquad \text{(II.1)}$$

where Γ is the space of hidden variables. Let the functions $A(\hat{a}, \lambda)$ and $B(\hat{b}, \lambda)$ take on the values +1 and -1, corresponding to the two possible results of a measurement on each particle; $\hat{a}$ and $\hat{b}$ are adjustable parameters of measuring devices 1 and 2, respectively.

We define the correlation function:

$$P(\hat{a}, \hat{b}) = \int \rho(\lambda)\ A(\hat{a}, \lambda)\ B(\hat{b}, \lambda) d\lambda \ . \qquad \text{(II.2)}$$

It should be emphasized that a strong but plausible locality condition is implicit in this definition: the result of each measurement does not depend upon the parameters of the other measuring device.

One could be more general by presuming the existence of additional hidden variables, residing in the measuring devices and affecting the outcome of measurements. In this case, the correlation function is given by the more general expression

$$\tilde{P}(\hat{a}, \hat{b}) = \int \rho(\lambda)\ \rho_1(\lambda_1)\ \rho_2(\lambda_2)\ A(\hat{a}, \lambda, \lambda_1)\ B(\hat{b}, \lambda, \lambda_2) d\lambda d\lambda_1 d\lambda_2 \quad \text{(II.3)}$$

where $\rho_1(\lambda_1)$ and $\rho_2(\lambda_2)$ are additional normalized distribution functions. It is easy to see, however, that Eq. II.3 can be recast in the form of Eq. II.2 without loss of generality.* Thus, the following discussion includes the possibility of hidden variables in the measuring devices even though the Eq. II.2 is used to define the correlation function.

Considering the four sets of measurement parameters $\hat{a}$, $\hat{b}$, $\hat{c}$, and $\hat{d}$, we have

---

* This is a formal transformation and does not mean that λ need be correlated with λ_1 and λ_2. One could just as well perform the λ_1- and λ_2-integrals first and define new functions $\tilde{A}(\hat{a}, \lambda) = \int \rho_1(\lambda_1) A(\hat{a}, \lambda, \lambda_1) d\lambda_1$ and $\tilde{B}(\hat{b}, \lambda) = \int \rho_2(\lambda_2) B(\hat{b}, \lambda, \lambda_2) d\lambda_2$. Then we have $|\tilde{A}(\hat{a}, \lambda)| \leq 1$ and $|\tilde{B}(\hat{b}, \lambda)| \leq 1$; these conditions are sufficient to derive the desired restriction (see Ref. B70).

$$|P(\hat{a}, \hat{b}) - P(\hat{a}, \hat{c})| = \left|\int \rho(\lambda) A(\hat{a}, \lambda) B(\hat{b}, \lambda) d\lambda - \int \rho(\lambda) A(\hat{a}, \lambda) B(\hat{c}, \lambda) d\lambda\right|$$

$$= \left|\int \rho(\lambda) A(\hat{a}, \lambda) B(\hat{b}, \lambda) [1 \pm A(\hat{d}, \lambda) B(\hat{c}, \lambda)] d\lambda \right.$$

$$\left. - \int \rho(\lambda) A(\hat{a}, \lambda) B(\hat{c}, \lambda) [1 \pm A(\hat{d}, \lambda) B(\hat{b}, \lambda)] d\lambda \right|$$

$$\leq \int \rho(\lambda) |A(\hat{a}, \lambda) B(\hat{b}, \lambda)| \; |[1 \pm A(\hat{d}, \lambda) B(\hat{c}, \lambda)]|$$

$$+ \int \rho(\lambda) |A(\hat{a}, \lambda) B(\hat{c}, \lambda)| \; |[1 \pm A(\hat{d}, \lambda) B(\hat{b}, \lambda)]| \; ;$$

hence

$$|P(\hat{a}, \hat{b}) - P(\hat{a}, \hat{c})| \leq 2 \int \rho(\lambda) d\lambda \pm \left(\int \rho(\lambda) A(\hat{d}, \lambda) B(\hat{c}, \lambda) \right.$$

$$\left. + \int \rho(\lambda) A(\hat{d}, \lambda) B(\hat{b}, \lambda) d\lambda \right)$$

and finally,

$$|P(\hat{a}, \hat{b}) - P(\hat{a}, \hat{c})| \leq 2 \pm [P(\hat{d}, \hat{c}) + P(\hat{d}, \hat{b})] \; .$$

This inequality can be written as two inequalities:

$$-2 \leq P(\hat{a}, \hat{b}) - P(\hat{a}, \hat{c}) + P(\hat{d}, \hat{c}) + P(\hat{d}, \hat{b}) \leq 2 \; . \qquad \text{(II.4)}$$

Inequalities II.4 are very general; in particular, the source of the particle pairs and the exact nature of the measurements have not been specified.

To test inequalities II.4 one must investigate a physical situation in which the locality condition can be expected to hold. Then a violation of inequalities II.4 by the experimentally determined correlation function rules out local hidden variables. One must choose an experiment in which the quantum-mechanical expectation value corre-

sponding to the correlation function violates the inequalities. A belief in local hidden variables would lead one to expect a breakdown of quantum mechanics for this situation.

For both idealized measurements considered in the Introduction, the quantum-mechanical expectation values (Eqs. I.2 and I.7) violate inequalities II.4 for suitably chosen measurement directions.

B. Application of the Generalized Inequality to the Present Experiment

In the present experiment, the particle pairs are pairs of photons emitted in a $0 \rightarrow 1 \rightarrow 0$ atomic cascade; the measuring devices each consist of a linear polarizer and a photomultiplier tube, and the adjustable parameter of each measuring device is the orientation of the polarizer about the z axis.

It would be natural to associate the results of a measurement on each photon with passage in either the ordinary ray or the extraordinary ray of the polarizer, but in any real polarizer some photons are not transmitted in either ray because of scattering losses or absorption. Thus, there are three possible results for a measurement, apparently violating the condition that measurements be two-valued. However, we are free to associate +1 with the transmission in the ordinary ray and -1 with nontransmission in the ordinary ray (regardless of the reason). This interpretation makes the measurements two-valued and has the practical advantage of making it unnecessary to detect photons in the extraordinary ray.

In order to express inequalities II.4 in terms of quantities

directly measured, it is convenient to introduce the following partition of Γ,

$$\Gamma_{ij}(\hat{a}, \hat{b}) = \{\lambda | A(\hat{a}, \lambda) = i \text{ and } B(\hat{b}, \lambda) = j\} ,$$

where i and j equal +1 or -1. Using this partition, we define the following quantities:

$$P_{ij}(\hat{a}, \hat{b}) = \int_{\Gamma_{ij}(\hat{a}, \hat{b})} \rho(\lambda) d\lambda .$$

$P_{++}(\hat{a}, \hat{b})$ is the probability of joint passage of the photons through the polarizers.

Using the definition of the correlation function (Eq. II.2) and the normalization condition on $\rho(\lambda)$ (Eq. II.1), we have

$$P(\hat{a}, \hat{b}) = P_{++}(\hat{a}, \hat{b}) - P_{+-}(\hat{a}, \hat{b}) - P_{-+}(\hat{a}, \hat{b}) + P_{--}(\hat{a}, \hat{b})$$

and

$$1 = P_{++}(\hat{a}, \hat{b}) + P_{+-}(\hat{a}, \hat{b}) + P_{-+}(\hat{a}, \hat{b}) + P_{--}(\hat{a}, \hat{b}) .$$

It is convenient to define the additional quantities

$$P_1(\hat{a}) = P_{++}(\hat{a}, \hat{b}) + P_{+-}(\hat{a}, \hat{b})$$

and

$$P_2(\hat{b}) = P_{++}(\hat{a}, \hat{b}) + P_{-+}(\hat{a}, \hat{b}) .$$

$P_1(\hat{a})$ and $P_2(\hat{b})$ are the probabilities of joint passage when one of the polarizers is absent.

Expressing the correlation function in terms of the probabil-

0 0 0 0 3 7 0 2 1 8 9

ities of joint passage, we have

$$P(\hat{a}, \hat{b}) = 4P_{++}(\hat{a}, \hat{b}) - 2P_1(\hat{a}) - 2P_2(\hat{b}) + 1 . \qquad \text{(II.5)}$$

On substitution of Eq. II.5 into inequalities II.4, we obtain

$$-1 \leq P_{++}(\hat{a}, \hat{b}) - P_{++}(\hat{a}, \hat{c}) + P_{++}(\hat{d}, \hat{c}) + P_{++}(\hat{d}, \hat{b}) - P_2(\hat{b}) - P_1(\hat{d}) \leq 0. \qquad \text{(II.6)}$$

Inequalities II.6 are obtained entirely within the framework of local hidden-variable theories.

If all transmitted photons were detected, we would have

$$P_{++}(\hat{a}, \hat{b}) = \frac{R(\hat{a}, \hat{b})}{R_o} , \qquad \text{(II.7a)}$$

$$P_1(\hat{a}) = \frac{R_1(\hat{a})}{R_o} , \qquad \text{(II.7b)}$$

and

$$P_2(\hat{b}) = \frac{R_2(\hat{b})}{R_o} , \qquad \text{(II.7c)}$$

where $R(\hat{a}, \hat{b})$, $R_1(\hat{a})$, $R_2(\hat{b})$, and R_o are the coincidence count rates (see Sect. I.F).

In the present experiment the detectors are not perfectly efficient (the efficiencies of the detectors are less than 30%), so all transmitted photons are not detected, and using Eq. II.7a-c to relate the probabilities of joint passage to the experimental count rates involves an additional assumption. We therefore assume that the detection probability for a photon is independent of whether or not the photon has

passed through a polarizer.*

Since for the present experiment $R_1(\hat{a})$ and $R_2(\hat{b})$ are independent of $\hat{a}$ and $\hat{b}$, and $R(\hat{a}, \hat{b})$ depends only on $\hat{a}\cdot\hat{b}$,† we have

$$-1 \leq \frac{R(\phi_1)}{R_o} - \frac{R(\phi_1 + \phi_2 + \phi_3)}{R_o} + \frac{R(\phi_2)}{R_o} + \frac{R(\phi_3)}{R_o} - \frac{R_1}{R_o} - \frac{R_2}{R_o} \leq 0, \quad \text{(II.8)}$$

where

$$\phi_1 = \cos^{-1}(\hat{a}\cdot\hat{b}) ,$$

$$\phi_2 = \cos^{-1}(\hat{d}\cdot\hat{c}) ,$$

$$\phi_3 = \cos^{-1}(\hat{d}\cdot\hat{b}) ,$$

and $$\phi_1 + \phi_2 + \phi_3 = \cos^{-1}(\hat{a}\cdot\hat{c}) .$$

Inequalities II.8 refer directly to the measured coincidence rates.

C. Quantum-Mechanical Predictions

In Section I.D the quantum-mechanical expectation value is calculated for the ideal case, in which the photons travel in opposite directions along the z axis and the polarizers are perfect. In this

---

* This assumption has been stated somewhat more strongly than necessary. In particular, a very special dependence is required in order that a violation of inequalities II.8 occur within the framework of local hidden-variable theories.

† These conditions are not required in a hidden-variable theory, but they are required by quantum mechanics. A slight systematic variation in R_1 and R_2 with angle would be expected if there were asymmetries in the interaction region (see Sect. III.B.5 and Appendix A). However, no deviation from angular independence is observed, and $R(\hat{a}, \hat{b})$ is found to depend only on $\hat{a}\cdot\hat{b}$.

0 0 0 0 3 7 0 2 1 9 0

section we consider a more realistic situation, in which the polarizers are imperfect and the detectors have finite solid angles.

First we consider the effect of imperfect polarizers, but retain the idealization of infinitesimal detector solid angles. In the representation in which Eq. I.7 is written, the operator

$$\pi_i = \begin{bmatrix} \epsilon_M^i & 0 \\ 0 & \epsilon_m^i \end{bmatrix}$$

represents the observation of transmission or nontransmission of a photon through a polarizer with polarization axis in the x direction ($\epsilon_M^i > \epsilon_m^i$). Transforming π_i by a rotation by ϕ_i about the z axis, we obtain the operator for arbitrary polarizer orientation:

$$\pi_i(\phi_i) = \begin{bmatrix} \tfrac{1}{2}(\epsilon_M^i + \epsilon_m^i) + \tfrac{1}{2}(\epsilon_M^i - \epsilon_m^i)\cos 2\phi_i & \tfrac{1}{2}(\epsilon_M^i - \epsilon_m^i)\sin 2\phi_i \\ \tfrac{1}{2}(\epsilon_M^i - \epsilon_m^i)\sin 2\phi_i & \tfrac{1}{2}(\epsilon_M^i + \epsilon_m^i) - \tfrac{1}{2}(\epsilon_M^i - \epsilon_m^i)\cos 2\phi_i \end{bmatrix}$$

(recall that ϕ_1 and ϕ_2 are defined in different right-handed coordinate frames).

In quantum mechanics, the matrix element that gives the probability that both photons are transmitted is

$$\frac{R(\phi)}{R_o} = \langle \gamma_1\gamma_2 | \pi_1(\phi_1)\ \pi_2(\phi_2) | \gamma_1\gamma_2 \rangle \ . \qquad \text{(II.9)}$$

In the present representation, $|\gamma_1\gamma_2\rangle$ is given by Eq. I.7, and Eq. II.9 is easy to evaluate; we have

$$\frac{R(\phi)}{R_o} = \tfrac{1}{4}(\varepsilon_M^1 + \varepsilon_m^1)(\varepsilon_M^2 + \varepsilon_m^2) + \tfrac{1}{4}(\varepsilon_M^1 - \varepsilon_m^1)(\varepsilon_M^2 - \varepsilon_m^2)\cos 2\phi \ , \quad \text{(II.10)}$$

where ϕ is the angle between the polarizer axes.

Similarly, we have

$$\frac{R_1'}{R_o} = \langle \gamma_1\gamma_2 | \pi_1(\phi_1) | \gamma_1\gamma_2 \rangle = \tfrac{1}{2}(\varepsilon_M^1 + \varepsilon_m^1) \quad \text{(II.11a)}$$

and

$$\frac{R_2}{R_o} = \langle \gamma_1\gamma_2 | \pi_2(\phi_2) | \gamma_1\gamma_2 \rangle = \tfrac{1}{2}(\varepsilon_M^2 + \varepsilon_m^2) \ . \quad \text{(II.11b)}$$

Because the detectors have finite solid angles, the coincident photons are not, in general, colinear. For this general case the two-photon state vector that replaces Eq. I.7 is constructed by coupling the eigenstates of total angular momentum of each photon. These eigenstates are themselves constructed by coupling eigenstates for the individual photons' orbital and spin (polarization) angular momentum. For colinear photons there is maximum correlation between the photon spins, but for noncolinear photons, the angular momentum contributes and the spin-spin correlation decreases.

The more general quantum-mechanical calculation for the joint passage probabilities is straightforward, but tedious. The calculation is done in detail by Horne (H70). Shimony (S70) has outlined a somewhat simpler derivation.

Clearly, even in the more general case, the predictions for R_1/R_o and R_2/R_o are given by Eqs. II.11a and II.11b.

The expression for $R(\phi)/R_o$ (Eq. II.10) is modified in the fol-

0 0 0 0 3 7 0 2 1 9 1

lowing way:

$$\frac{R(\phi)}{R_o} = \tfrac{1}{4}(\epsilon_M^1 + \epsilon_m^1)(\epsilon_M^2 + \epsilon_m^2) + \tfrac{1}{4}(\epsilon_M^1 - \epsilon_m^1)(\epsilon_M^2 - \epsilon_m^2)F_1(\Theta)\cos 2\phi \ , \quad \text{(II.12)}$$

where

$$F_1(\Theta) = \frac{(7 - 3\cos\Theta - 3\cos^2\Theta - \cos^3\Theta)^2}{12(8 - 16\cos\Theta + 9\cos^2\Theta - 2\cos^4\Theta + \cos^6\Theta)} \ , \quad \text{(II.13)}$$

and Θ is the half angle of the cone defining the detector solid angles (the detector solid angles are assumed equal). For infinitesimal solid angles $F_1(\Theta) = 1.0$; $F_1(\Theta)$ decreases monotonically with increasing Θ, slowly at first [$F_1(34°) = 0.98$] and then somewhat faster [$F_1(68°) = 0.80$]; see Ref. H70. For the detector solid angles in this experiment ($\Theta \approx 30°$), $F_1(\Theta)$ is 0.988. Thus, the effect of the finite detector solid angles in the present experiment changes the polarization correlation very little from the ideal case.

D. Requirements for a Decisive Test

Consider the function

$$\Delta(\phi_1, \phi_2, \phi_3) = \frac{R(\phi_1)}{R_o} - \frac{R(\phi_1 + \phi_2 + \phi_3)}{R_o} + \frac{R(\phi_2)}{R_o} + \frac{R(\phi_3)}{R_o} - \frac{R_1}{R_o} - \frac{R_2}{R_o} \ , \quad \text{(II.14)}$$

whose value is restricted by inequalities II.8.

Inserting the quantum-mechanical predictions into Eq. II.14 and differentiating with respect to each of the three angles, we obtain a

set of equations which gives the angles at which $\Delta(\phi_1, \phi_2, \phi_3)$ has maximum and minimum values. One finds that $\Delta(\phi_1, \phi_2, \phi_3)$ is maximum when $\phi_1 = \phi_2 = \phi_3 = 22\frac{1}{2}°$ and minimum when $\phi_1 = \phi_2 = \phi_3 = 67\frac{1}{2}°$. Since the maximum and minimum values occur when the three angles are equal, it is convenient to consider the function

$$\Delta(\phi) = \frac{3R(\phi)}{R_o} - \frac{R(3\phi)}{R_o} - \frac{R_1}{R_o} - \frac{R_2}{R_o} . \qquad \text{(II.15)}$$

The angle between the polarizer axes is, by definition, less than 90°, so we can combine the inequalities at maximum expected violation,

$$\frac{3R(22\frac{1}{2}°)}{R_o} - \frac{R(67\frac{1}{2}°)}{R_o} - \frac{R_1}{R_o} - \frac{R_2}{R_o} \leq 0$$

and

$$-1 \leq \frac{3R(67\frac{1}{2}°)}{R_o} - \frac{R(22\frac{1}{2}°)}{R_o} - \frac{R_1}{R_o} - \frac{R_2}{R_o} ,$$

into a simpler inequality that does not contain R_1/R_o and R_2/R_o. Thus we obtain $\delta \leq 0$, where

$$\delta = \frac{R(22\frac{1}{2}°)}{R_o} - \frac{R(67\frac{1}{2}°)}{R_o} - \frac{1}{4} . \qquad \text{(II.16)}$$

Inserting the quantum-mechanical prediction into Eq. II.16, we have

$$\delta = \frac{1}{2\sqrt{2}} (\varepsilon_M^1 - \varepsilon_m^1)(\varepsilon_M^2 - \varepsilon_m^2) F_1(\Theta) - \frac{1}{4} .$$

0 0 0 0 3 7 0 2 1 9 2

In order to insure that the quantum-mechanical predictions violate the local hidden-variable inequalities, the experiment must be designed so that

$$\frac{1}{2\sqrt{2}} (\epsilon_M^1 - \epsilon_m^1)(\epsilon_M^2 - \epsilon_m^2) F_1(\Theta) - \frac{1}{4} > 0 \ .$$

This requirement sets a maximum limit on the size of the detector solid angles and a minimum limit on the efficiencies of the polarizers. With perfect polarizers and infinitesimal solid angles, δ is predicted to be 0.104. For the present experiment, with the measured polarizer efficiencies (Table I) and with ~30° solid angles, δ is 0.051. Therefore, according to quantum mechanics, the polarization correlation measured in the present experiment is expected to violate the restrictions of local hidden-variable theories.

III. THE EXPERIMENTAL METHOD

A. Introductory Remarks: Design Criteria

Two-particle coincidence techniques are much more easily applied in nuclear physics than in atomic physics. The difficulty in the latter field is the generally low detection efficiencies for the low-energy particles encountered (E71). In particular, the best photomultipliers available for photon counting in the visible region have quantum efficiencies of less than 30%. Along with solid-angle losses, imperfect filter transmissions, and other losses, overall counter efficiencies of even a few tenths of a percent are difficult to obtain. This makes coincidence experiments especially difficult, as the count rate is proportional to the product of two efficiencies.

Another consideration in this experiment is the need for a high cascade-excitation rate. To the extent that the atomic beam is optically thin for excitation light, the cascade excitation rate N is proportional to the product of the atomic beam density n, the excitation lamp intensity I_o, and the volume V of the interaction region. Several excitation lamps were investigated in an attempt to maximize I_o.

Limitations on n are of a more fundamental nature. The second photon of the cascade corresponds to a resonance transition and is readily scattered by ground-state calcium atoms. This "trapping" of γ_2 photons is expected to lengthen the apparent lifetime of the intermediate state, and, to some extent, destroy the polarization correlation (B59a, B59b, B59c, DP65).

"Trapping" increases with beam density, and since lengthened

0 0 0 0 3 7 0 2 1 9 3

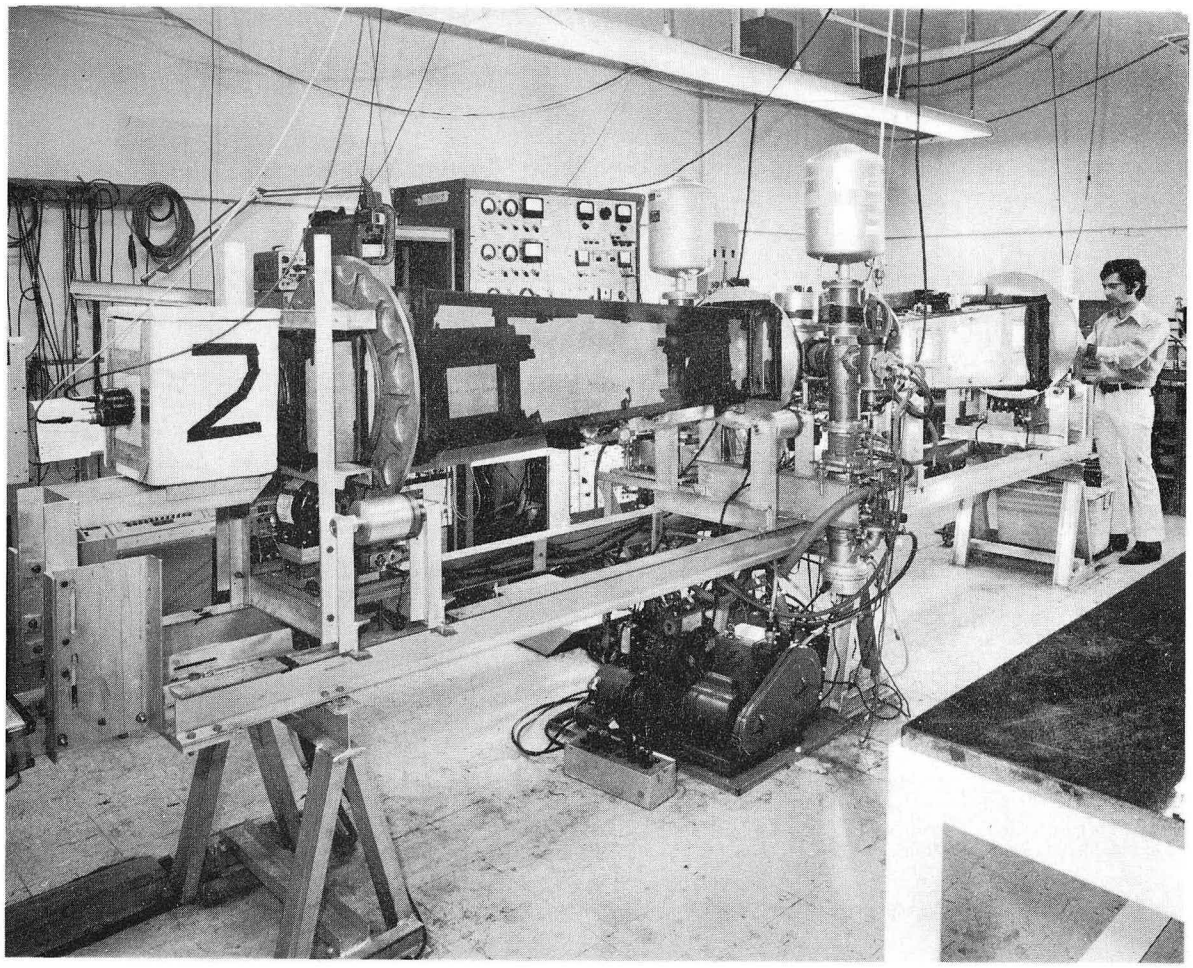

XBB 7112-5794

Fig. 3. Overall view of the apparatus. The distance between the detectors is about 5 meters.

lifetimes are observed at densities greater than ~10^{10} atoms/cm^3, the density is restricted to roughly this value for the final runs of the experiment.* It is found, however, that the effects of "trapping" on the polarization are slight even when significant lifetime lengthening is observed (see Sect. IV.A and Appendix C).

As an additional precaution against "trapping," the main chamber is designed so that the atomic beam intersects the axis of each detector optical system at 60° (see Fig. 5). The detector for γ_2 sees atoms which move relative to one another owing to the distribution of atom velocities in the beam. The Doppler-shifted photons emitted by these atoms have a lower probability of being rescattered than do the unshifted photons emitted perpendicular to the beam axis (for a discussion of this point see K67a).

The volume of the interaction region and the size of the detector optical systems are complementary considerations. The minimum linear dimension of the interaction region is determined by the size of the excitation light beam. Of course, this light could be collimated, but only at the expense of a decreased excitation rate. To utilize most of the excitation light, the interaction region must have a minimum dimension equal to the diameter of the light beam (roughly 4 mm). On the other hand, to minimize the divergence of light rays from the first lens of each detector optical system, the focal lengths of the lenses

---

* The amount of "trapping" also depends on the thickness of the interaction region, but it will be seen that this dimension is constrained by other considerations.

0 0 0 0 3 7 0 2 1 9 4

must be large compared to the maximum dimension of the interaction region. In addition, detector solid angles must be large or counter efficiencies will suffer, so larger-diameter lenses must be used. The upper limit on the detector solid angles discussed in Sect. II.D is not a real constraint. The maximum solid angles are determined by more practical considerations, such as the availability of large-diameter, high f-number lenses that are corrected for spherical aberrations (see Sect. III.B.4).

Large optical systems require that large linear polarizers be used. Furthermore, a decisive test of local hidden-variable theories requires that the polarizers be highly efficient. Neither polaroid sheet nor calcite prisms satisfies both these requirements, polaroid being too inefficient and calcite prisms being too small. This problem is solved by employing pile-of-plates-type polarizers which are specifically constructed to satisfy the requirements of this experiment.

Despite efforts to maximize the rate of data collection, the apparatus is designed with the expectation of long integration times. To facilitate this, data collection is automatic, and the apparatus runs without attendance.

Figure 3 shows an overall view of the apparatus.

B. Description of the Apparatus

1. Vacuum System

The vacuum system consists of an oven chamber and a main chamber connected by a narrow tube, as shown in Figs. 4 and 5. The system is

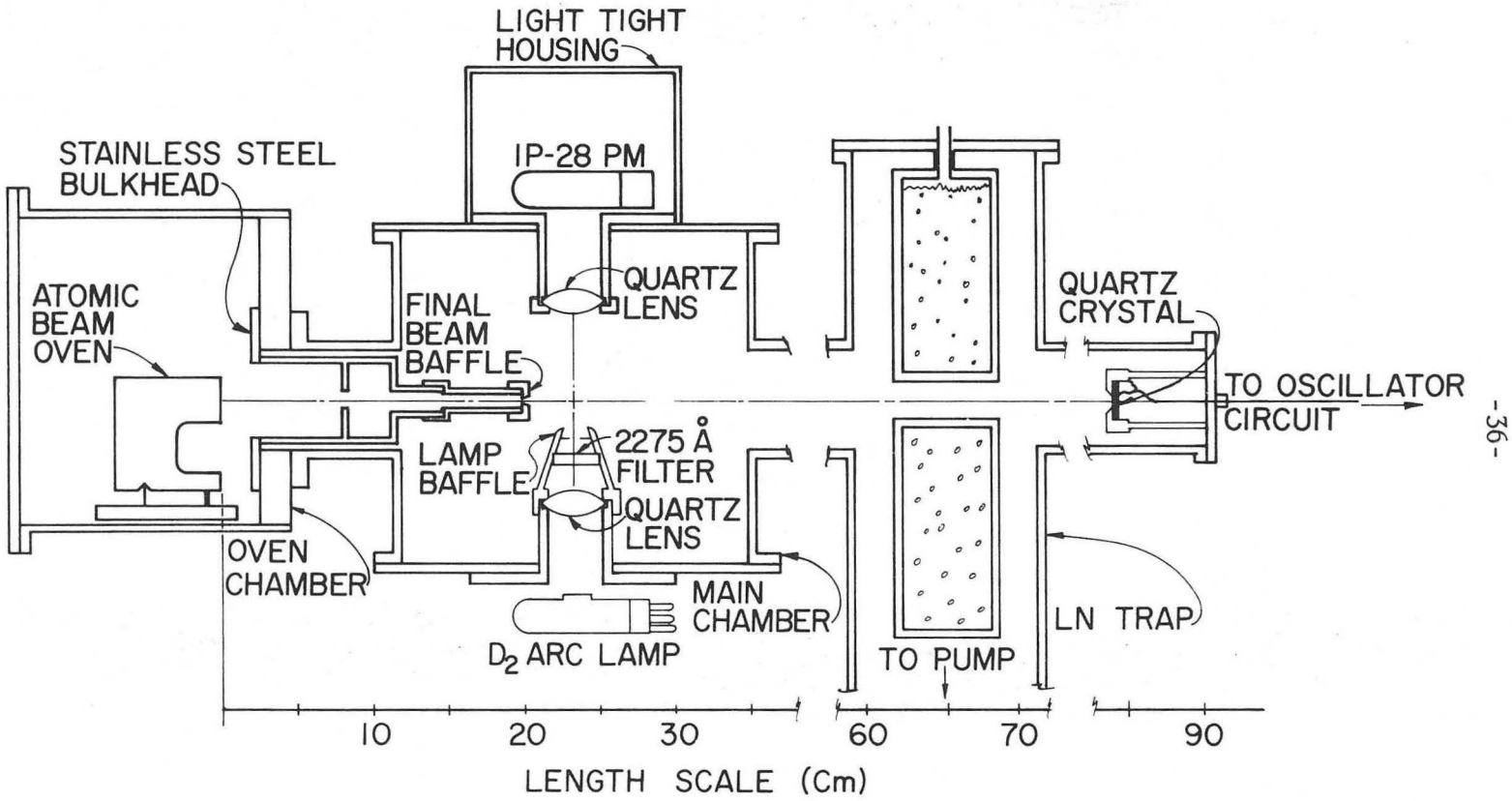

XBL 723-532

Fig. 4. Cross-sectional view of the vacuum system along the path of the atomic beam.

0 0 0 0 3 7 0 2 1 9 5

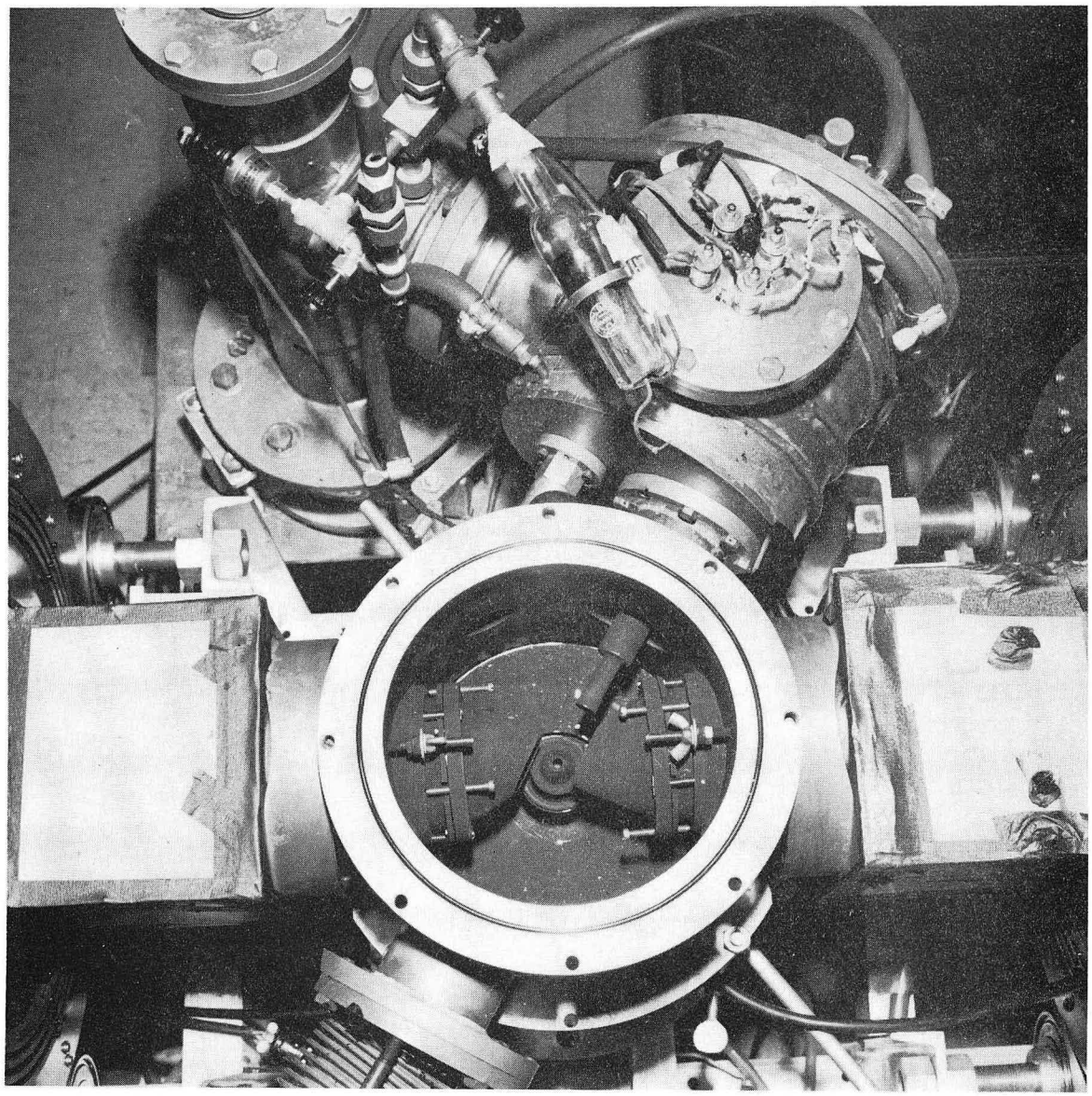

XBB 7112-5800

Fig. 5. The open main chamber, top view. The first lens of each detector optical system is held in each of the symmetrically-placed cone-shaped light baffles. The oven chamber is in the upper right-hand corner.

constructed of brass, and standard O-ring seals are used throughout. Mechanical motion of the atomic-beam cutoff flag is provided through a Wilson seal. An oil-diffusion pump and a liquid-nitrogen trap pump each chamber, and VG-1A vacuum gauges monitor the pressure.

The pressure during runs, $\lesssim 10^{-5}$ Torr, corresponds to a residual-gas density of $\lesssim 3\times10^{11}$ atoms/cm^3 and a calcium mean free path of $\gtrsim$20 m. The distance traveled by calcium atoms in the beam is less than 1 m, so this modestly low pressure is quite sufficient.

2. The Atomic Beam Oven and Beam Monitors*

The atomic beam oven is large, facilitating long runs (see Fig. 6). The oven is 7.0 cm long by 7.6 cm high by 3.8 cm wide, and is constructed of tantalum. A full charge consists of about 15 gm of calcium in the form of a rod 2.4 cm in diameter by 5 cm long. The calcium is originally of high purity (99.999%), but tends to absorb contaminants when stored. An initial premelting in vacuo eliminates these contaminants which would otherwise cause an unstable beam. A tapered plug seals the oven after the premelting precedure.

To reduce heat loss by conduction, the oven rests on a three-pin mount. The front heater coils are powered separately from the rear coils, allowing the front to be kept ~20°C warmer and thereby preventing condensation in the oven channel. The coils are wound from 0.5-mm

---

* Although highly reactive, calcium vapor can be sucessfully contained in cells constructed from single crystals of MgO (KOZ69). This method is a possible alternative to the use of an atomic beam in this experiment.

0 0 0 0 3 7 0 2 1 9 6

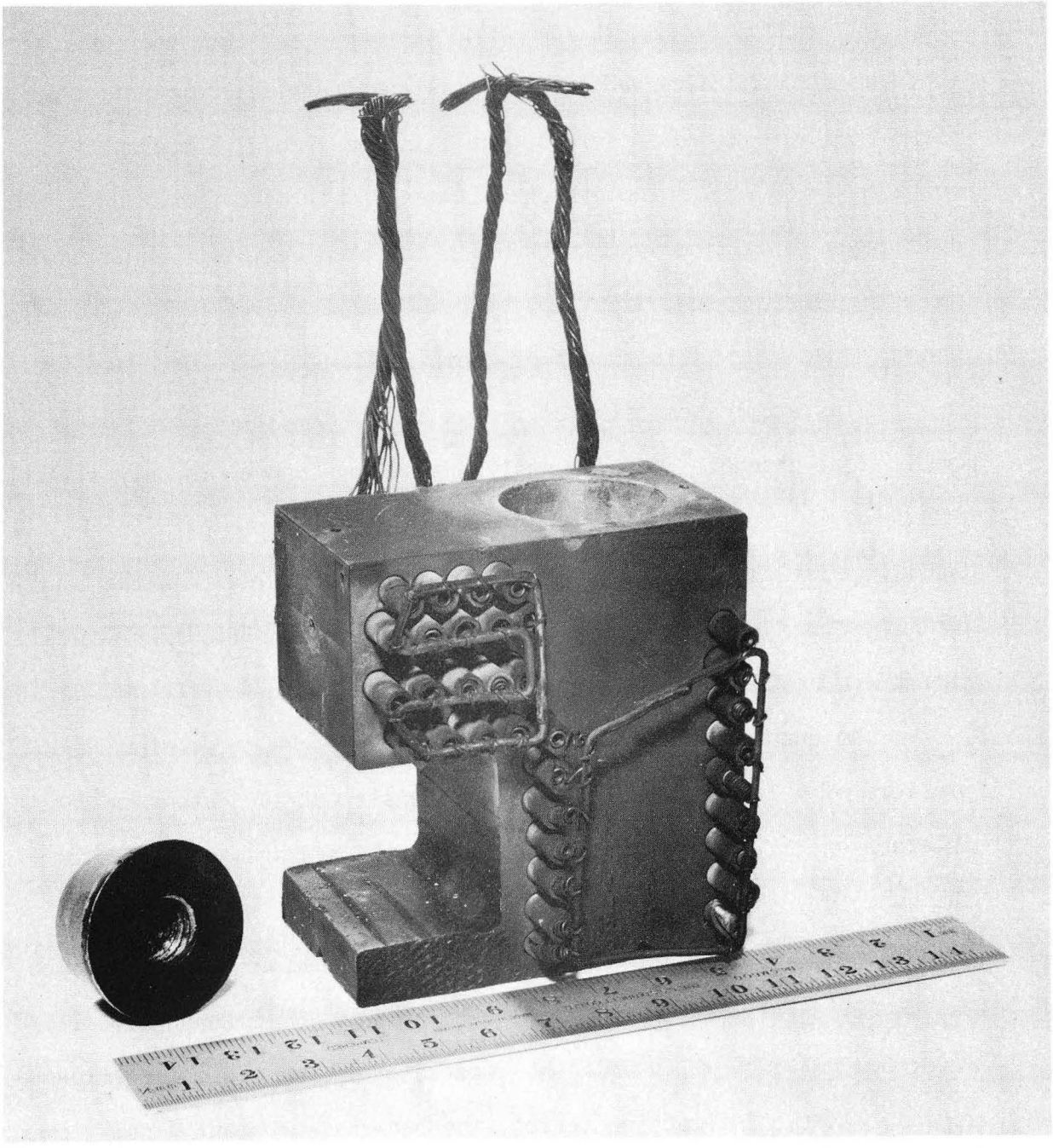

XBB 7112-5797

Fig. 6. The atomic beam oven and the oven plug. The small holes in the top of the oven are for thermocouples.

tantalum wire and arranged in low-resistance parallel combinations. At first they were wired in series, but this required high operating voltages (~150 VAC). These high voltages led to the formation of discharges in calcium vapor present in the oven chamber, resulting in undesirable background light. Step-down transformers provide the higher currents necessary with the lower operating voltages (~20 VAC).

The atomic beam effuses from a 3.5-cm long by 0.25-cm diameter cylindrical channel. Unfortunately, this long channel is only slightly effective in providing a directed beam. The mean free path in the oven during operation is about 0.3 cm; this is much smaller than the length of the channel, and is too small to satisfy the condition for well-channeled flow (R56, L67).

An oven temperature of 725°C corresponds to a calcium vapor pressure of 0.2 Torr (N63) and a beam density of 10^{10} atoms/cm^3 at the interaction region. At this temperature, the average speed of atoms in the beam, $\overline{v}_B$, is 8.5×10^4 cm/sec.

The cross-sectional dimensions of the beam at the interaction region are determined by the final beam baffle – a rectangular collimator 3.3 mm wide by 5.0 mm high, located 3 cm from the interaction region. At the interaction region, the beam has constant density over a 3.4- by 5.3-mm rectangle surrounded by a 0.38-mm wide penumbra region in which the density decreases to zero. Thus the nominal beam cross section is 3.8 by 5.7 mm FWHM. The beam width corresponds, approximately, to the diameter of the exciting light beam. The height is small enough for the interaction region to be within the detectors' field

0 0 0 0 3 7 0 2 1 9 7

of view; it is slightly larger than the width, to take advantage of a higher excitation rate due to increased interaction volume.

The beam density at the interaction region is inferred by three methods:

(1) After each run, a measurement of the calcium deposited on a stainless-steel bulkhead (shown in Fig. 4) gives an integrated measure of the beam density.* Runs are normally made at approximately constant beam density, so this method also gives an indication of the density at any time.

With an interaction-region beam density n that is constant for a run of length T, we have

$$n = \frac{D}{T} \frac{\ell^2 \rho}{L^2 \bar{v}_B m} \qquad \text{(III.1)}$$

where D = the deposit thickness in cm, ℓ = the distance from the oven to the stainless-steel bulkhead = 8.1 cm, L = the distance from the oven to the interaction region = 23.2 cm, m = the mass of calcium atoms = 6.62×10^{-23} gm, and ρ = the bulk density of calcium = 1.54 gm/cm^3. Neglecting the slight variation of $\bar{v}_B$ with oven temperature and using the value at 725°C, we obtain $n = 0.33\times10^{17}$ (D/T) atoms/cm^3. A run lasting 100 hr with $n = 10^{10}$ atoms/cm^3 gives an easily measurable deposit of ~1 mm. The accuracy of this method is limited by the difficulty in accounting for variations in beam density during a run

---

* This method was used by Kocher (K67a) who found that calcium adheres uniformly to #304 stainless steel.

and from errors in measuring the deposit thickness. The accuracy is ±20%.

(2) A deposition-thickness monitor provides a more continuous measure of the beam density. A quartz-crystal wafer* forms part of a resonance circuit oscillating at ~5 MHz; calcium depositing on the face of the crystal decreases the resonance frequency. The frequency shift is linearly proportional to the deposit thickness (WS63). A Hewlett Packard 524 electronic frequency counter measures the shift by sampling the frequency during alternate 10-sec periods. The system is calibrated in an evaporator by relating an observed frequency change ΔF to a known calcium thickness (the thickness being measured with an interferometer). The resulting calibration is consistent with calculations†: $\Delta F = 0.9d$, where d is the deposit thickness in Å.

The interaction region beam density in terms of the frequency shift is given by an expression similar to Eq. III.1; we obtain $n = 0.2\times10^{10}\ \Delta F'$ atoms/cm^3, where $\Delta F'$ is the change in frequency between successive samples. At the typical beam density, $\Delta F'$ is 5 Hz.

The sensitivities of this device to mechanical vibrations and vacuum contaminants severely limit its dependability. Reproducibility is also poor – perhaps owing to a dependence of the calcium sticking

---

* The quartz wafer is a standard 0.75×0.75×0.015" AT-cut Sloan crystal held in a water-cooled brass mount which exposes a 1-cm disk of the crystal.

† The Sloan manual (Technical Note T-1a) gives the approximate calibration $\Delta F \approx (\rho/2)d$, where ρ is the bulk density of calcium, yielding $\Delta F \approx 0.8d$.

0 0 0 0 3 7 0 2 1 9 8

fraction on the mass already deposited.* Despite these problems, this method is useful for making quick estimates (~50%) of the beam density.

(3) The ratio of the γ_2-singles rate N_2, corrected for the counting background B_2, to the intensity of the excitation lamp, I_o, provides a third measure of the beam density. The atomic beam is optically thin for 2275-Å radiation; hence $n = K(N_2 - B_2)/I_o$, where K is a constant dependent upon the geometry and excitation probability. The lamp intensity is monitored by a RCA-1P28 photomultiplier wired as a photodiode and mounted above the atomic beam as shown in Fig. 4. As a relative measure this method has an accuracy better than 1%, but the necessity of inferring K from other measurements (method 1) limits the absolute accuracy to ~20%.

3. Excitation Lamp

Investigations of the possibility of electron-bombardment excitation of the $4p^2\ ^1S_0$ state lead to conclusions similar to Kocher's (K67a). It is likely that the $4s4p\ ^1P_1$ excitation rate would be large compared to the $4p^2\ ^1S_0$ rate, resulting in a large background of γ_2 photons. However, electron excitation cross sections are difficult to estimate (MS68), and the possibility remains that the ratio of excitations may be acceptable – certainly a higher total excitation rate is to be expected. On the other hand, the use of electron-bombardment

---

* This effect has been observed for Zn, Cd, and Hg (MNSSG64); when the crystal is cooled to LN temperature, the sticking fraction approaches unity, but cooling introduces many complications (APJ70).

excitation presents many technical difficulties, so it was decided to use the indirect optical excitation method of Kocher and Commins (KC67).

An early attempt to build a radio-discharge calcium-flow lamp of the type described by Budick, Novick and Lurio (BNL65) was unsuccessful in producing a suitable excitation source. The lamp's output at 2275 Å was not competitive with the H_2-flow lamp designed by Kocher (K67b).

The use of continuum lamps in conjunction with interference filters as sources of atomic excitations is a standard technique (RCA67). The ultraviolet continuum generated by dischargesin H_2 is particularly well suited to this experiment, the spectral output being 100 times brighter at 2275 Å than at 4227 Å. The H_2 uv continuum extends from 1675 Å to 4500 Å; it arises from transitions between the stable $^3\Sigma_g^+$ molecular state and the lower repulsive $^3\Sigma_u^+$ state (C69). For reasons not well understood, the intensity is greater for deuterium than for hydrogen (LS61). Three types of discharge lamps were used in the course of this work: a lamp similar to the one designed by Kocher, and two commercial deuterium lamps.

The Kocher lamp is water cooled and constructed of brass. H_2 or D_2 pumped through it prevents cathode material from depositing on the exit window – a suprasil quartz lens, which also serves to focus the lamp output. A pressure of 3 Torr maintains the discharge. The intensity is increased by replacing Kocher's cylindrical cathode by a cone-shaped cathode of the same material – porous tungsten impregnated with Ca, Ba, and Al. The new cathode is 1.25 cm long with a maximum diameter of 0.75 cm (Spectromat Inc. design SK #691210); it operates with

0 0 0 0 3 7 0 2 1 9 9

a concentric tantalum anode having a minimum diameter of 1.2 cm. The lamp's operation with the new cathode is similar to Kocher's description (K67a, K67b). However, the intensity is greatest when the lamp current is 30 A, corresponding to 20 V between the anode and the cathode (lamp power is provided by a current-regulated supply – Perkins 0-36 V, 0-32 A). An additional increase in intensity (~30%) is obtained when D_2 replaces H_2.

This lamp's rather large discharge volume* prevents the output from being focused to a region smaller than 1.5 cm in diameter. Full utilization of the lamp output would require an interaction region of comparable dimensions, resulting in unreasonably large detector optical systems. Therefore, less powerful commercial lamps that have smaller discharge volumes are more convenient for this experiment. Two types of commercial deuterium lamps are used; each has a discharge region of 1 mm diameter and can easily be focused to a region ~4 mm in diameter.†

The most often-used lamp is an Oriel C-42-72-12 deuterium-filled lamp – a small, sealed-off, quartz lamp which is normally used in uv spectrometers. The lamp cathode is a cylinder of nickel. To start, the cathode is heated by an enclosed filament. As with most D_2-discharge lamps, further heating is not required during operation, the cathode being heated by positive ion bombardment. A current-regulated power

---

* The desire to decrease the discharge volume of Kocher's lamp led to the new cathode design.

† Spherical aberrations in the biconvex quartz condenser lens (f-1, 3.8 cm diameter) used with these lamps prevents the output from being focused to the limit implied by geometric optics.

supply (model 651, constructed by UCB Physics Department Electronics Shop) provides ~0.7 amps at ~90 V during operation.

Light is emitted into a 30° (half angle) cone through a hole in a half cylinder of nickel and molybdenum which forms the anode. A fan provides cooling during operation (see Fig. 7). The lamp has a finite lifetime; its intensity decreases by 50% after about 300 hours of operation.

A more powerful, water-cooled deuterium lamp, the type WHS-200 manufactured by the Dr. Kern GMbH, is used in some runs.* It operates with a current-regulated Varian 2200-A magnet power supply which provides ~1.3 A at ~120 V. The intensity of the Kern lamp decreases quite rapidly,† and it is more difficult to operate than the Oriel lamp.

Any of the three lamps can be mounted below the main chamber. An additional Oriel lamp, mounted above the main chamber, provides an increased excitation rate during some runs. Lamps are fitted with interference filters having transmissions of ~20% at 2275 Å and bandpasses of ~250 Å FWHM. Various baffle and filter arrangements were tried, utilizing either a 2.5 or a 1.5-cm diameter filter. The most convenient arrangement is shown in Fig. 4.

An RCA 1P-28, calibrated against an Eppley thermopile, measures

---

* A comparison of the intensity of the Kern and Oriel lamps at 2275 Å gives results consistent with a previous comparison (LE69).

† The short lifetime, ~50 hours to 50% intensity, may be due to the non-recommended buring position used in this experiment. The lamp manual recommends an orientation with light emitted horizontally; however, vertical emission is more convenient here.

0 0 0 0 0 6 7 0 2 4 0 0

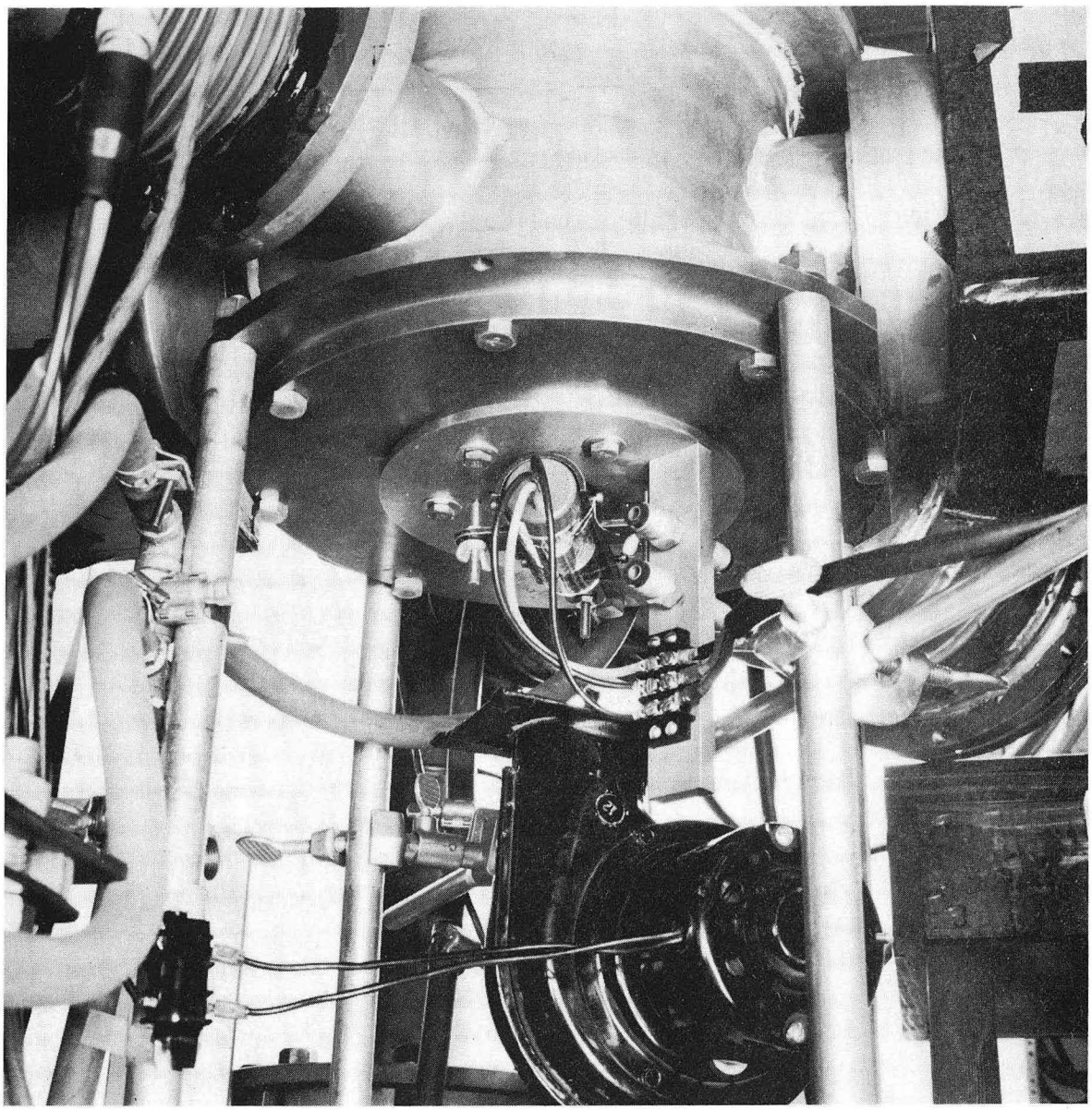

XBB 7112-5799

Fig. 7. An excitation lamp (Oriel-type) mounted below the main chamber. The Kern lamp fits on the same mounting.

the intensities of the lamps. Measurements are made at the interaction region with lamp, lens, and filter in place. The intensities are roughly 3×10^{12}, 2×10^{12}, and 5×10^{12} photons/cm^2/sec/Å for the Kocher, Oriel, and Kern lamps, respectively. These are typical values; the intensity of the commercial lamps depends upon age. The intensity during runs also depends upon the condition of the interference filter; the high lamp intensities cause the filter to deteriorate quite rapidly. Transmission decreases at about 0.5% per hour during runs, and the filter is visibly discolored after ~100 hours of use. The decrease is verified with a Beckman DK-1A spectrophotometer. Consequently, the ultraviolet filter must be replaced periodically.

4. Detector Optics

The interference filter in each detector optical system is 10 cm in diameter. Filter No. 1 has 50% transmission at 5513 Å and a 10-Å-FWHM bandpass; No. 2 has 20% transmission at 4227 Å and a 6-Å-FWHM bandpass. The filters are mounted just outside the main vacuum chamber.

The first lens of each optical system is 8.0 cm in diameter, with a 6.6-cm focal length. Each is held in a cone-shaped light baffle (see Fig. 5) and positioned one focal distance from the interaction region. The first lens is a critical element, since it determines the detector solid angle and affects the performance of the pile-of-plates polarizers.

Spherical aberrations in ordinary lenses lead to serious reductions in counter efficiencies, resulting from nonparallel focusing of

0 0 0 0 3 7 0 2 2 0 1

light rays.* Therefore, the first lenses are aspheric condensers which are largely corrected for spherical aberrations. These lenses are manufactured by a molding procedure which produces strains. Strained glass is optically active, so the lenses are annealed to prevent distortion of the polarization correlation.†

Because of the finite dimensions of the interaction region, the light rays emerging from the first lens diverge slightly (~2½°), and subsequent optical components must be of increasing size. The second lens is located 180 cm from the first; it is a 20.0-cm diameter plano-convex condenser having a 25.4-cm focal length. An adjustment insuring that the presence of the polarizer does not affect the aperture of the optical system resulted in each second lens being stopped to 18.0-cm diameter. The photomultiplier faces are large enough so that spherical aberrations in the second lenses do not cause losses. In addition, annealing is not necessary because polarization analysis takes place before light reaches the second lens.

A He-Ne laser initially aligns the two optical systems, insuring colinearity. A point source positioned at the center of the interaction region provides for final alignment of each optical component. With detectors in place, the field of view of each optical system is deter-

---

* Nonparallel focusing causes light to be lost for two reasons: the bandpass of the filters is shifted to shorter wavelengths for obliquely incident light, and rays at angles more extreme than 2½° can not strike the second lens of the optical system.

† A run made before the optical activity was discovered yielded a greatly distorted polarization correlation.

mined by measuring the count rate for various positions of the point light source. In this way, one insures that the interaction region is entirely in view of both detectors.*

Some of the glass surfaces intersecting the optical path are coated with MgF_2, reducing reflection losses. The vacuum windows, the second lenses, and the exterior of the evacuated cells affixed to the detectors (see Sect. III.B.6 and Fig. 10) are coated, while the first lenses and the interiors of the evacuated cells are not.

5. Pile-of-Plates Polarizers

Ordinary glass can be used in the construction of the polarizers because the photons are in the visible region. Each polarizer contains ten sheets of 0.3-mm glass (Corning Microsheet 0211) inclined at nearly Brewster's angle. The sheets are spaced to prevent multiple reflections and graduated in size to accommodate the 2½° divergence of light from the first lens.

Each sheet is attached to a hinged aluminum frame which can be folded completely out of the optical path. In the "out" position, all sheets are hidden from view of the detectors by the adjacent aluminum frame, preventing spurious counts due to scattered light. In the "in" position, the angle of each sheet is determined by an adjustable stop, and set to an optimum angle slightly larger than Brewster's angle. The

---

* A serious reduction in the signal-to-background for coincidence counting results when the interaction volume exceeds the field of view of the detectors (DC68).

0 0 0 0 3 7 0 2 2 0 2

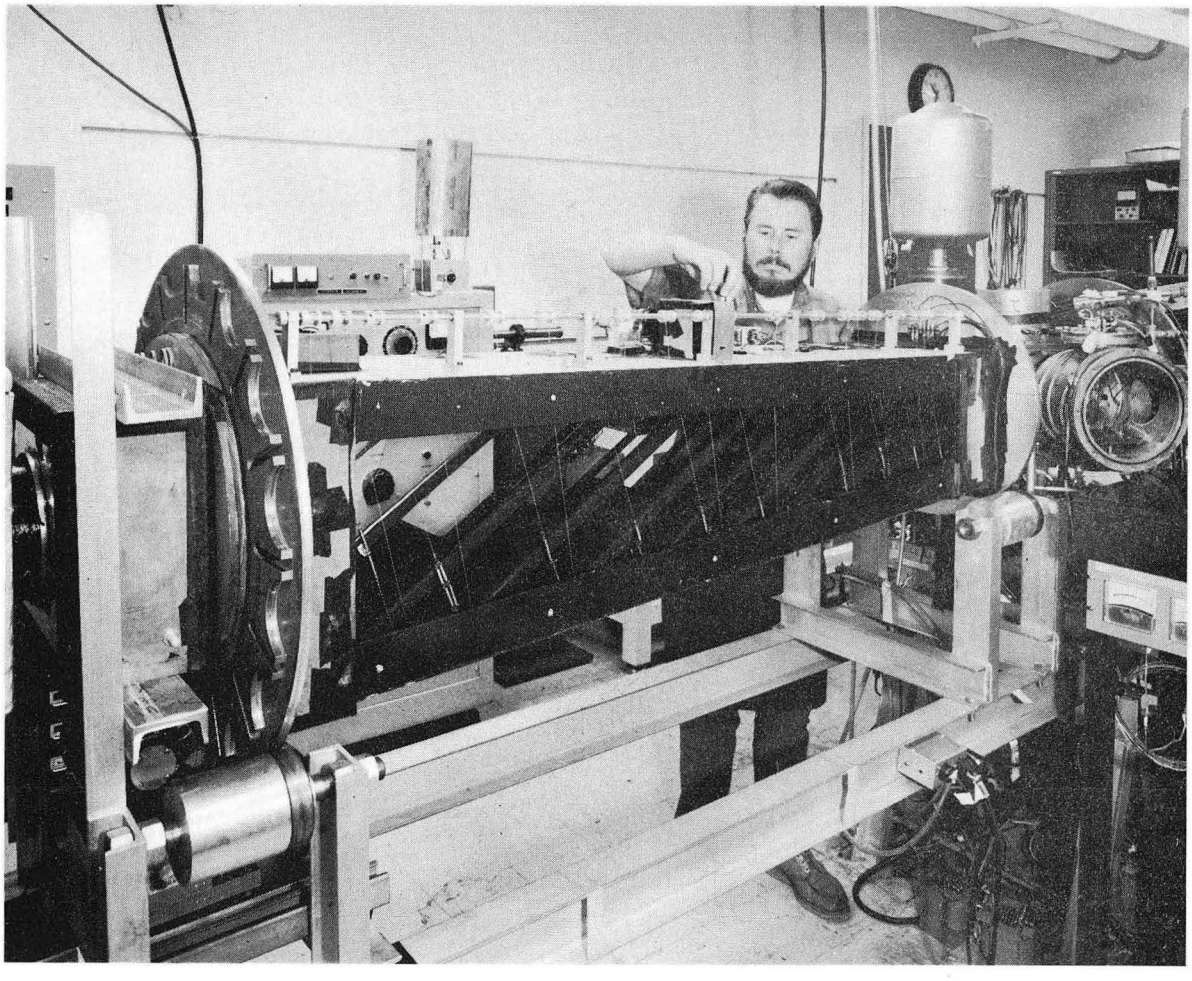

XBB 7112-5796

Fig. 8. A view of polarizer No. 1 with light shielding removed. The rear support disc (at left) is a large Geneva gear. Power to the glass sheet-lifting mechanism is connected through commutator rings (not shown) on the front support disc, at right. An adjustment to the lifting mechanism is being made by Machinist D. Rehder.

optimum angle is determined according to the theory of pile-of-plates polarizers (see Appendix A). The polarizers have slightly different efficiencies because of differences in the index of refraction and the absorption coefficient of the glass at 5513 Å and 4227 Å (see Table III).

A motor-driven system of wires, winches, and pulleys moves the glass sheets in and out of the optical path (see Fig. 8). Four large bearings support each polarizer. A motor-driven Geneva mechanism rotates each polarizer in 22½° increments about the optical axis. Electrical power for the lifting mechanism is connected through four brass commutator rings. Rotatable light seals are constructed of 2-cm-thick black felt compressed between flat metal plates. An entire polarizer unit is about 180 cm long, and weighs about 75 kg.

A constant-intensity polarized light source shaped like the interaction region is used in conjunction with the photodetectors for measurements of the polarizer efficiencies. The transmission of each polarizer – the ratio of the background corrected count rates: polarizer "in" to polarizer "out" – is measured for various polarizer orientation angles. The results are fitted with the function $\varepsilon_M \cos^2(\Phi - \Lambda) + \varepsilon_m \sin^2(\Phi - \Lambda)$, where Φ is the angle of orientation of the polarizer and Λ is the initial angle offset of the polarization axis of the light source. Figure 9 shows the results of measurements of polarizer 2 with an extended and a point light source. The poorer efficiencies measured with the extended source result from the geometry of the pile-of-plates polarizers. The transmission of these polarizers depends upon the angle of the incident light, and thus the efficiencies

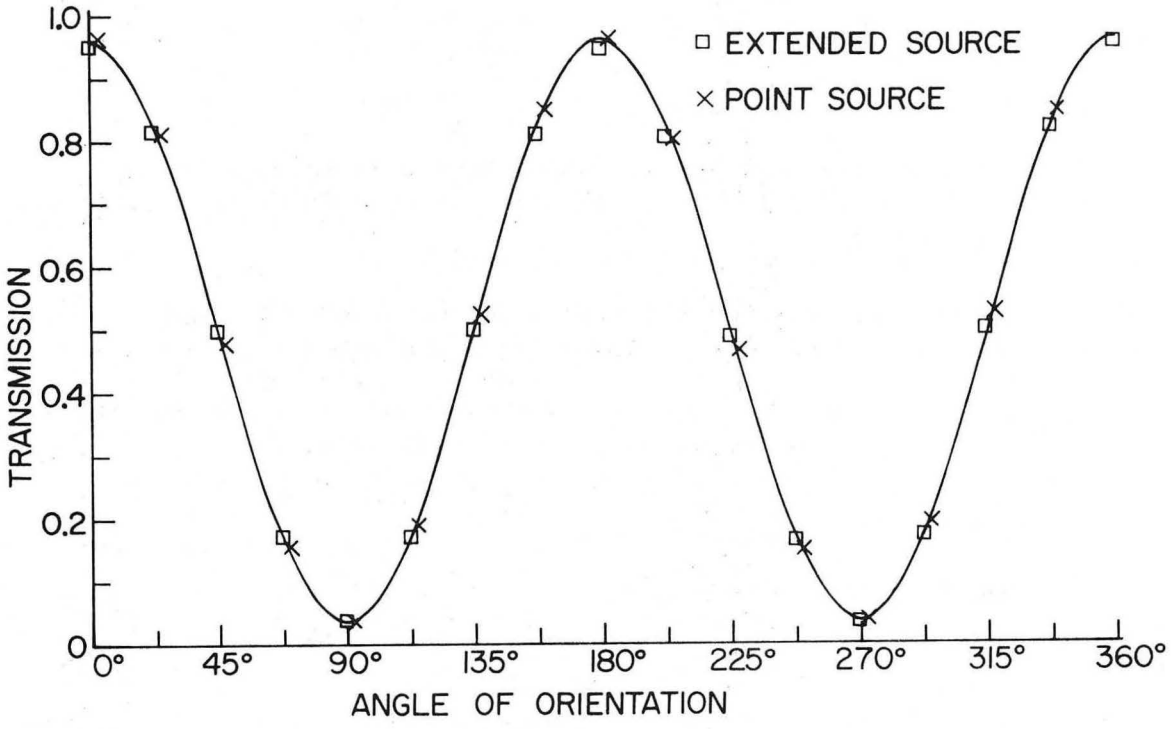

XBL 723-531

Fig. 9. Results of a measurement of the transmission of polarizer no. 2 as a function of angle of orientation of the polarizer, Φ.

Table I. Measured polarizer efficiencies (using a polarized light source shaped like the interaction region).

	Polarizer No. 1	Polarizer No. 2
ε_M:	0.97 ± 0.01	0.96 ± 0.01
ε_m:	0.038 ± 0.004	0.037 ± 0.004

differ for light rays originating from different parts of the interaction region. This point is discussed in Appendix A.

The measured polarizer efficiencies for a source geometry similar to the interaction region are given in Table I.

6. Photon Detectors

Efficient single-photon counting is essential to this experiment.* Fortunately, two newly developed photomultipliers with relatively good quantum efficiencies at the appropriate wavelengths became available shortly before work began.

Photomultiplier 1, an RCA-C31000E,† has a multialkali photocathode and a quantum efficiency (QE) of 12.8% at 5513 Å ; this QE was measured at the factory . No. 2, an RCA-8850, has a bialkali photocathode and a QE of 28% at 4227 Å (QE was measured at 4200 Å by comparison with an RCA-8575 of known QE). These tubes have a 12-stage focused dynode structure. The first dynode is coated with gallium-phosphide, providing an electron secondary-emission ratio that is about 10 times higher than ordinary dynode material.‡ This feature serves to

---

* Many conflicting approaches to single-photon counting are described in the literature (FJOP69, Y69, M68, R71, RM70). The techniques employed here — type of equipment, use of amplifiers, discriminator levels, etc. — were chosen after much experimentation.

† The C31000E is a developmental tube which eventually became the RCA-8852.

‡ It is well known that end-on phototubes are somewhat sensitive to the polarization of the incident light because a fraction of the output pulses arise from photons striking the first dynode at oblique angles. For the tubes used here, this effect is greatly reduced because normal pulses (due to photocathode electrons) are ~50 times larger.

0 0 0 0 3 7 0 2 2 0 3

increase the anode-pulse-height resolution (MSK69, LL72), making it easier to discriminate between single-photon pulses and dynode-noise pulses.

The tube bases are standard low-current grounded-anode resistor chains; the cathode grid potentials are adjusted for maximum collector efficiency. Careful high-frequency wiring techniques (PT61) preserve the fast rise times (~2.5 nsec) and narrow pulse widths (~6 nsec) of the tubes. In particular, the base resistors and capacitors are attached directly to the tube sockets. The bases are potted in RTV-3110 encapsulent, insuring proper operation during coolings.

Cooling the detectors is necessary for the reduction of dark pulse rates. The phototube coolers are constructed of brass and insulated with 5-cm-thick styrofoam; a brass tube surrounded by coolant holds the phototube assembly. A cone-shaped evacuated Pyrex cell attached to the phototube extends out of each cooler, preventing condensation on the tube face. A cooler and a phototube assembly are shown in Fig. 10.

The C31000E is cooled to -78°C by a slurry of dry ice and ethanol, and the 8850 is cooled to 0°C with ice water (temperatures below 0°C do not further reduce the 8850 dark rate, and may cause a loss of sensitivity (MM60)). Extra precautions are taken against radio-frequency pickup by the detectors; this is an especially serious possible cause of systematic error in a low count-rate coincidence experiment. Mu-metal shields maintained at cathode potential provide both magnetic and rf shielding. In addition, the phototubes are

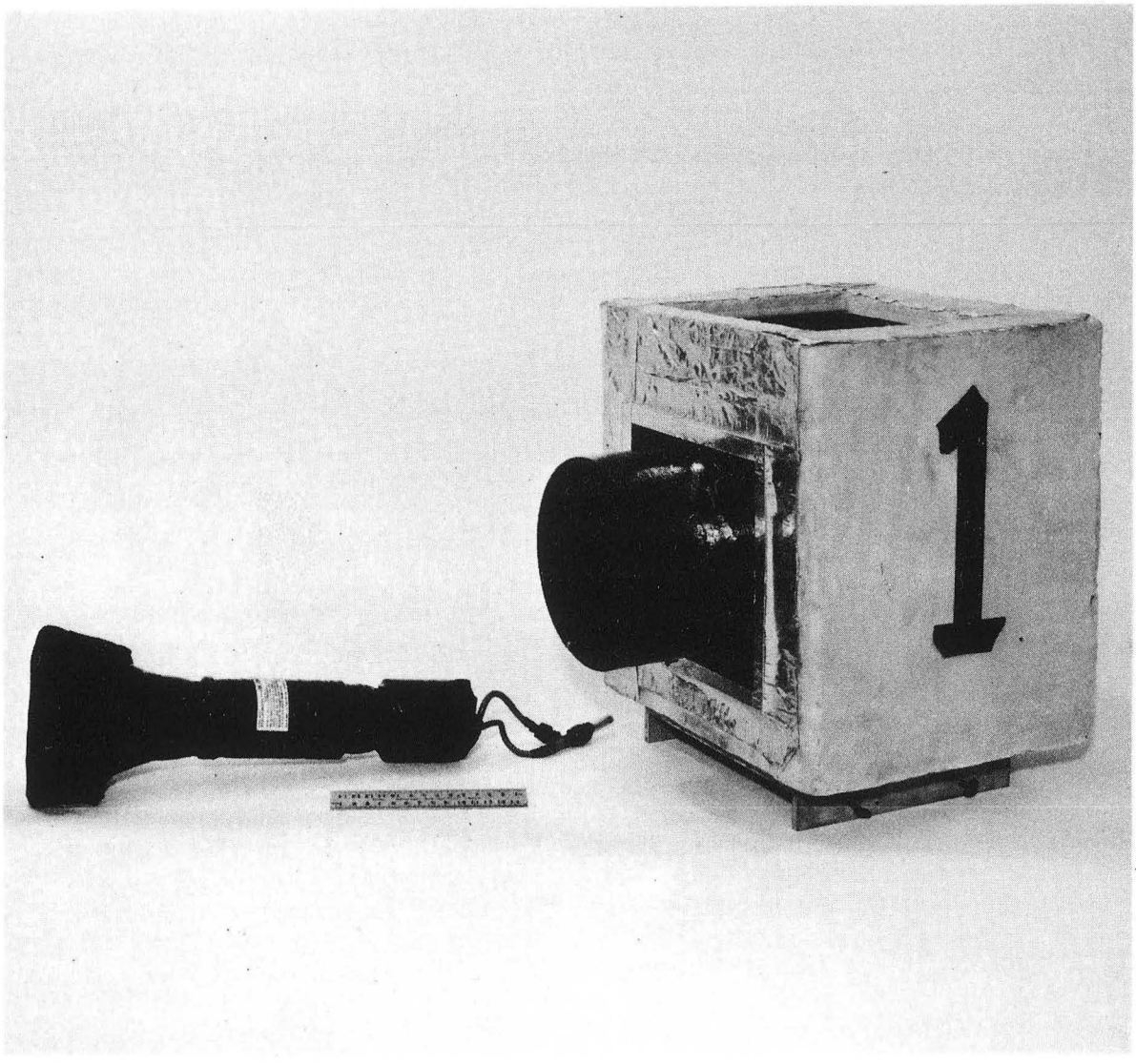

XBB 7112-5798

Fig. 10. Photomultiplier assembly No. 1 and associated cooler. The photomultiplier, the base, and the cone-shaped evacuated cell form a sealed unit. (The end of the cell is covered to prevent damage from room light.)

0 0 0 0 3 7 0 2 2 0 4

enclosed in additional metal shields which are constructed and grounded according to standard rf-shielding procedures (M67). As a precaution against leakage currents from high-voltage areas, the tubes are encased in high-dielectric-strength Teflon tape.

It has been pointed out that photomultipliers are themselves excellent low-noise pulse amplifiers (FJOP69), and thus should be operated at high voltages, making a minimum amount of external amplification necessary. An additional advantage of this procedure is better time resolution , resulting from decreased electron transit-time spread (LL72). However, too high a voltage results in a high dark rate. The arrangement found to be best is to use the 8850 without external amplification and the C31000E with a single ×10 amplifier. The amplifier (a Chronetics 156B) is very stable, and, having a rise time of 2 nsec, does not appreciably distort the photomultiplier pulses.

The negative photomultiplier pulses, after amplification in the case of the C31000E, feed-level discriminators (identical sections of EG&G 204 A/N dual discriminator module) which are triggered by pulses exceeding a -0.100-V threshold. The dynode-string high voltage necessary to insure that nearly every single-photon induced anode pulse leads to a discriminator output is determined by a method suggested by Camhy-Val et al. (CDDM68). Each phototube is illuminated with a constant-intensity light source, and the discriminator output pulse rate is measured for various tube voltages. The observed count rate levels off at a characteristic voltage; this voltage provides enough gain so that nearly all single-photon pulses register as counts. For each tube,

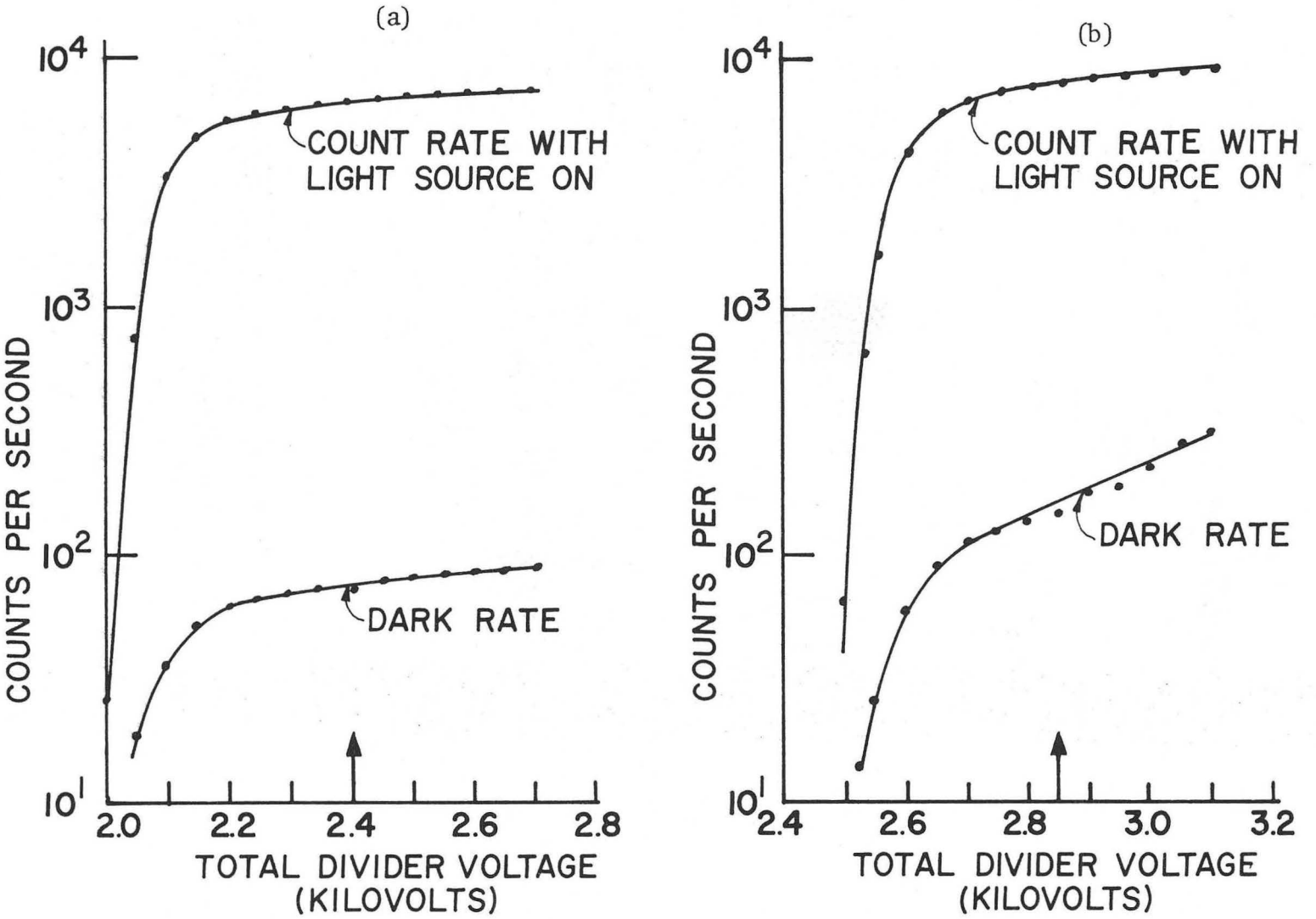

Fig. 11. Discriminator output rate as a function of dynode-string voltage with and without a constant intensity light source: (a) for the C 31000E (PM No. 1) and (b) for the 8850 (PM No. 2). The signal due to the light source (the rate with light on minus the dark rate) is insignificantly different from the total rate in this log plot. The arrows indicate the chosen operating voltages. XBL 723-525

0 0 0 0 3 7 0 2 2 0 5

the operating voltage is chosen to be larger than the characteristic voltage, as shown in Fig. 11a and 11b.

Tube voltages are provided by separate supplies (power design HV-1556). The tube dark rates vary somewhat, the dark rate vs voltage curves shown in Fig. 11a,b being typical.

7. Counting Electronics

The primary data are obtained from a standard coincidence counting arrangement, having a coincidence and an accidental-coincidence channel. The single-photon count rates (singles rates) are monitored at the same time; they provide performance information and an alternate way of inferring the accidental rate. A detailed block diagram of the counting electronics is shown in Fig. 12.

Each discriminator converts a photomultiplier pulse of sufficient amplitude into a standard fast-logic pulse; this pulse is simultaneously presented at four output connectors. The output pulses are ~5.5 nsec wide and -0.900 V high. The coincidence circuits (EG&G 102 B/N dual coincidence module) are overlap type – an output is generated if the two input pulses overlap in time. The minimum overlap is 2.5 nsec, and the output pulse width is equal to the overlap.* Discriminator and coincidence outputs are monitored by Ortec 430 scalers,

---

* The effective width of the coincidence and accidental windows is determined by random pulse counting, by using the relation $N_C = wN_1N_2$, where N_1 and N_2 are the singles rates and N_C is the coincidence rate. The effective width is 8.14 ± 0.02; to this accuracy it is the same for both windows.

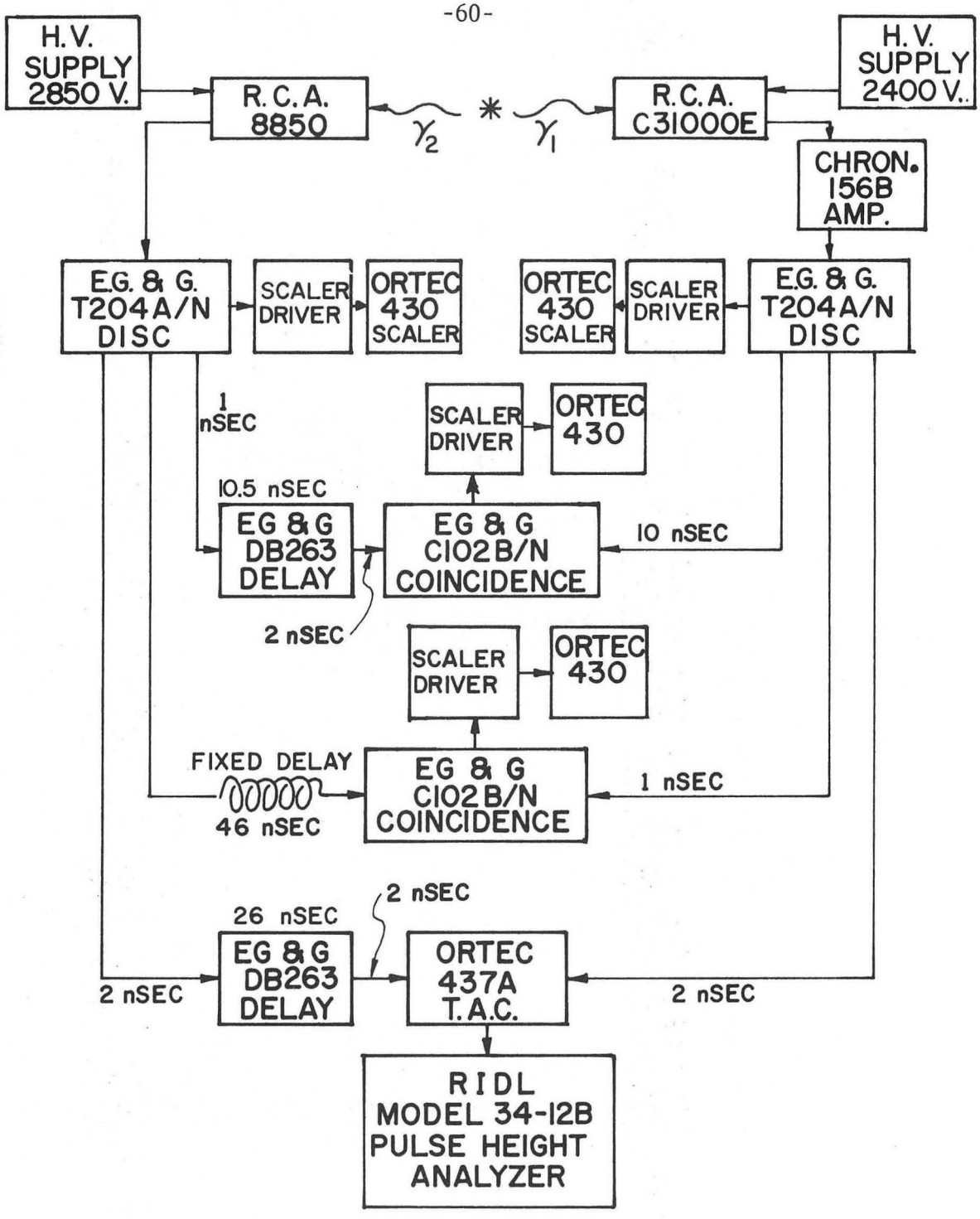

Fig. 12. Detailed block diagram of the counting electronics.

0 0 0 0 3 7 0 2 2 0 6

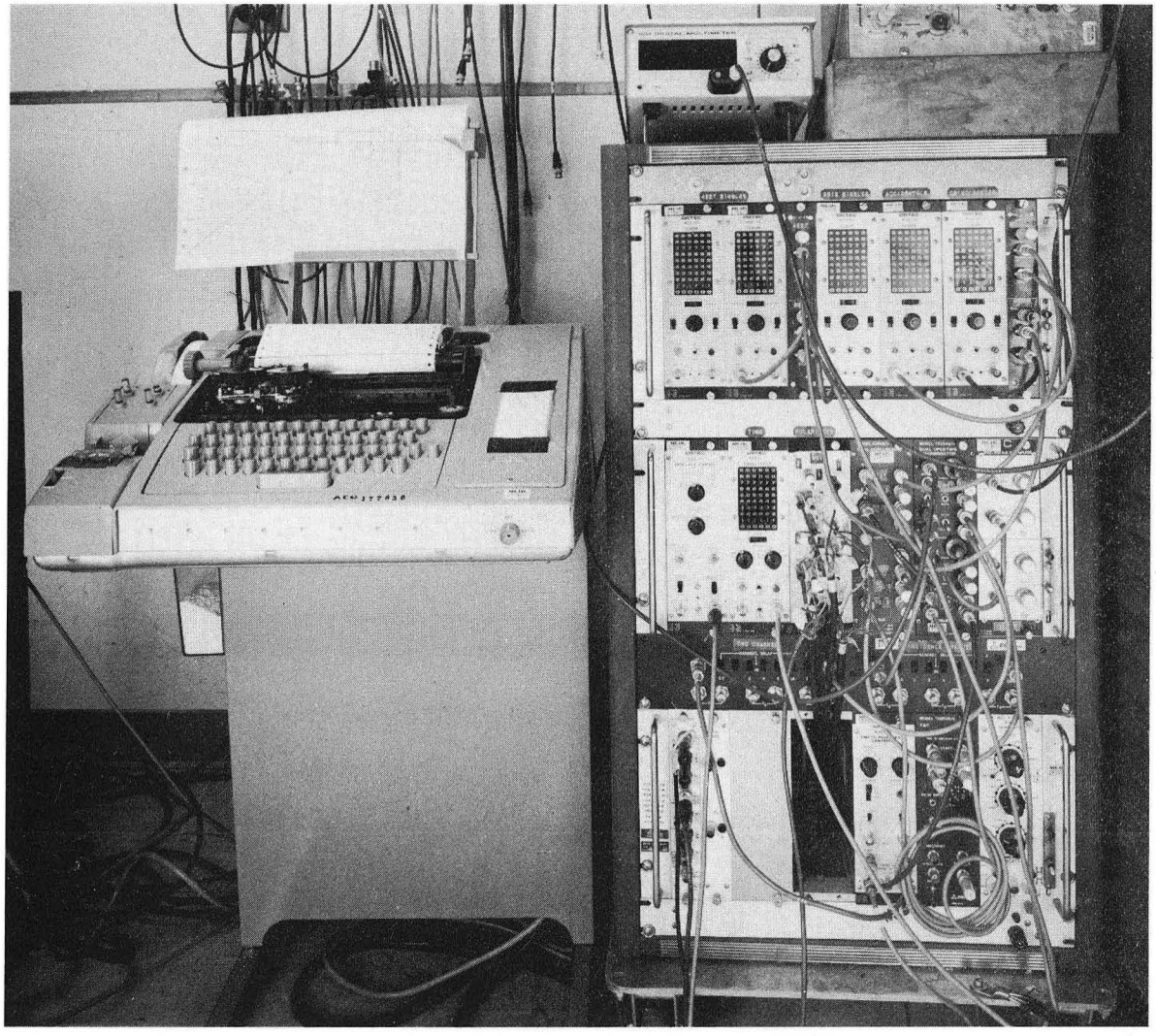

XBB 7112-5795

Fig. 13. The counting-electronics rack and the Teletype.

whose maximum count rate, 16 MHz, is much higher than any count rate encountered in this experiment. However, the scalers do not respond dependably to narrow pulses, hence scaler drivers interface the scalers to the other electronics. The scaler drivers convert logic pulses having widths greater than ~3 nsec into positive-going 5-V-high, 25-nsec-wide pulses that are reliably detected by the scalers.

Cable delays in the coincidence channel are adjusted so that an output pulse corresponds to two detected photons, γ_1 and γ_2, which could have been emitted by the same atom. The accidental channel has the γ_2 pulse delayed by an additional 45 nsec, insuring that an output does not correspond to photons emitted from a single atom.

Time analysis is performed by a time-to-amplitude converter (TAC) pulse-height analyzer (PHA) combination. The TAC (Ortec 437) is a start-stop type: a γ_1 (start) pulse activates the unit; if a γ_2 (stop) pulse is detected within 50 nsec, the TAC generates an output pulse having an amplitude proportional to the start-stop time difference. The output of the TAC feeds the PHA (RIDL 34-12B); each input pulse results in a count in a PHA channel with memory location proportional to pulse amplitude. Two hundred channels of the PHA are normally used, and the time base is adjusted so that 5 channels roughly correspond to 1 nsec.

The best estimate of the time resolution of the counting system (including the detector) comes from the slope of the front edge of the intermediate-state lifetime curve (see Fig. 20). Assuming a gaussian response function, this gives a time resolution of 1.5 to 2.0 nsec FWHM.

0 0 0 0 3 7 0 2 2 0 7

This time error comes from two sources: (1) transit-time spread in the phototubes and (2) discriminator walk (walk is a variance in the discriminator trigger times caused by the varying amplitudes of the photomultiplier pulses).

The time resolution of the electronics is quite sufficient for the primary measurement, but it could be improved by employing higher tube voltages (reducing transit-time spread) and by utilizing constant-fraction discriminators (newly developed discriminators which greatly reduce walk).

A pulsed-light source is used to make cable adjustments in the coincidence channel. This system, built by LBL for timing applications, consists of a 3-kV pulse generator which simultaneously powers up to four barium-titinate lamps. The lamps, which normally produce 20,000 photons in each 2-nsec-wide pulse, are attenuated, giving 1 photon per pulse. With two lamps as light sources, the coincidence count rate is measured as a function of cable delay of the γ_2 pulse. The delay is set to the minimum value at which the maximum coincidence rate is obtained as shown in Fig. 14. The slope of the edges of the coincidence-rate-vs-delay curve gives an upper limit of the time resolution of the system which is consistent with the previously discussed inference. (This gives only an upper limit because of the 2-nsec time spread coming from the light pulser.) A further calibration is obtained with simultaneous electronic pulses instead of photomultiplier pulses. The resulting coincidence-rate-vs-delay curve (not shown) jumps from zero to the maximum rate in a time less than 0.5 nsec. This gives confir-

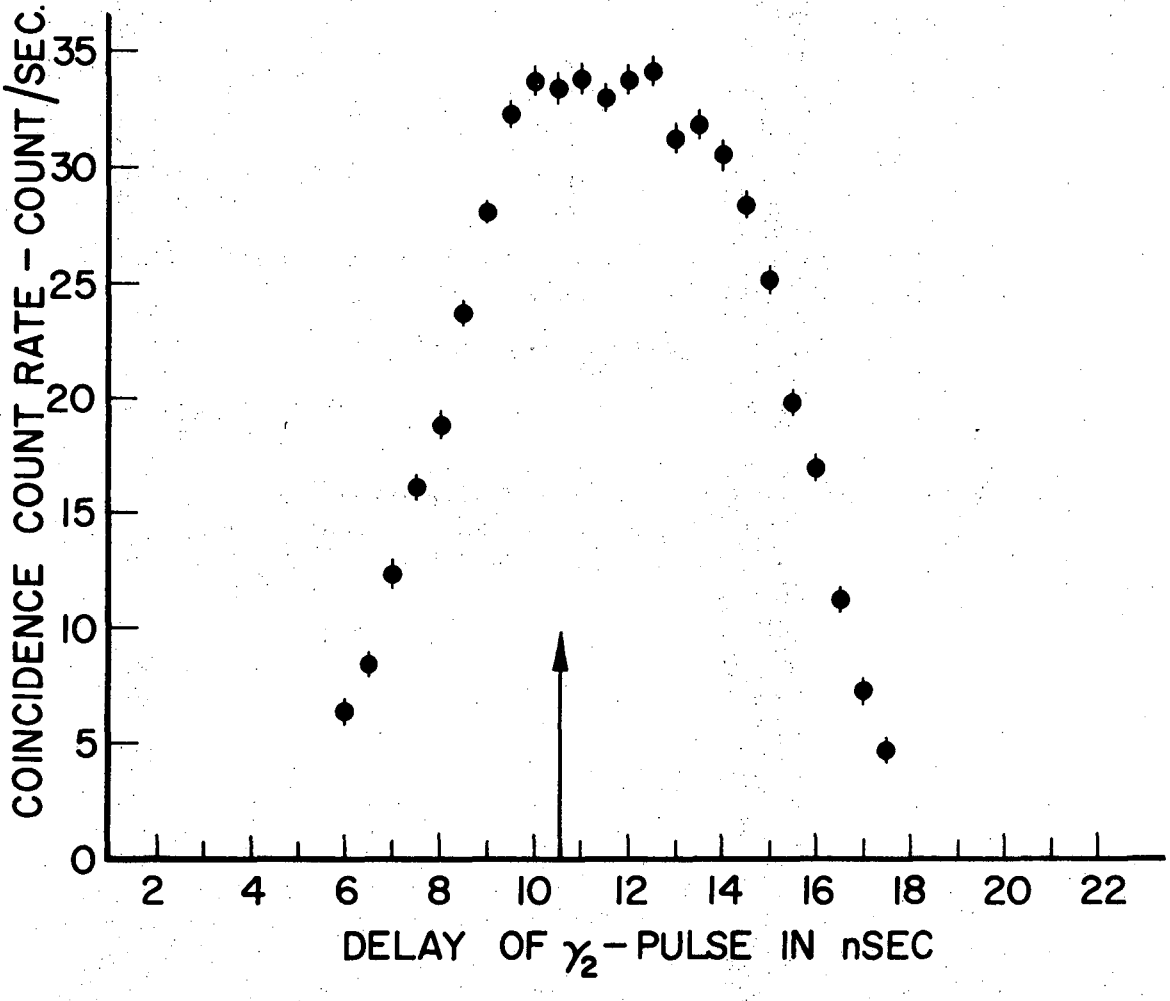

XBL 723-518

Fig. 14. Pulsed coincidence channel timing curve obtained with simultaneous light sources. The slight distortion in the curve is due to time variation of the intensity of the light sources. The arrow indicates the delay chosen.

mation that the major time spread comes from the phototubes.

8. Automatic Sequencing and Data Collection System

The data contained in the scalers is read out on a Teletype by an Ortec scaler-printout system. The heart of this system is a 432 printout control and a 431 timer-scaler. Normally the printout control causes the system to be read out after a preset count period. The system then resets and another count period begins. This system is modified slightly for the present experiment, allowing the experimental parameters to be changed before a new count period begins. A block diagram of the modified system is shown in Fig. 15.

A data module, similar to one of the Ortec 430 scalers, reads out the polarizer orientations. Four microswitches riding against the front support disc of each polarizer are activated by screwheads arranged in a sequence around the disc. Each polarizer orientation corresponds to a permutation of closed and open switches which is interpreted by the data module. Additional microswitches indicate if the glass sheets are "in" or "out" of the optical system.

The experimental sequencer (basically a 10-position stepping relay) is advanced by the same pulse that instigates readout. Once advanced, the sequencer inhibits the timer-scaler from restarting until all parameter changes are complete. Each step of the program is associated with four rotary switches which are preset to the desired parameter change sequence. For each step of the program, the glass sheets of the polarizers can be put "in" or "out" of the optical system,

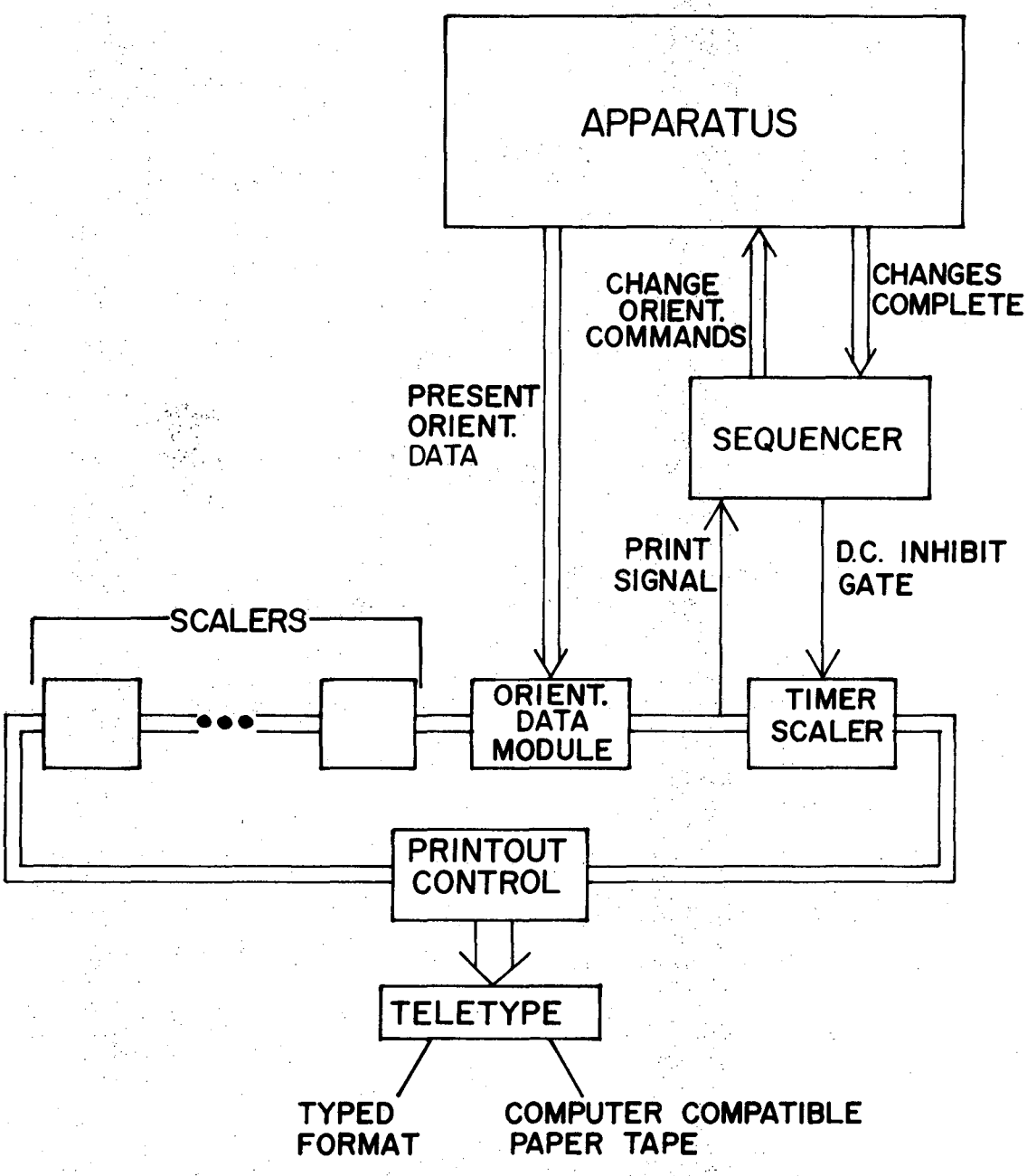

XBL 723-520

Fig. 15. The automatic readout and sequencing system. The lower part of the diagram shows the Ortec scaler readout system.

0 0 0 0 3 7 0 2 2 9

and the polarizers can be rotated by one, two, or three 22½° steps. The inhibit to the timer-scaler releases ~0.5 seconds after completion of parameter changes, and another count period begins.

The PHA is gated off during the time the orientations of the polarizers are being changed, so as to prevent spurious counts from electrical noise from motors and relays.

C. Experimental Considerations

1. The Excitation and Decay Process

Figure 16 shows the portion of the calcium term scheme that is relevant to this experiment. The lamp emits light over a wide spectrum, causing excitations to several of the upper $^1P_1$ resonance states. Using the transition probabilities tabulated by Wiese et al. (WSM69) and the transmission spectrum of the lamp filter, it is estimated that the proportions of atoms excited to the 4s8p, 4s7p, 3d4p, and 4s6p $^1P_1$ states are 2%, 18%, 52%, and 28%, respectively. Excitations to states other than the 4s6p $^1P_1$ state (which lies below the $4p^2$ $^1S_0$ state) can lead to the desired cascade, with excitations to the $3d4p^1$ $^1P_1$ state probably predominating.

A calculation of the effectiveness of this excitation method requires a knowledge of the transition probabilities between many levels. Unfortunately, as pointed out by Wiese et al. (WSM69), very few A-coefficients have been measured accurately, and there is presently no consistent theoretical method for calculating them in calcium. Estimates were made by Kocher (K67a) using the Bates-Damgaard (BD49)

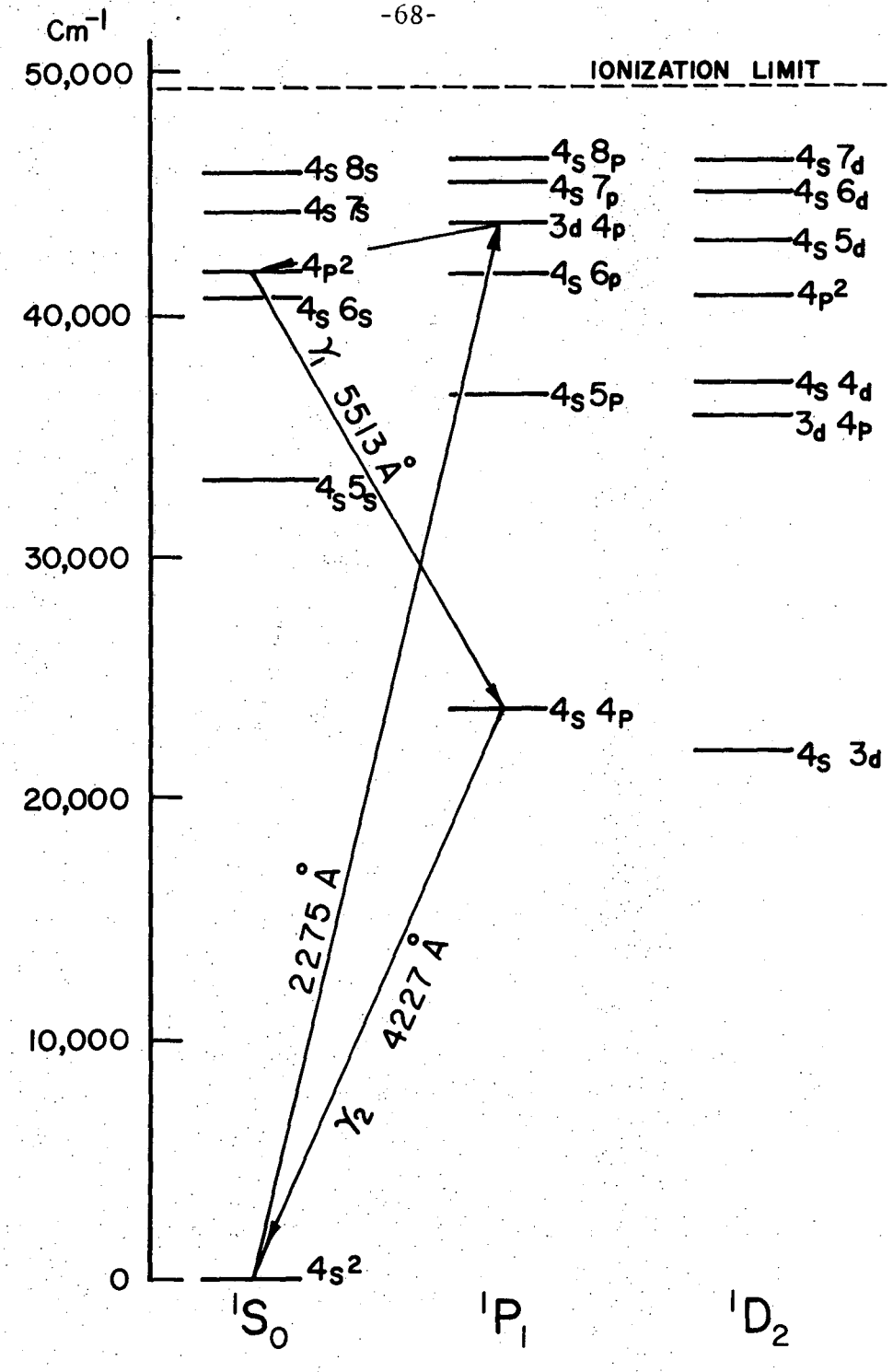

Fig. 16. Partial term scheme of calcium.

0 0 0 0 3 7 0 2 2 1 0

approximation and the electron configuration assignments of Moore (M49). Moore assigns single-electron excitations to all the relevant levels; however, a Bates-Damgaard approximation is not appropriate for the presently accepted assignments (WSM69), in which many of the important levels are two-electron excitations.

It will be useful in subsequent discussions to note that the $4s4p\,^1P_1$–$4s3d\,^1D_2$ transition probability is very small compared to the $4s4p\,^1P_1$–$4s^2\,^1S_0$ probability. The Bates-Damgaard approximation (appropriate for this single-electron transition) and more sophisticated calculations (FT69) predict that $4s4p\,^1P_1$–$4s3d\,^1D_2$ transitions are $\sim 10^5$ times less likely than direct transitions to the ground state. Thus, to a good approximation, atoms which emit γ_1 also emit γ_2.

During runs, the γ_1 signal is unpolarized, but the γ_2 signal is partially polarized in the direction perpendicular to the excitation-light beam. About 10% of the γ_2 signal is polarized. Scattered light from wall fluorescence caused by the lamp cannot account for this, because the background due to the lamp is less than 10% of the signal. Resonance-scattered light originating from 4227-Å light leaking through the lamp filter is expected to have the observed polarization. To test this possibility, a piece of Pyrex glass was put in front of the excitation lamp. (Pyrex blocks uv light, but passes 4227-Å light.) With the glass in place, both the γ_1 and the γ_2 singles rates were reduced to dark rate levels. Therefore, the observed polarization must arise from initial polarization in the upper $^1P_1$ states, caused by the excitation light and transferred to the $4s4p\,^1P_1$ state through indirect

transitions. Transitions through $^1S_0$ states cannot transfer polarization, but transitions through $^1D_2$ states can easily account for the observed polarization of the γ_2 signal (see Fig. 16).

2. Coincidence Counting

Much effort is directed at maximizing the rate of data collection. This rate is determined by the details of the atomic cascade, the detector efficiencies, the excitation rate, and the counting background. In this section, a figure of merit related to the rate of data collection will be defined and the relative importance of the quantities determining it will be discussed.

Let N be the cascade excitation rate. The γ_1 singles rate N_1, with polarizer absent, is

$$N_1 = \eta_1 N + B_1 , \qquad \text{(III.2)}$$

where η_1 is the overall counter efficiency of detector system 1, and B_1 is the counting background. The γ_2 singles rate is

$$N_2 = \eta_2 \xi N + B_2 , \qquad \text{(III.3)}$$

where ξ is a factor (>1) depending on the details of the excitation and decay process. ξ accounts for all the decays in addition to the desired cascade in which a γ_2 photon is emitted.

The coincidence rate N_c is given by

$$N_c = \eta_1 \eta_2 P(\Theta) E(w) N .$$

0 0 0 0 3 7 0 2 2 1 1

$P(\Theta)$ is a factor accounting for the angular distribution of the emission directions of γ_1 and γ_2. Let $\hat{n}_i$ be the emission direction of γ_i, then the angular distribution probability is proportional to $1 + (\hat{n}_1 \cdot \hat{n}_2)^2$. Integrating $\hat{n}_1$ and $\hat{n}_2$ over the solid angle of each detector, we obtain $P(30°) \approx 1.3$ [the proper normalization has been included so that $P(180°) = 1$].

$E(w)$ accounts for the finite width w of the coincidence window. For optimum timing we have

$$E(w) = 1 - e^{-w/\tau} ,$$

where τ is the lifetime of the intermediate state. For $w \approx 8$ nsec and $\tau \approx 5$ nsec, $E(w)$ is approximately 0.8. Since $P(30°)E(8 \text{ nsec}) \approx 1$, we will use the approximate equation

$$N_C = \eta_1 \eta_2 N . \qquad \text{(III.4)}$$

The expression for the accidental coincidence rate is

$$N_A = wN_1N_2 = w(\eta_1 N + B_1)(\eta_2 \xi N + B_2) .$$

The magnitude of the signal-to-noise ratio (with polarizers removed) indicates the statistical significance of the data collected during a time T; it is given by the following expression:

$$\frac{N_C T}{(N_C T + 2N_A T)^{\frac{1}{2}}} .$$

In analogy to this we define Q (the quality factor) by

$$Q = \frac{N_c}{(N_c + 2N_A)^{\frac{1}{2}}} = \frac{\eta_1\eta_2 N}{[\eta_1\eta_2 N + 2w(\eta_1 N + B_1)(\eta_2 \xi N + B_2)]^{\frac{1}{2}}} \quad . \qquad \text{(III.5)}$$

The time required to complete the experiment (assuming the results must have a certain degree of statistical significance) is proportional to $1/Q^2$.

Q increases with N and asymptotically approaches a maximum value:

$$Q \underset{N\to\infty}{\longrightarrow} Q_M = \sqrt{\frac{\eta_1\eta_2}{2w\xi}} \quad . \qquad \text{(III.6)}$$

An ideal cascade has $\xi = 1$. A short intermediate-state lifetime allows w to be small.* The importance of high counter efficiencies in determining Q and Q_M is clear from Eqs. III.5 and III.6. It can be seen from Eq. III.5 that, as long as B_1 and B_2 are not the dominant contributions to N_1 and N_2, respectively, further background reduction does not significantly reduce the time necessary to complete the experiment.

If B_1 and B_2 are small, Q increases rapidly in the region around $N \approx \frac{1}{2w\xi}$. For excitation rates much larger than $1/2w\xi$, the accidental rate begins to dominate, and Q increases slowly. If either B_1 or B_2 is large, the rapid increase in Q occurs at higher N. In any case, Q always levels off at high N, and it is generally not worth the effort to increase N beyond the region of rapid increase of Q.

---

* In a coincidence experiment of this kind, w would ordinarily be chosen larger than τ. Note that, if the factor $P(\Theta)E(w)$ is different from 1, it must be included in the definition of Q and Q_M.

0 0 0 0 5 7 0 2 2 1 2

3. Counter Efficiencies, Count Rates, and Rate of Data Accumulation

Reductions in counter efficiencies because of finite solid angles, imperfect filter transmissions, and limited quantum efficiencies are unavoidable. With only these losses, the counter efficiencies are given by the expression

$$\eta_i = \left(\frac{\Omega_i}{4\pi}\right) T_i \varepsilon_i \ , \qquad \text{(III.7)}$$

where Ω_i = the solid angle of the detector optical system

$$\left(\frac{\Omega_1}{4\pi} = \frac{\Omega_2}{4\pi} \approx 0.065 \right) ,$$

T_i = the transmission of the interference filter

$$(T_1 \approx 0.50, \quad T_2 \approx 0.20) \ ,$$

and ε_i = the quantum efficiency of the detector

$$(\varepsilon_1 \approx 0.128, \quad \varepsilon_2 \approx 0.28) \ .$$

We obtain $\eta_1 \approx 4.2\times10^{-3}$ and $\eta_2 \approx 3.6\times10^{-3}$.

The actual counter efficiencies are expected to be lower than these estimates for several reasons. Reflection losses and losses due to uncorrected spherical aberrations have been neglected. In addition, the collector efficiency of each phototube may be significantly less than 1.* Therefore we have

---

* The determination of phototube collector efficiencies – the probability that an electron ejected from the photocathode will strike the first dynode – is a controversial issue. Foord et al. (FJOP69, FJOP71) have reported collector efficiencies smaller than 50% for some phototubes, but these findings have been disputed by Young (Y71, YS71).

$$\frac{\eta_1}{\eta_2} = \frac{T_1\varepsilon_1}{T_2\varepsilon_2} = 1.14 \ ,$$

and

$$\eta_1 = (1.7 \pm 0.1)\times 10^{-3} \ .$$

With the same assumption, ξ can be estimated from the data for N_c, N_2, and B_2 by using Eq. III.3. We obtain $\xi \approx 12.5$. With these values for η_1, η_2, and ξ and the known width of the coincidence window, the maximum possible quality factor Q_M is ~3.5.

The counting backgrounds, B_1 and B_2, are due to the photomultiplier dark pulses and to stray light originating from wall fluorescence caused by excitation light. The former contribution is reduced by cooling the detectors (see Sect. III.B.6), the latter by a system of baffles and by covering reflecting surfaces with highly absorbant flat black enamel (Nextel-101). The use of narrow-band interference filters in the detector optical systems also reduces the scattered light contributions.* Figures 17a and 17b show the various contributions to the singles rate as a function of lamp intensity. These graphs are constructed by averaging data from several runs. In each run a single Oriel lamp is used, and the beam density is ~10^{10} atoms/cm^3.

Because of the narrow coincidence window, low counting backgrounds, and moderately low excitation rates, the coincidence-to-accidental-coincidence ratio is normally high (as large as 50 to 1

---

* These measures are sufficient to eliminate the background originating from scattered oven light.

0 0 0 0 3 7 0 2 2 1 3

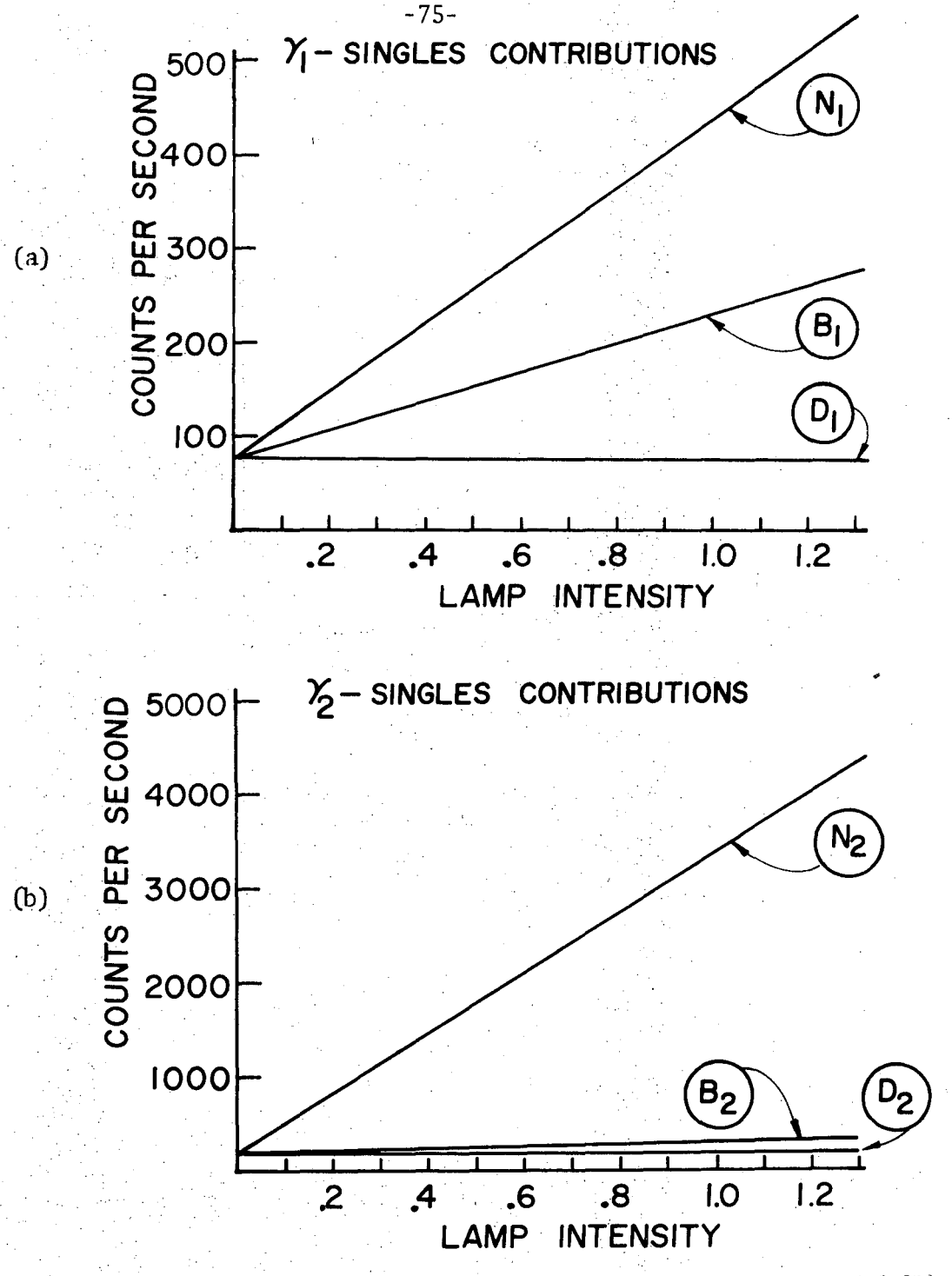

XBL 723-523

Fig. 17. Single-photon count-rate contributions. The lamp intensity is measured in arbitrary units. These curves are constructed by averaging data from several runs in which a single Oriel lamp is used. B_1, B_2, D_1, and D_2 are independent of beam density; the remaining contributions N_1 - B_1 and N_2 - B_2 correspond to a beam density of $\sim 10^{10}$ atoms/cm^3.

during some runs). Runs are made with Q ranging from 0.3 to 0.9. The experimental Q is high enough to that statistically significant results can be obtained in less than a day of counting.*

D. Preparation and Procedure for Runs

Each run corresponds to one charge of calcium and lasts from two to four days, depending upon the beam density and the amount of calcium lost during the premelting procedure. Data are collected for only a portion of this time; some time is lost during oven warmup (3 to 5 hr) and during data readout (10 to 20 sec for every 100-sec counting period). In addition, malfunctions account for lost counting time.†

Preparation for a run begins with cleaning of the oven chamber and the lamp-associated optics. The polarizers are checked for proper operation of the glass-sheet lifting mechanism and proper adjustment of stops. After the oven is loaded and the calcium premelted, the vacuum system is sealed and pumped out.

Before the oven is warmed, the phototubes are cooled and left to stabilize for a day with high voltages on. The system is then checked for light leaks – as an additional precaution, runs are made with room lights turned out.

---

* The values of Q for other atomic two-photon coincidence experiments are given in Table IV.

† Occasionally, one or the other photomultiplier developed a greatly increased dark pulse rate – 2000 to 3000 counts/sec. The phenomenon – more often occurring in the C31000E – was remedied by shutting down the experiment and storing the phototube at room temperature for several days; when recooled, the dark rate returns to normal.

0 0 0 0 5 7 0 2 2 1 4

The oven is warmed slowly to avoid overshooting the desired beam density. The crystal oscillator monitors the density for the first part of this procedure. As the density nears the desired value, the γ_2 singles-to-lamp-intensity ratio is used.

At the desired density, a check of the count rates, with atomic-beam-cutoff flag open and closed and with lamp on and off, indicates proper operation of the system. The experimental sequencer is set to the desired program, the automatic readout system turned on, and the run commenced. During runs, the oven temperature is occasionally readjusted to compensate for a slight decrease in the beam density with time.*

---

* The front of the oven being warmer than the rear results in a decrease in beam density as the level of calcium decreases in the oven reservoir.

IV. RESULTS

A. Results of a Measurement of the Polarization Correlation

In this section the data from the final series of runs will be discussed and compared to the predictions of quantum mechanics. In the next section these data will be analyzed in terms of the restrictions imposed by local hidden-variable theories. Some additional data representative of other runs made under different conditions are presented in Appendix C.

The final runs were made over a period of 2 months and represent about 280 h actual (timer-scaler on) counting time. The experimental setup is similar for each run. A single Oriel lamp mounted below the main chamber provides excitation light, and the atomic beam density is $(1.1 \pm 0.3)\times 10^{10}$ atoms/cm^3. As previously mentioned, the coincidence rate depends upon the lamp intensity, which decreases during runs. For these runs, the typical coincidence rate with polarizers removed is about 0.18 counts/sec, the typical Q is about 0.4, and the coincidence-to-accidental ratio is about 35 to 1.

Of the five runs that made up the series, two are devoted to measurements of $R(\phi)/R_o$, with ϕ varying from 0 to 360° in 22½° steps; one to R_1/R_o and R_2/R_o, averaged over the angle of the inserted polarizer; one to $R(\phi)/R_o$, with ϕ varying from 11¼° to 348¾° in 22½° steps; and one to $R(\phi)/R_o$ at the critical angles corresponding to 22½° and 67½°.

In all runs, measurements of $R(\phi)$, R_1, or R_2 are alternated with measurements of R_o, the count periods being 100 sec long. For example, to measure $R(\phi)/R_o$ for 22½° increments between 0° and 360°, the experi-

0 0 0 0 3 7 0 2 4 1 5

mental sequencer is set to the following program: A-1 (A-2) indicates a command to advance polarizer No. 1 (2) by one 22½° increment, I-1 (I-2) a command to insert polarizer No. 1 (2), R-1 (R-2) a command to remove polarizer No. 1 (2); and a dash indicates no change:

Step 1: A-1, R-1, A-2, R-2 ;

Step 2: — , I-1, — , I-2 ;

Step 3: — , R-1, A-2, R-2 ;

Step 4: — , I-1, — , I-2 ;

Step 5: — , R-1, A-2, R-2 ;

Step 6: — , I-1, — , I-2 ;

Step 7: — , R-1, A-2, R-2 ;

Step 8: — , I-1, — , I-2 ;

Step 9: — , R-1, A-2, R-2 ;

Step 10: — , I-1, — , I-2 .

If the polarizer axes are initially parallel or perpendicular, repetition of this sequence causes data to be taken at all relative angles, with data at 0°, 90°, 180°, and 270° being taken (approximately) twice as often. When the data are summed according to physically different relative angles (0° to 90°), there are an (approximately) equal number of count periods for each angle.

A ten-step sequence is not sufficient to take data at all 256 possible combinations of individual polarizer orientations, so the sequence is restarted at Step 1 once every 24 h, after both polarizers have been manually advanced by one step. Taking data at all possible orientations of the individual polarizers in approximately equal

amounts helps to average out possible systematic errors due to experimental asymmetries.

The data are analyzed by an IBM 1620-II computer. For a run measuring $R(\phi)/R_o$, the analysis program sums the counts in all 100-sec periods corresponding to relative angle ϕ, and divides by half the sum of the counts in adjacent periods of the sequence in which both polarizers are removed, after correcting for the accidental background. Data for R_1/R_o and R_2/R_o are analyzed in a similar fashion.

Background corrections are made by two procedures. In the first, the number of counts collected by the accidental-coincidence channel is used; in the second, the accidental counts are inferred from the singles rates by the prescription $N_A = wN_1N_2$. These procedures give results that are consistent to a small fraction of a standard deviation. The former procedure is used for the data presented here.

Statistical errors are estimated according to the standard prescription for counting experiments (Bv69), in which the total counts accumulated are assumed to follow a Poisson parent distribution, and estimates of the standard deviations are given by the square root of the total counts.

Another analysis procedure is to use all counts collected with polarizers removed to determine R_o. This procedure gives results consistent with the previous procedure and, in addition, gives smaller error estimates. It was decided, however, to use data for R_o taken only during count periods adjacent to those for which the other rates are measured, in calculating the ratios. The procedure chosen is more

0 0 0 0 0 3 7 0 2 2 1 6

effective in eliminating possible errors from long-term drifts in the excitation rate.

Even in the present procedure, smaller error estimates would result if the sums of counts instead of averages were used to calculate R_o. The approach adopted is therefore expected to yield conservative error estimates.

The predictions of quantum mechanics are repeated here for convenience:

$$\frac{R(\phi)}{R_o} = \frac{1}{4}(\varepsilon_M^1 + \varepsilon_m^1)(\varepsilon_M^2 + \varepsilon_m^2) + \frac{1}{4}(\varepsilon_M^1 - \varepsilon_m^1)(\varepsilon_M^2 - \varepsilon_m^2)F_1(\Theta)\cos 2\phi \ ;$$

$$\frac{R_1}{R_o} = \frac{1}{2}(\varepsilon_M^1 + \varepsilon_m^1) \ ;$$

and

$$\frac{R_2}{R_o} = \frac{1}{2}(\varepsilon_M^2 + \varepsilon_m^2) \ .$$

Using the measured polarizer efficiencies (Table I) and the value of $F_1(\Theta)$ [$F_1(30°) = 0.988$], we have

$$\frac{R(\phi)}{R_o} = (0.251 \pm 0.004) + (0.213 \pm 0.004)\cos 2\phi \ , \qquad \text{(IV.1)}$$

$$\frac{R_1}{R_o} = 0.504 \pm 0.005 \ , \qquad \text{(IV.2)}$$

and

$$\frac{R_2}{R_o} = 0.499 \pm 0.005 \ , \qquad \text{(IV.3)}$$

where the uncertainties reflect the uncertainties in the measurements of the polarizer efficiencies and the detector solid angles.

In Fig. 18 the polarization correlation is plotted for angles between 0° and 360°. Figure 19 shows these results plotted for physically different relative angles. The solid curve in each figure is not a fit to the data; this is the curve given by Eq. IV.1, and therefore is a definite prediction of quantum mechanics based on parameters measured by other methods. Obviously, the data are in excellent agreement with these predictions.

The measured values of R_1/R_o are also in excellent agreement, and are given in Table II along with the numerical values for results displayed in Fig. 19.

It is expected that there is some error in the initial alignment of the axes of the polarizers (~1°). When the data are plotted from 0° to 360°, this shift can cause systematic deviations at angles that are equivalent modulo 180°.* The data for relative angles which are multiples of 22½° appear to show this trend (see Fig. 18), the only exception being the point at 225°. The data for relative angles which are odd multiples of 11¼° represent a setup in which the initial relative polarizer angle was readjusted. These data are therefore not expected to show the same angular shift. When the data are plotted for physically different angles, the effect of an angular shift is elminated to first order in the shift angle. To second order, this effect of the angular shift is much smaller than the statistical uncertainties.

---

* The precession of the $4s4p\,^1P_1$ state inducted by stray magnetic fields can also result in an angular shift (for example, the earth's field). This precession would also tend to decrease the amplitude of the resulting polarization correlation.

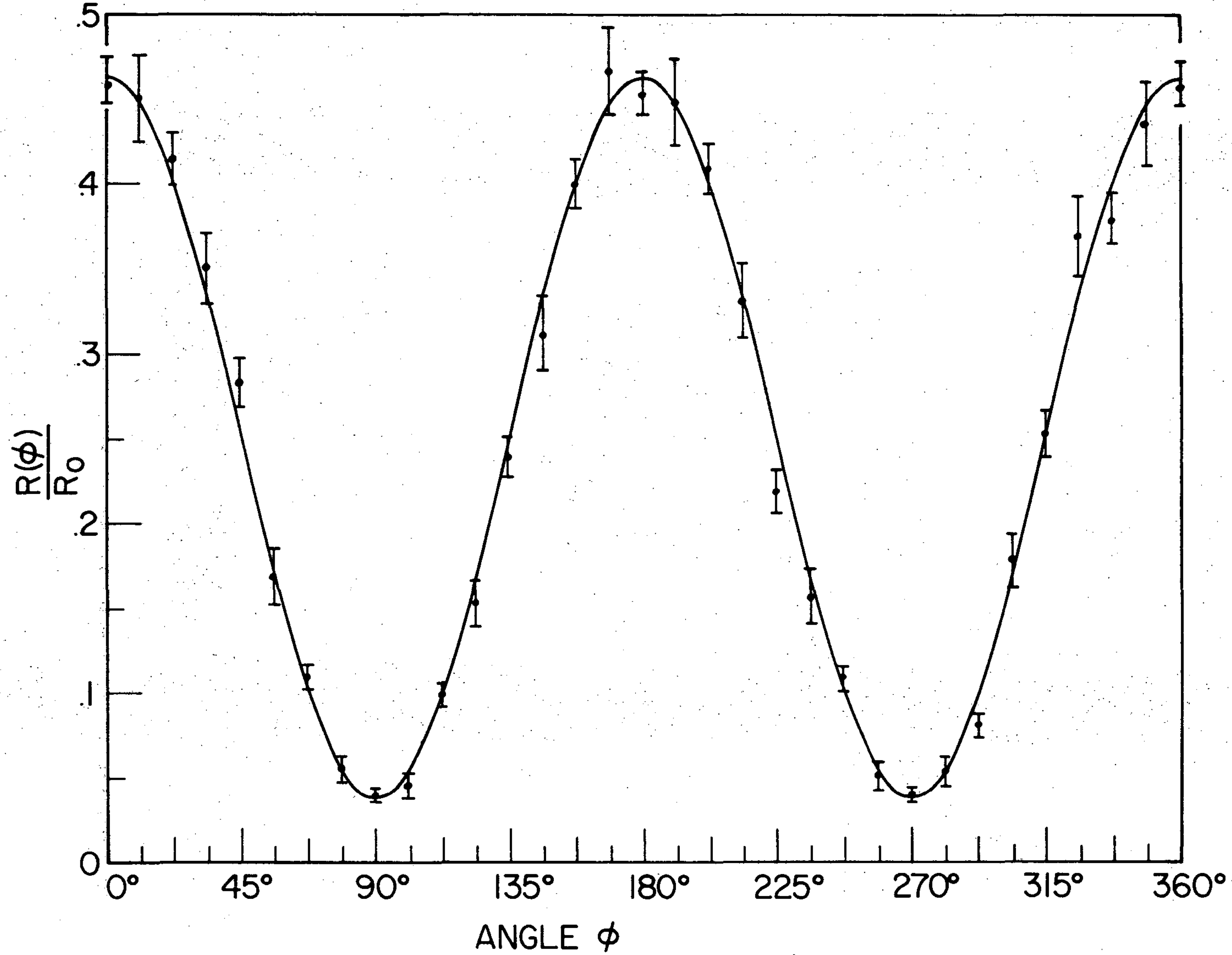

Fig. 18. The experimentally determined polarization correlation $R(\phi)/R_o$ for ϕ between 0° and 360° (the point at 0° is repeated at 360°). The solid curve is the quantum-mechanical predictions (Eq. IV.1).

XBL 723-530

0 0 0 0 3 7 0 2 2 1 7

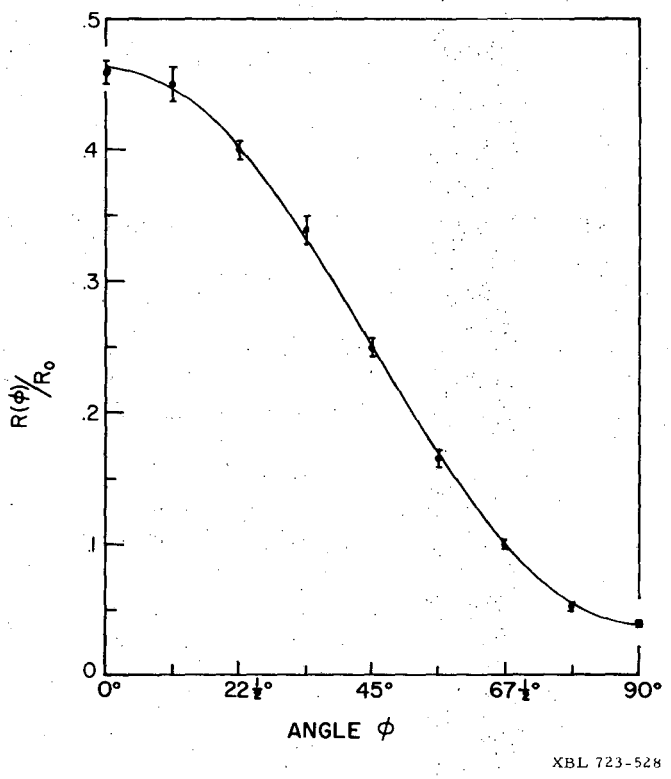

Fig. 19. The experimentally determined polarization correlation for physically different angles.

Table II. Polarization correlation (values plotted in Fig.19).

	Measured value	QM prediction
$R(0°)/R_o$	0.457 ± 0.009	0.464
$R(11\frac{1}{4}°)/R_o$	0.451 ± 0.013	0.448
$R(22\frac{1}{2}°)/R_o$	0.400 ± 0.007	0.401
$R(33\frac{3}{4}°)/R_o$	0.340 ± 0.010	0.333
$R(45°)/R_o$	0.249 ± 0.007	0.251
$R(56\frac{1}{4}°)/R_o$	0.164 ± 0.007	0.170
$R(67\frac{1}{2}°)/R_o$	0.100 ± 0.003	0.100
$R(78\frac{3}{4}°)/R_o$	0.052 ± 0.004	0.055
$R(90°)/R_o$	0.041 ± 0.003	0.039
R_1/R_o	0.497 ± 0.009	0.504
R_2/R_o	0.499 ± 0.009	0.499

0 0 0 0 3 7 0 2 2 1 8

Figure 20 shows the time-delay-coincidence spectrum for the final series of runs. The lifetime obtained from this curve is $\tau = 5.5 \pm 0.5$ nsec. The accepted lifetime for the $4s4p\,^1P_1$ state of calcium is 4.6 ± 0.5 nsec (WSM69). Although the present determination is roughly consistent with the accepted value, it is expected that the lifetime is slightly lengthened because of trapping.*

The polarization correlation for these runs is apparently unaffected by "trapping" – at least in terms of the agreement with quantum mechanics. A run made at a higher density, $\sim 10^{11}$ atoms/cm^3, gives a much longer apparent lifetime, $\tau \approx 9$ nsec. Even at this density, however, the polarization correlation is not significantly different from the one associated with the lower density (see Appendix C).

B. Direct Comparison With the Local Hidden-Variable Inequalities

It is hardly necessary to point out that the results presented in the previous section must violate the restrictions of local hidden-variable theories. The results are consistent with quantum-mechanical predictions which themselves violated these restrictions. On the other hand, a direct comparison of the results with the local hidden-variable inequalities will indicate the statistical validity of the violation.

---

* Wiese et al. get $\tau = 4.6 \pm 0.5$ nsec from a compilation of three roughly consistent determinations, each of which is reported with an error that is much smaller than 10% (see Refs. LDG64, HPP64, SG66). Kluge et al. (KOZ69) have accurately measured the lifetime at various densities and find the lifetime levels off to ~4.6 nsec at low densities. They observe "trapping" at densities greater than $\sim 10^{10}$ atoms/cm^3, which is consistent with the present observations, despite significant differences in the experimental arrangements.

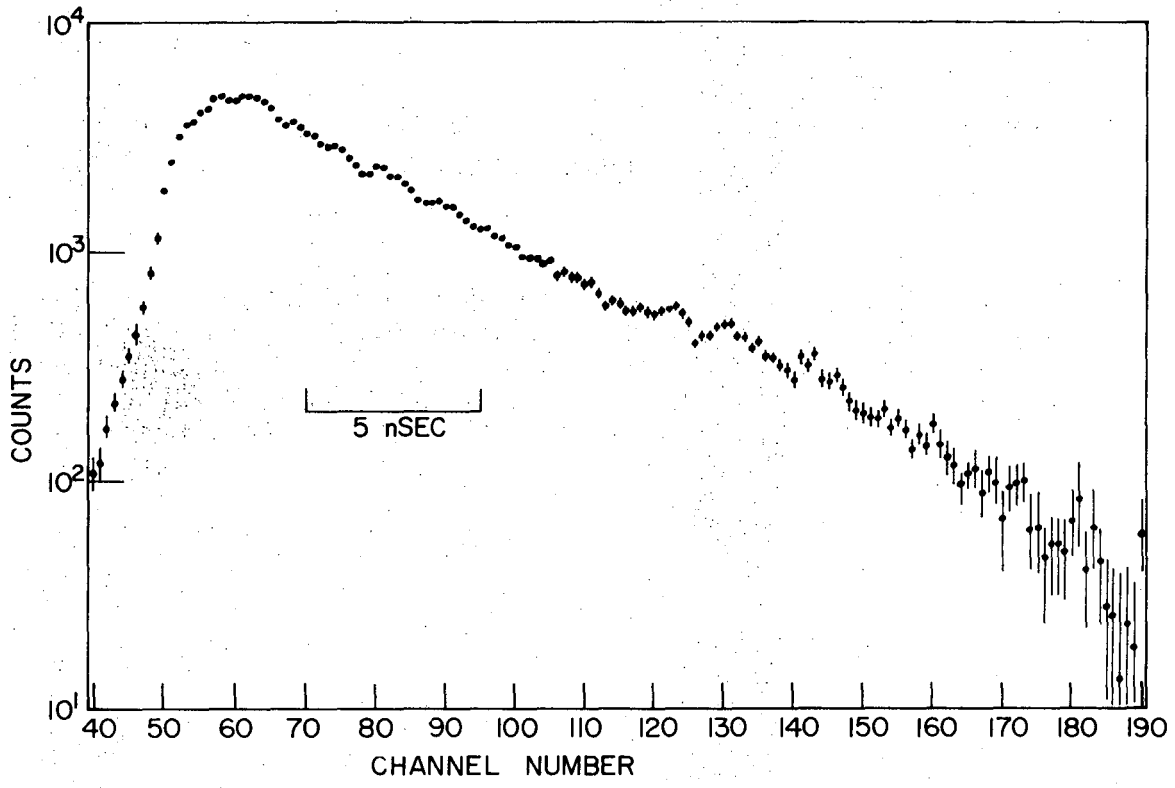

XBL 723-529

Fig. 20. Time delay coincidence spectrum accumulated during the final series of runs. Counts are collected whenever the timer-scaler is on, including those 100-sec count periods in which one or both polarizers are inserted. Some distortion of the curve is expected because of variations in the beam density and from nonlinearities in the TAC-PHA system.

0 0 0 0 3 7 0 2 2 1 9

A convenient way to display the discrepancy between the theories is to consider the angular dependence of $\Delta(\phi)$:

$$\Delta(\phi) = \frac{3R(\phi)}{R_o} - \frac{R(3\phi)}{R_o} - \frac{R_1}{R_o} - \frac{R_2}{R_o} .$$

The solid curve in Fig. 21 displays the quantum-mechanical dependence. The local hidden-variable inequalities require that $\Delta(\phi)$ lie between the broken lines in the figure. The experimentally determined points are consistent with the solid curve, and show significant deviations from the local hidden-variable restrictions at $22\frac{1}{2}°$ and $67\frac{1}{2}°$.

The inequality

$$\delta = \left[\frac{R(22\frac{1}{2}°)}{R_o} - \frac{R(67\frac{1}{2}°)}{R_o}\right] - \frac{1}{4} \leq 0$$

provides a more sensitive test, because the expression for δ contains the fewest experimental values and is therefore determined with the smallest uncertainty.

Using the data from the final series of runs, we obtain

$$\delta = 0.050 \pm 0.008 .$$

This quantity exceeds the maximum value allowed by a local hidden-variable theory by more than six standard deviations, implying a probability of 1 in 10^9 (conservatively) that this violation occurs by random fluctuation.

Due to the high coincidence-to-accidental ratio for coincidence counting, the background corrections necessary in the analysis of the

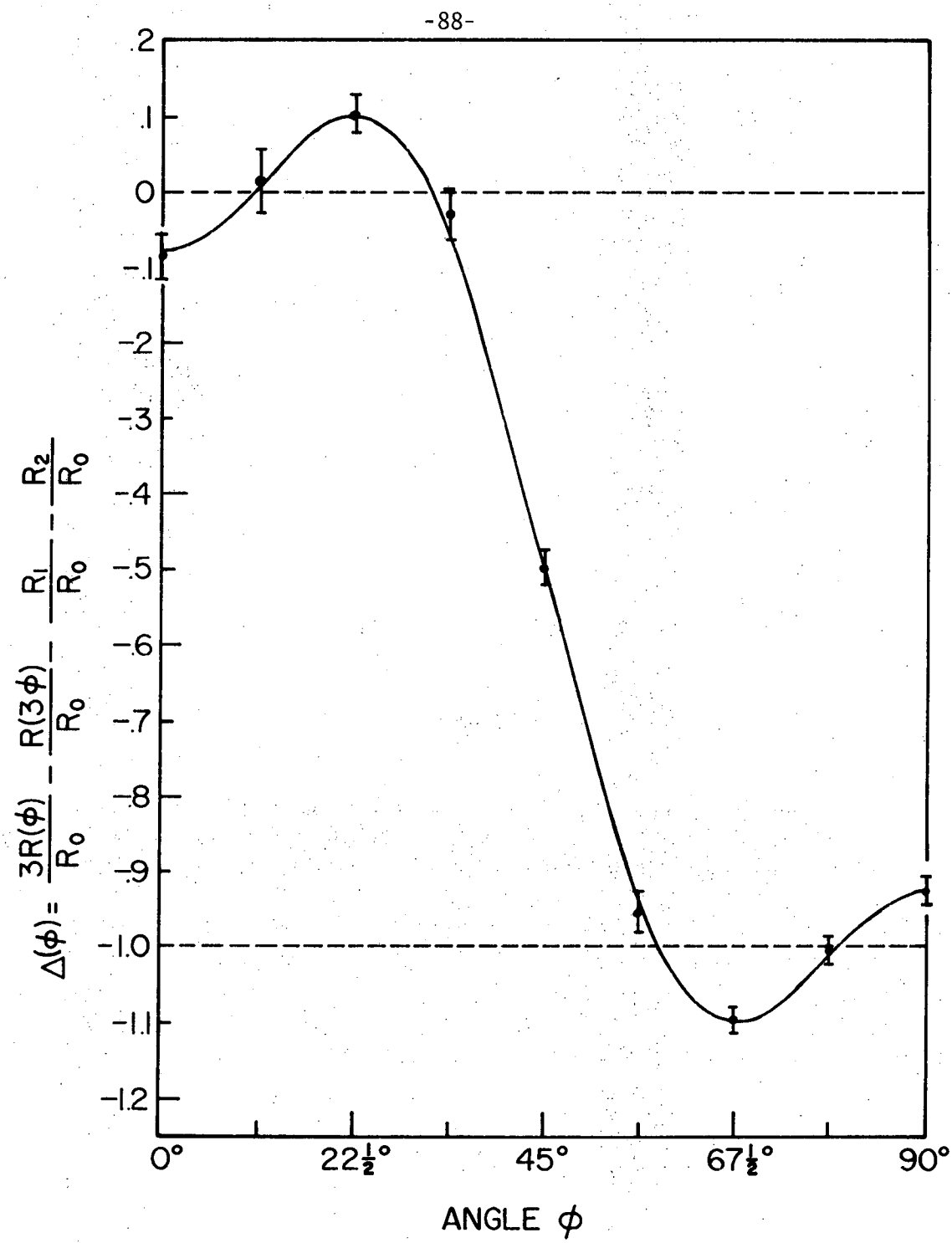

XBL 723-526

Fig. 21. Experimentally determined dependence of $\Delta(\phi)$ on the angle ϕ. The solid curve is the dependence predicted by quantum mechanics. The local hidden-variable inequalities constrain all points to lie between the broken lines.

0 0 0 0 3 7 0 2 2 2 0

data are slight. In fact, if no correction for accidental coincidences is made, the results are still roughly consistent with the quantum-mechanical predictions, and we obtain $\delta = 0.043 \pm 0.007$.

C. Discussion of Results

If the polarization correlation had been found to be of the form $A + B\cos 2\phi$, but with B small enough to satisfy the inequalities, it would be necessary to exhaustively eliminate many possible systematic errors before this result could be considered as evidence favoring local hidden-variable theories. A correlation of this sort could be consistent with quantum mechanics, the low amplitude being due to "trapping" or other depolarizing effects.

Since the results violate the inequalities, the discussion of systematic errors is greatly simplified. The inequalities are derived without reference to the specific experimental arrangement, so most systematic errors are irrelevant. In general, one need consider only those effects which could cause one of the basic assumptions to be violated.

The necessity of relating the ratio $R(\phi)/R_o$ to the probability of joint passage leads to a possible systematic error. Suppose that the coincidence rate with polarizers removed were systematically low; then, a low-amplitude correlation of the form $A + B\cos 2\phi$, which satisfies the inequalities, would appear to have greater amplitude and might violate the inequalities. This effect could arise from the slight displacement

of light rays caused by the presence of the polarizers* or from enhancement of signal owing to scattering. However, one would also expect a discrepancy in the effective values of $(\epsilon_M^1 + \epsilon_m^1)/2$ and $(\epsilon_M^2 + \epsilon_m^2)/2$ during the experiment. These quantities are directly related to the ratios of the background-corrected single-photon count rates with polarizers "in" and "out." The singles rates measured during runs give values for these ratios that are consistent with the measured polarizer efficiencies.†

One is left with the possibility that the detector efficiencies depend upon whether or not the photon has passed through a polarizer. It has already been noted that photomultipliers are somewhat polarization dependent.‡ However, a polarization dependence could not account for a violation; the detector efficiencies must depend on some (as yet unknown) hidden variable. The best argument against this possibility is the excellent agreement with quantum mechanics that has been

---

* Because of refraction by the glass sheets, light rays passing through the polarizers are displaced by ~1.5 mm. For this to yield an enhancement of R_o, the intensity distribution from the interaction region must have a peculiar shape, e.g., a ring of high intensity that is ordinarily not detected unless displaced by the polarizers.

† At least a 10% discrepancy is required for the violation to occur by this mechanism. The agreement is compatible with the errors in the measured polarizer efficiencies.

‡ No polarization dependence of the detectors is found in this experiment. It has already been noted that the photomultipliers used are relatively insensitive to photon polarization. Also, the second lenses in the optical systems, being optically active, effectively depolarize the light before it is detected. In any case, any residual polarization dependence is eliminated by averaging the data over individual polarizer orientations.

0 0 0 0 3 7 0 2 4 2 1

found. To account for the results, one requires a very pathological dependence which somehow changes a local hidden-variable correlation emerging from the polarizers into one that is consistent with quantum mechanics.

APPENDIX A

PILE-OF-PLATES POLARIZERS

Pile-of-plates type polarizers, being fragile and bulky, are normally employed only when more convenient polarizing materials are not applicable. They have been used successfully at both infrared (S62) and ultraviolet (Wa70) wavelengths. Recently, with the development of thin plastics of uniform thickness, they have become more competitive with other types of polarizers even at visible wavelengths (Sc70). In this appendix the theory of pile-of-plates polarizers will be discussed as it applies to the ten-element polarizers constructed for the present experiment.

Consider a light ray striking the surface of a glass sheet with angle of incidence θ_i.* The transmission through the first glass surface for light polarized parallel ($t_\parallel$) and perpendicular ($t_\perp$) to the incident plane is

$$t_\parallel = 1 - \frac{\tan^2(\theta_i - \theta_r)}{\tan^2(\theta_i + \theta_r)} \qquad \text{(A1)}$$

and

$$t_\perp = 1 - \frac{\sin^2(\theta_i - \theta_r)}{\sin^2(\theta_i + \theta_r)} \ , \qquad \text{(A2)}$$

where θ_r is the angle of refraction. Taking the index of refraction of air as unity, then θ_r is related to θ_i and the index of refraction of

---

* Angles of incidence and refraction are taken between the light ray and the normal to the surface.

0 0 0 0 3 7 0 4 4 2 2

the glass by

$$\theta_r = \sin^{-1}\left(\frac{\sin\theta_i}{n}\right) . \qquad \text{(A3)}$$

Equations A1, A2, and A3 are obtained by imposing the electromagnetic boundary conditions on the incident, reflected, and refracted rays at the glass surface (S48).

With the inclusion of multiple reflections within the glass, the transmissions $T_\parallel$ and $T_\perp$ through the sheet are given by

$$T_\parallel = \frac{t_\parallel}{2 - t_\parallel}$$

and

$$T_\perp = \frac{t_\perp}{2 - t_\perp} .$$

Finally, the transmissions through ten glass sheets, that are widely spaced to eliminate multiple reflections between adjacent sheets, are

$$\varepsilon_M = T_\parallel^{10} = \left[\frac{\tan^2(\theta_i + \theta_r) - \tan^2(\theta_i - \theta_r)}{\tan^2(\theta_i + \theta_r) + \tan^2(\theta_i - \theta_r)}\right]^{10} \qquad \text{(A4)}$$

and

$$\varepsilon_m = T_\perp^{10} = \left[\frac{\sin^2(\theta_i + \theta_r) - \sin^2(\theta_i - \theta_r)}{\sin^2(\theta_i + \theta_r) + \sin^2(\theta_i - \theta_r)}\right]^{10} , \qquad \text{(A5)}$$

where, by definition, the transmissions for parallel and perpendicular polarizations are the polarizer efficiencies ε_M and ε_m, respectively.

Figure A1 displays the results of a computer calculation of ε_M

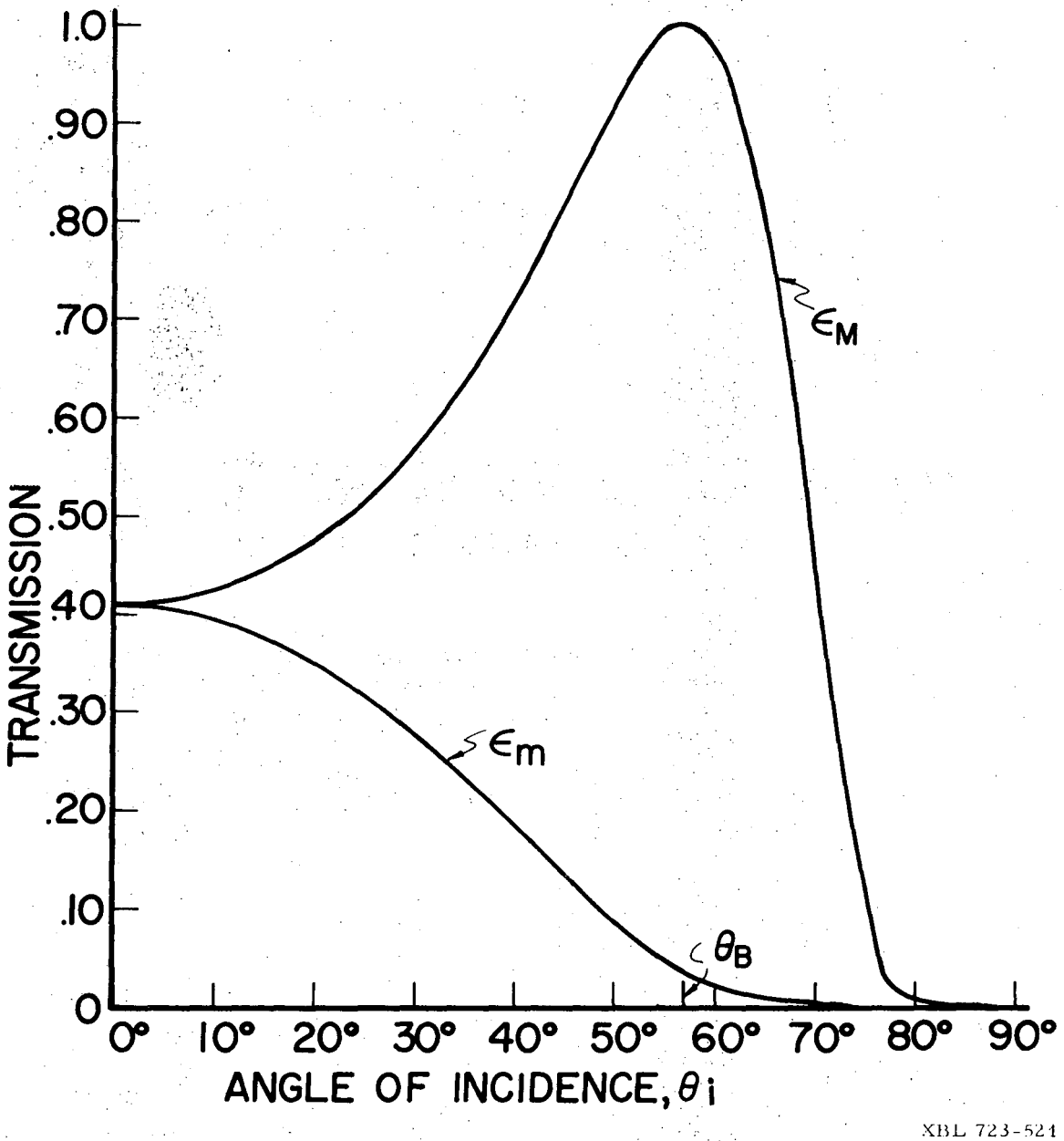

Fig. A1. The dependences of the efficiencies of a ten-element pile-of-plates polarizer on the angle of an incidence light ray. The index of refraction of the glass is 1.525.

0 0 0 0 3 7 0 2 2 2 3

and ε_m as a function of θ_i (n = 1.525). At Brewster's angle, defined by $\theta_B = \tan^{-1} n$, the efficiencies are $\varepsilon_M = 1.0$ and $\varepsilon_m = 0.036$. In the present experiment, the maximum discrepancy between quantum mechanics and local hidden-variable theories occurs when $\varepsilon_M - \varepsilon_m$ is maximized. For each polarizer, this occurs to an incident angle θ_o slightly larger than θ_B ($\theta_o - \theta_b \approx 1°$).

Table III gives the predicted efficiencies for polarizers Nos. 1 and 2 with the inclusion of losses owing to absorption in the glass. The efficiencies measured with an on-axis polarized point source are also given.

For light rays that are not parallel to the axis of rotation, a rotation of the polarizer will change the angle of incidence on the glass sheets. In terms of the geometry of Fig. A2, a unit vector $\hat{\alpha}$ taken in the y-z plane and making an angle α with the axis of rotation is

$$\hat{\alpha} = \hat{k} \cos\alpha + \hat{j} \sin\alpha \ ;$$

the unit vector normal to the glass sheet by

$$\hat{n} = \hat{k} \cos\theta_o + \hat{j} \sin\theta_o \cos\Phi - \hat{i} \sin\theta_o \sin\Phi \ ,$$

where Φ is the angle of orientation of the polarizer; and a unit vector in the direction of the electric component of the incident light ray, also taken in the y-z plane, by

$$\hat{e} = -\hat{k} \sin\alpha + \hat{j} \cos\alpha \ .$$

Then, for arbitrary Φ, the angle θ_i appropriate for calculating the

Table III. Properties of the polarizers, including calculated and measured efficiencies.

	Polarizer No. 1 (5513 Å)	Polarizer No. 2 (4227 Å)
Index of Refraction, n	1.525	1.537
Absorbance	0.16% per mm	0.41% per mm
θ_B	56.745	56.951
θ_o	~57.8	~58.0
ε_M(calculated)	0.992	0.983
ε_M(measured)*	0.98 ± 0.01	0.97 ± 0.01
ε_m(calculated)	0.0342	0.0313
ε_m(measured)*	0.035 ± 0.004	0.035 ± 0.004

* Measured with an on-axis polarized point source.

0 0 0 0 5 7 3 2 2 4

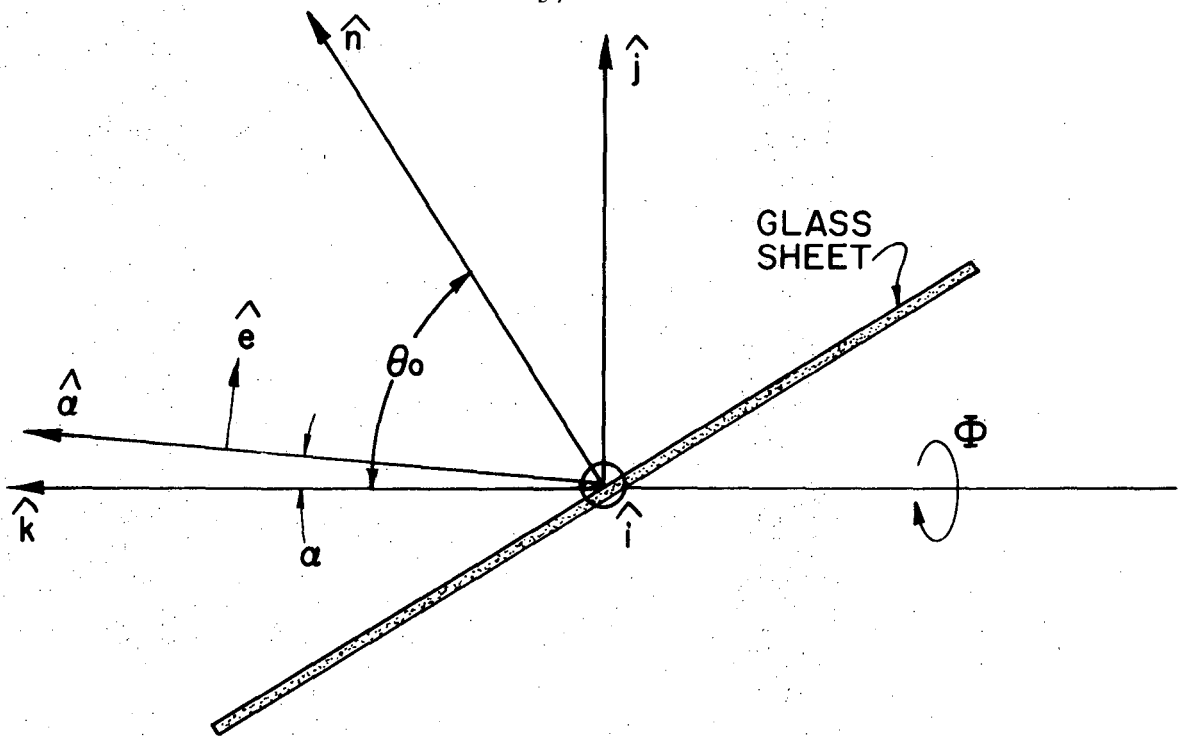

XBL 723-519

Fig. A2. Geometry convention for a nonaxial incident light ray.

polarizer efficiencies is

$$\theta_i = \cos^{-1}(\hat{n}\cdot\hat{\alpha}) = \cos^{-1}[\cos\theta_o \cos\alpha + \sin\theta_o \sin\alpha \cos\Phi] \ .$$

The transmission for linearly polarized light for any polarizer having efficiencies ε_M and ε_m is

$$T(\Phi') = \varepsilon_M \cos^2 \Phi' + \varepsilon_m \sin^2 \Phi' \ ,$$

where Φ' is the angle between the polarization direction of the light and the polarizer axis. For a pile-of-plates polarizer, the polarizer axis lies in the incident plane and is perpendicular to the incident light ray. Hence, for nonaxial light, the angle Φ' is

$$\Phi' = \sin^{-1}\left[\frac{\hat{e}\cdot(\hat{n}\times\hat{\alpha})}{|\hat{n}\times\hat{\alpha}|}\right] = \sin^{-1}\left[\frac{\sin\theta_o \sin\Phi}{[1 - (\cos\theta_o \cos\alpha + \sin\theta_o \sin\alpha \cos\Phi)^2]^{\frac{1}{2}}}\right] .$$

Figures A3a and A3b display the Φ dependence of the difference in transmission between axial and nonaxial light, for various values of α, in the cases of polarized and unpolarized incident light. Measurements with an off-axis point source verify the predicted behavior.

The major implication of the above discussion is slightly poorer efficiencies for the (extended) experimental source geometry. Any possible systematic error resulting from rotational variance of the efficiencies cannot change the basic conclusion of this thesis.

0 0 0 0 3 7 0 2 2 2 5

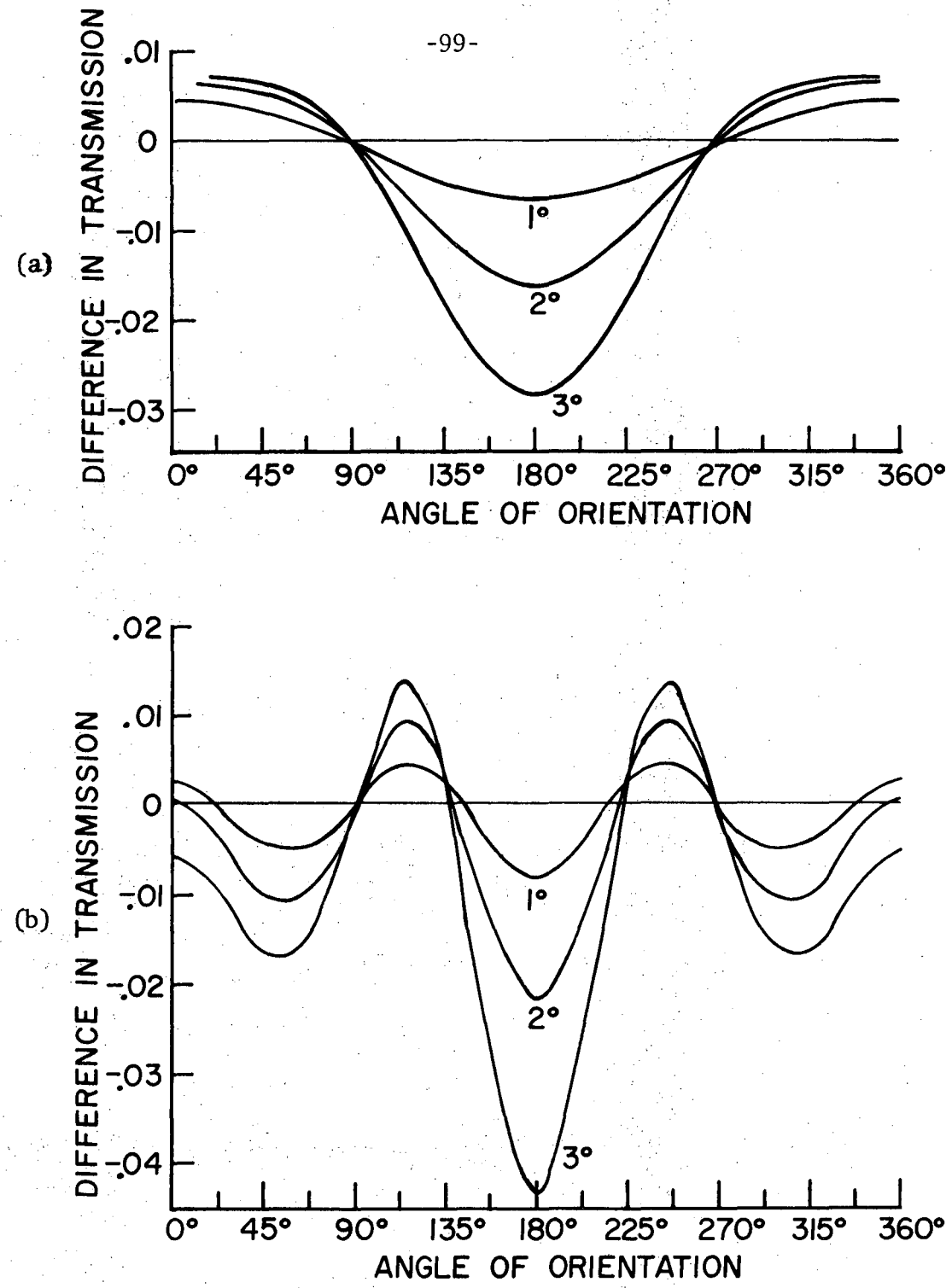

XBL 723-524

Fig. A3. The difference in transmission between nonaxial and axial light as a function of the angle of orientation of the polarizer (the index of refraction is 1.525): (a) for unpolarized incident light and (b) for polarized incident light (see Fig. A2 for conventions). Curves are plotted for three values of the angle of the incident light ray.

APPENDIX B

TWO-PHOTON COINCIDENCE TECHNIQUE IN ATOMIC PHYSICS

The first successful atomic two-photon coincidence experiment was reported by Brannen et al. (Table IV) in 1955. Their experiment and the subsequent applications of the technique were made possible by the development of the photomultiplier tube, which occurred during the 1940's and 1950's.

The technique has been applied primarily to the measurement of atomic lifetimes and to the observation of Brown-Twiss correlations (BT56). Angular distributions were observed by Lipeles et al. (LNT65) from a two-photon decay in singly ionized helium ($2s \rightarrow 1s$), and by Popp et al. (Table IV) from a two-photon cascade of mercury ($7^3S_1 \rightarrow 6^3P_1 \rightarrow 6^1S_0$). Kocher and Commins were the first to observe a polarization correlation. Dumont et al. (Table IV) observed the perturbation of a polarization correlation due to an external magnetic field.

To observe a polarization correlation, one must choose a cascade from which both emitted photons have wavelengths that allow the use of available polarizers and photomultipliers. This limits possible experiments to a small class of well-chosen cascades.

A search of the literature resulted in the list of experiments given in Table IV, involving observations of two photons from atomic cascades. For some experiments, the highest Q obtained is estimated

0 0 0 0 3 7 0 2 2 2 6

from published data and also given in the table.*

---

* Q, the quality factor, is defined in Sect. III.C.2. A high Q means a result with a given statistical accuracy can be obtained quickly. The time required to complete the experiment is proportional to $1/Q^2$.

Table IV. Atomic two-photon coincidence experiments.

Date	Element and Cascade	Photon Wavelengths	Phototube Type	Q	What was observed
1955[a]	(Hg) Ionization limit→ $7^3S_1 \rightarrow 6^3P_1$	$\lambda_1 \approx 4900$ Å $\lambda_2 = 4359$ Å	RCA 1P21 RCA 1P21		$\tau(7^3S_1) =$ 11.2±.2 nsec
1963[b]	(H) $n=3 \rightarrow n=2 \rightarrow n=1$	$\lambda_1 = 6562$ Å $\lambda_2 = 1216$ Å	RCA 7265 Bendix 306		QE of Bendix 306
1966[c]	(Hg) $6D \rightarrow 6^3P_1 \rightarrow 6^1S_0$	$\lambda_1 \approx 3130$ Å $\lambda_2 = 2537$ Å		.05[d]	$\tau(6^3P_1) \approx$ 118 nsec
1967[e]	(Hg) 6^1P_0 and $6p^1D_2$ $\rightarrow 7^3S_1 \rightarrow 6^3P_1$ or 6^3P_2 or 6^3P_0	$\lambda_1 = 6072$ Å and 6123 Å $\lambda_2 = 4358$ Å or 5401 Å or 4047 Å	Amperex 56TVP RCA 1P21 or Amperex 56AVP	.08[d]	$\tau(7^3S_1) =$ 9.7±.2 nsec
1967[f]	(Ca) $4p^2\ ^1S_0 \rightarrow 4^1P_1 \rightarrow 4^1S_0$	$\lambda_1 = 5513$ Å $\lambda_2 = 4227$ Å	RCA 7265 RCA 8575	.1[g]	Polarization correlation
1967[h]	(Hg) $7^3S_1 \rightarrow$ $6^3P_1 \rightarrow$ 6^1S_0	$\lambda_1 = 4358$ Å $\lambda_2 = 2537$ Å	Amperex 56DVP Amperex 56UVP	.1[d]	$\tau(6^3P_1)$ as a function of pressure of Hg
1968[i]	(Ar II) $^4P_{5/2} \rightarrow 4p\ ^4S_{3/2} \rightarrow\ ^4P_{3/2}$	$\lambda_1 = 3869$ Å $\lambda_2 = 3851$ Å	Amperex 56UVP Amperex 56UVP	.005[d]	$\tau(4p\ ^4S_{3/2}) =$ 5.2±2.3 nsec
1969[j]	(Ar II) $^2D_{5/2} \rightarrow 4p\ ^2D_{3/2} \rightarrow\ ^2D_{5/2}$	$\lambda_1 \approx 4449$ Å $\lambda_2 = 4482$ Å	Amperex 56DVP Amperex 56DVP	.02[d]	$\tau(4p\ ^2D_{5/2}) =$ 6.27±.06 nsec
1970[k]	(Hg) 6^1P_0 and 6^1D_2 $7^3S_1 \rightarrow 6^3P_1$	$\lambda_1 = 6073$ Å and 6123 Å $\lambda_2 = 4358$ Å			$\tau(7^3S_1) =$ 8.4±.4 nsec
1970[k]	(Ar II) $^2P_{3/2} \rightarrow 4p\ ^4D_{7/2} \rightarrow\ ^4P_{5/2}$	$\lambda_1 = 4104$ Å $\lambda_2 = 4348$ Å			$\tau(4p\ ^4D_{7/2}) =$ 5.06±.12 nsec

(continued on next page)

0 0 0 0 3 7 0 2 2 7

Table IV *(continued)*

Date	Element and Cascade	Photon Wavelengths	Phototube Type	Q	What was observed
1970[ℓ]	(Hg) $7^3S_1 \rightarrow 6^3P_1 \rightarrow 6^1S_0$	λ_1 = 4358 Å λ_2 = 2537 Å	RCA 31000D Amperex 56TUVP	.1[ℓ]	$\tau(6^3P_1)$ = 120±2 nsec Angular correlation with and without a perturbing field $g(6^3P_1)$ = 1.35±0.10
1970[m]	(Ar II) $^2P_{3/2} \rightarrow 4p\ ^4D_{7/2} \rightarrow {}^4P_{5/2}$	λ_1 = 4104 Å λ_2 = 4348 Å			Polarization correlation in a perturbing magnetic field $g(4p\ ^4D_{7/2})$ = 1.2±0.3

[a] E. Brannen, F. R. Hunt, R. H. Adlington, and R. W. Nichols, Nature 175, 810 (1955).
[b] F. Cristofori, P. Fenici, G. E. Figerio, N. Molho, and P. G. Sona, Phys. Letters 6, 171 (1963).
[c] R. D. Kaul, J. Opt. Soc. Am. 56, 1262 (1966).
[d] C. Camhy-Val and A. M. Dumont, Astron. and Astrophys. 6, 27 (1970).
[e] J. Pardiès, Thèse de Doctorat, Bordeaux, 1967.
[f] C. A. Kocher and E. D. Commins, Phys. Rev. Letters 18, 575 (1967).
[g] C. A. Kocher, Ph.D. Thesis (University of California, Berkeley, 1967), p. 56. Lawrence Radiation Laboratory Report UCRL-17587.
[h] G. H. Nussbaum and F. M. Pipkin, Phys. Rev. Letters 19, 1089 (1967).
[i] C. Camhy-Val and A. M. Dumont, Compt. Rend. 267 (Series B), 689 (1968).
[j] A. M. Dumont, Thèse de Doctorat, Paris, 1970.
[k] C. Camhy-Val, A. M. Dumont, M. Dreux, and R. Vitry, Phys. Letters 32A, 233 (1970).
[ℓ] M. Popp, G. Schäfer, and E. Bodenstedt, Z. Physik 240, 71 (1970).
[m] A. M. Dumont, C. Camhy-Val, M. Dreux, and R. Vitry, Compt. Rend. 271 (Series B), 1021 (1970).

APPENDIX C

ADDITIONAL DATA

This appendix contains the results of some runs that were not included in Sect. IV. Table V gives the results of three separate determinations of the polarization correlation.

For Run 1 the polarizer efficiencies are slightly poorer than during the other runs. The efficiencies for Run 1 are: $\varepsilon_M^1 = 94 \pm 0.01$, $\varepsilon_m^1 = 0.04 \pm 0.01$, $\varepsilon_M^2 = 0.92 \pm 0.01$, and $\varepsilon_m^2 = 0.04 \pm 0.01$. Subsequent to Run 1 the efficiencies were improved by cleaning and readjusting the glass sheets in each polarizer. The efficiencies for all other runs discussed in this thesis correspond to the values given in Table I.

In Run 3 the beam density is much higher than during the final series of runs, yet the polarization correlation is not significantly different from the ones associated with the lower densities.

0 0 0 0 3 7 0 2 2 8

Table V. Additional data.

	1[a]	2	3
Excitation Source	Two Oriel Lamps	One Kern Lamp	One Kern Lamp
Average Atomic Beam Density	~3×10^{10} atoms/cm^3	~3×10^{10} atoms/cm^3	~10^{11} atoms/cm^3
Total Counting Time	53 h	16 h	6.5 h
Average Coincidence Rate[b]	0.52 counts/sec	0.65 counts/sec	0.52 counts/sec
Average Coincidence-to-Accidental Ratio[b]	2.5	5.2	12.4
Average Quality Factor[b]	0.53	0.69	0.67
Apparent Lifetime, τ	7.8 ± 0.7 nsec	7.5 ± 0.7 nsec	9 ± 1 nsec
$R(0°)/R_o$	0.442 ± 0.013	0.473 ± 0.015	0.452 ± 0.024
$R(22\frac{1}{2}°)/R_o$	0.382 ± 0.009	0.407 ± 0.014	0.395 ± 0.022
$R(45°)/R_o$	0.237 ± 0.008	0.258 ± 0.011	0.255 ± 0.018
$R(67\frac{1}{2}°)/R_o$	0.096 ± 0.006	0.116 ± 0.008	0.123 ± 0.012
$R(90°)/R_o$	0.048 ± 0.007	0.050 ± 0.007	0.055 ± 0.009
R_1/R_o	0.492 ± 0.016		
R_2/R_0	0.471 ± 0.015		
δ	0.035 ± 0.012	0.040 ± 0.016	0.022 ± 0.025

[a] The polarizer efficiencies were poorer than usual for this run.

[b] Polarizers removed.

ACKNOWLEDGMENTS

I wish first of all to thank my advisor, Professor Eugene Commins, for his wise guidance, his encouragement, and his friendship.

I am indebted to Dr. John Clauser, who brought the experimental proposal (CHSH69) to Berkeley and collaborated with me on the experimental work and the published report of the experiment (FC72).

I wish to thank my friend andcolleague Mel Simmons for many discussions and for several important suggestions.

I wish to thank David Rehder, an extremely clever and competent machinist, who did much of the machining and mechanical construction of the apparatus.

I am grateful to Professor Howard Shugart and the other members of the Atomic Beams Group for much valuable assistance.

This work relies heavily on the previous work of Dr. Carl Kocher (while a student of Prof. Commins) and Dr. Michael Horne (while a student of Prof. Abner Shimony), and I wish to acknowledge both of them for their excellent theses.

I am grateful to Ms. Joyce Freedman for her moral support and for typing the rough draft of this thesis, and to Jean Atteridge for typing the final copy.

This work was supported by the U.S. Atomic Energy Commission.

0 0 0 0 3 7 0 2 2 2 9

REFERENCES

APJ70 R. Apjean, A. Pochat, and A. Johannin-Gilles, Vacuum 20, 193 (1970).

BB48 E. Bleuler and H. L. Bradt, Phys. Rev. 73, 1398 (1948).

BD49 D. R. Bates and A. Damgaard, Phil. Trans. Roy. Soc. London 242, 101 (1949).

B51 D. Bohm, Quantum Theory (Prentice-Hall, Inc., New York, 1951), Chapter XXII.

B52a D. Bohm, Phys. Rev. 85, 166 (1952).

B52b D. Bohm, Phys. Rev. 85, 180 (1952).

BBL55 G. Bertolini, M. Bettoni, and E. Lazzarini, Nuovo Cimento 2, 661 (1955).

BT56 R. Hanbury Brown and R. Q. Twiss, Nature 177, 27 (1956).

B57 D. Bohm, Causality and Chance in Modern Physics (Harper & Bros., New York, 1957).

BA57 D. Bohm and Y. Aharonov, Phys. Rev. 108, 1070 (1957).

B59a J. P. Barrat, J. Phys. Radium 20, 541 (1959).

B59b J. P. Barrat, J. Phys. Radium 20, 633 (1959).

B59c J. P. Barrat, J. Phys. Radium 20, 657 (1959).

B65 J. S. Bell, Physics 1, 195 (1965).

BNL65 B. Budick, R. Novick, and A. Lurio, Appl. Opt. 4, 229 (1965).

B66 J. S. Bell, Rev. Mod. Phys. 38, 447 (1966).

BB66 D. Bohm and J. Bub, Rev. Mod. Phys. 38, 453 (1966).

Bv69 P. R. Bevington, Data Reduction and Error Analysis for the Physical Sciences (McGraw-Hill, New York, 1969).

B70 J. S. Bell, "Hidden Variables," lecture notes, International School of Physics "Enrico Fermi," I.L. course: Foundations of Quantum Mechanics, 29 June-11 July 1970 at Varenna (to be

published by Academic Press).

B72 F. J. Belinfante, A Survey of Hidden-Variable Theories (Revised Edition), (to be published by Pergamon Press).

CDDM68 C. Camhy-Val, M. Dreux, A. M. Dumont, and J. Marchal, Nucl. Instr. and Methods 60, 333 (1968).

C69 M. W. P. Cann, Appl. Opt. 8, 1645 (1969).

CHSH69 J. F. Clauser, M. A. Horne, A. Shimony, and R. A. Holt, Phys. Rev. Lett. 23, 1969).

D61 T. B. Day, Phys. Rev. 121, 1204 (1961).

DP65 M. I. D'Yakonov and V. I. Perel, Sov. Phys.-JETP 20, 997 (1965).

DC68 A. M. Dumont and C. Camhy-Val, Nucl. Instr. and Methods 60, 329 (1968).

DG71 B. Dewitt and N. Graham, Am. J. Phys. 39, 724 (1971).

EPR35 A. Einstein, B. Podolsky, and N. Rosen, Phys. Rev. 47, 777 (1935).

E71 H. Ehrhardt, Coincidence techniques in scattering, in Atomic Physics 2, Proc. Second Conference on Atomic Physics July 21-24, 1970, ed. P. G. H. Sandars (Plenum Press, Oxford, 1971).

F36 W. H. Furry, Phys. Rev. 49, 392 (1936).

FJOP69 R. Foord, R. Jones, C. J. Oliver, and E. R. Pike, Appl. Opt. 8, 1975 (1969).

FT69 H. Friedrich and E. Trefftz, J. Quant. Spectrosc. Radiat. Transfer 9, 333 (1969).

F71 R. Fox, Lett. Nuovo Cimento 2, 565 (1971).

FJOP71 R. Foord, R. Jones, C. J. Oliver, and E. R. Pike, Appl. Opt. 10, 1683 (1971).

FR71 R. Fox and B. Rosner, Phys. Rev. D 4, 1243 (1971).

FC72 S. J. Freedman and J. F. Clauser, Phys. Rev. Lett. 28, 938 (1972).

0 0 0 0 3 7 0 2 2 3 0

G57 A. M. Gleason, J. Math. & Mech. 6, 885 (1967).

G68 S. Gudder, Proc. Am. Math. Soc. 19, 319 (1968).

G70 S. Gudder, J. Math. Phys. 11, 431 (1970).

Gr70 N. Graham, The Everett Interpretation of Quantum Mechanics (Ph.D. Thesis), Univ. of North Carolina, Chapel Hill, 1970 (unpublished).

H48 R. C. Hanna, Nature 162, 332 (1948).

H51 F. L. Hereford, Phys. Rev. 81, 482 (1951).

HPP64 E. Hulpke, E. Paul, and W. Paul, Z. Physik 177, 257 (1964).

H70 M. A. Horne, Experimental Consequences of Local Hidden-Variable Theories (Ph.D. Thesis), Harvard University, 1970 (unpublished).

I61 D. R. Inglis, Rev. Mod. Phys. 33, 1 (1961).

JP63 J. Jauch and C. Piron, Helv. Phys. Acta. 36, 827 (1963).

K67a C. A. Kocher, Polarization Correlation of Photons Emitted In An Atomic Cascade (Ph.D. Thesis), Lawrence Radiation Laboratory Report UCRL-17587, 1967 (unpublished).

K67b C. A. Kocher, Rev. Sci. Instr. 38, 1674 (1967).

KC67 C. A. Kocher and E. D. Commins, Phys. Rev. Lett. 18, 575 (1967).

KS67 S. Kochen and E. Specker, J. Math. Mech. 17, 59 (1967).

KOZ69 H. J. Kluge, E. W. Otten, and G. Zimmerman, J. Phys. Radium 30, C1-15 (1969).

K70 L. R. Kasday, "Experimental Test of Quantum Predictions for Widely Separated Photons," lecture notes, International School of Physics "Enrico Fermi," I.L. course: Foundations of Quantum Mechanics, 29 June-11 July 1970 at Varenna (to be published by Academic Press).

KUW70 L. R. Kasday, J. Ullman, and C. S. Wu, Bull. Am. Phys. Soc. 15, 586 (1970).

L60 H. Langhoff, Z. Physik 160, 186 (1960).

LS61 S. I. Levikos and L. P. Shishatskaya, Opt. Spectrosc. 11, 371 (1961).

LDG64 A. Lurio, R. L. DeZafra, and R. J. Goshen, Phys. Rev. 134, A1198 (1964).

LNT65 M. Lipeles, R. Novick, and N. Tolk, Phys. Rev. Lett. 15, 690 (1965).

L67 H. Lew, in Methods of Experimental Physics, Vol. 4A: Atomic and Electron Physics - Atomic Sources and Detectors, ed. V. W. Hughes and H. L. Schultz (Academic Press, New York, 1967).

LHP67 C. M. Lederer, J. M. Hollander, and I. Perlman, Table of Isotopes, 6th Edit. (J. Wiley, New York, 1967).

LE69 P. A. Liebman and G. Entine, Appl. Opt. 8, 1502 (1969).

LL72 B. Leskovar and C. C. Lo, Lawrence Berkeley Laboratory Report LBL-399 (to be published in IEEE Trans. Nucl. Sci.).

M49 C. E. Moore, Atomic Energy Levels (NBS, Washington, D.C., 1949), Vol. I.

MM60 R. B. Murray and J. J. Manning, IRE Trans. Nucl. Sci. NS-7, No. 2-3, 80 (1960).

MNSSG64 M. Mayer, R. Niedermayer, W. Schroen, D. Stünkel, and M. Göhre, in Vacuum Microbalance Techniques (Plenum Press, New York, 1964), Vol. 3, p. 87.

M67 R. Morrison, Grounding and Shielding Techniques in Instrumentation (J. Wiley, New York, 1967).

Mi67 B. Misra, Nuovo Cimento 47, 843 (1967).

M68 G. A. Morton, Appl. Opt. 1, 1 (1968).

MS68 B. L. Moiseiwitsch and S. J. Smith, Electron Impact Excitations of Atoms, NSRDS-NBS 25 (NBS, Washington, D.C., 1968).

MSK69 G. A. Morton, H. M. Smith, and H. R. Krall, IEEE Trans. Nucl. Sci. NS-16, 92 (1969).

N63 A. N. Nesmeyanov, Vapor Pressure of the Chemical Elements, ed. Robert Gary (Elsevier Publ. Co., New York, 1963).

PS60 A. Peres and P. Singer, Nuovo Cimento 15, 907 (1960).

0 0 0 0 3 7 0 2 2 3 1

PT61 RCA Photomultiplier Manual, RCA Technical Series PT-61 (1970).

R56 N. F. Ramsey, Molecular Beams (Clarendon Press, Oxford, 1956).

RCA67 W. Raith, R. L. Christensen, and I. Ames, in Methods of Experimental Physics, Vol. 4A: Atomic and Electron Physics - Atomic Sources and Detectors, ed. V. W. Hughes and H. L. Schultz (Academic Press, New York, 1967), p. 284.

RM70 J. Rolfe and S. E. Moore, Appl. Opt. 9, 63 (1970).

R71 F. Robben, Appl. Opt. 10, 776 (1971).

S48 F. W. Sears, Principles of Physics III – Optics (Addison-Wesley, New York, 1948), pp. 167-176.

S62 W. A. Shurcliff, Polarized Light – Production and Use (Harvard University Press, Cambridge, Mass., 1962).

SG66 W. W. Smith and A. Gallagher, Phys. Rev. 145, 26 (1966).

S70 A. Shimony, "Experimental Test of Local Hidden Variables," lecture notes, International School of Physics "Enrico Fermi," I.L. course: Foundations of Quantum Mechanics, 29 June-11 July 1970 at Varenna (to be published by Academic Press).

Sc70 M. J. Schwartz, Electro-Optical Systems Design, August 1970, p. 88.

V32 J. Von Neumann, Mathematische Grundlagen der Quantenmechanik, (Springer, Berlin, 1932); English translation The Mathematical Foundations of Quantum Mechanics (Princeton Univ. Press, Princeton, N.J., 1955).

VD49 N. A. Vlasow and B. S. Dzehelepov, Dokl. Akad. Nauk. SSSR 69, 777 (1949).

W46 J. A. Wheeler, Ann. N. Y. Acad. Sci. 48, 219 (1946).

WS50 C. S. Wu and J. Shaknov, Phys. Rev. 77, 136 (1950).

WS63 A. W. Warner and C. D. Stockbridge, in Vacuum Microbalance Techniques (Plenum Press, New York, 1963), Vol. 2, p. 55.

WSM69 W. L. Wiese, M. W. Smith, and B. M. Miles, Atomic Transition Probabilities, Vol. II, NSRDS-NBS 22 (NBS, Washington, D.C., 1969).

W70 E. P. Wigner, Am. J. Phys. 38, 1005 (1970).

Wa70 W. C. Walker, Appl. Opt. 3, 1457 (1964).

Y69 A. T. Young, Appl. Opt. 8, 2431 (1969).

Y71 A. T. Young, Appl. Opt. 10, 1681 (1971).

YS71 A. T. Young and R. E. Schild, Appl. Opt. 10, 1668 (1971).

LEGAL NOTICE

This report was prepared as an account of work sponsored by the United States Government. Neither the United States nor the United States Atomic Energy Commission, nor any of their employees, nor any of their contractors, subcontractors, or their employees, makes any warranty, express or implied, or assumes any legal liability or responsibility for the accuracy, completeness or usefulness of any information, apparatus, product or process disclosed, or represents that its use would not infringe privately owned rights.

TECHNICAL INFORMATION DIVISION
LAWRENCE BERKELEY LABORATORY
UNIVERSITY OF CALIFORNIA
BERKELEY, CALIFORNIA 94720